

การพัฒนาวิธีการวิเคราะห์การไหลแบบอัตโนมัติร่วมกับแอนดริกสทริปปิงโวลแทมเมตรีสำหรับการ
ตรวจวัดโลหะหนัก

นางสาววนิดา วอนสวัสดิ์

วิทยานิพนธ์นี้เป็นส่วนหนึ่งของการศึกษาตามหลักสูตรปริญญาวิทยาศาสตรดุษฎีบัณฑิต
สาขาวิชาเคมี ภาควิชาเคมี
คณะวิทยาศาสตร์ จุฬาลงกรณ์มหาวิทยาลัย
ปีการศึกษา 2554

บทคัดย่อและแฟ้มข้อมูลฉบับเต็มของวิทยานิพนธ์ตั้งแต่ปีการศึกษา 2554 ที่เก็บถาวรในคลังปัญญาจุฬาฯ (CUIR)
เป็นแฟ้มข้อมูลของนิสิตเจ้าของวิทยานิพนธ์ที่ส่งผ่านทางบัณฑิตวิทยาลัย

The abstract and full text of theses from the academic year 2011 in Chulalongkorn University Intellectual Repository (CUIR)
are the thesis authors' files submitted through the Graduate School.

METHOD DEVELOPMENT OF AUTOMATED FLOW ANALYSIS
COUPLED WITH ANODIC STRIPPING VOLTAMMETRY FOR
DETERMINATION OF HEAVY METALS

Miss Wanida Wonsawat

A Dissertation Submitted in Partial Fulfillment of the Requirements
for the Degree of Doctor of Philosophy Program in Chemistry

Department of Chemistry

Faculty of Science

Chulalongkorn University

Academic Year 2011

Copyright of Chulalongkorn University

Thesis Title DEVELOPMENT OF AUTOMATED FLOW ANALYSIS
 COUPLED WITH ANODIC STRIPPING VOLTAMMETRY
 FOR DETERMINATION OF HEAVY METALS

By Miss Wanida Wonsawat

Field of Study Chemistry

Thesis Advisor Associate Professor Orawon Chailapakul, Ph.D.

Thesis Co-advisor Assistant Professor Suchada Chuanuwatanakul, Ph.D.

Accepted by the Faculty of Science, Chulalongkorn University in Partial
Fulfillment of the Requirements for the Doctoral Degree

..... Dean of the Faculty of Science

(Professor Supot Hannongbua, Dr. rer. nat.)

THESIS COMMITTEE

..... Chairman
(Assistant Professor Warinthorn Chavasiri, Ph.D.)

..... Thesis Advisor
(Associate Professor Orawon Chailapakul, Ph.D.)

..... Thesis Co-advisor
(Assistant Professor Suchada Chuanuwatanakul, Ph.D.)

..... Examiner
(Associate Professor Nattaya Ngamrojanavanich, Ph.D.)

..... Examiner
(Assistant Professor Pakorn Varanusupakul, Ph.D.)

..... Examiner
(Passapol Ngamukot, Ph.D.)

..... External Examiner
(Weena Siangproh, Ph.D.)

วนิดา วอนสวัสดิ์ : การพัฒนาวิธีการวิเคราะห์การไหลแบบอัตโนมัติร่วมกับแอนโอดิกสทริปปิงโวลแทมเมตรีสำหรับตรวจวัดโลหะหนัก. (METHOD DEVELOPMENT OF AUTOMATED FLOW ANALYSIS COUPLED WITH ANODIC STRIPPING VOLTAMMETRY FOR DETERMINATION OF HEAVY METALS) อ. ที่ปริกษาวิทยานิพนธ์หลัก: รศ. ดร.อรวรรณ ชัยลภากุล อ. ที่ปริกษาวิทยานิพนธ์ร่วม: ผศ. ดร.สุชาดา จูอนูวัฒนกุล; 150 หน้า.

ในงานวิจัยนี้ได้พัฒนาวิธีการวิเคราะห์การไหลแบบอัตโนมัติสำหรับการตรวจวัดโลหะหนักปริมาณน้อยมากด้วยดิฟเฟอเรนเชียลพัลส์แอนโอดิกสทริปปิงโวลแทมเมตรีและสแควร์เวฟแอนโอดิกสทริปปิงโวลแทมเมตรีโดยใช้ตัวรับรู้แบบไมโครโพลาร์ ซึ่งประกอบด้วยเมมเบรนเพิ่มความเข้มข้นและส่วนไฟฟ้าเคมีแบบสามขั้วที่มีขั้วไฟฟ้าคาร์บอนเป็นขั้วไฟฟ้าใช้งาน เป็นตัวตรวจวัด จิตจำกัดการตรวจวัดแคดเมียมและตะกั่วคือ 2.37 และ 0.15 ไมโครกรัมต่อลิตร ด้วยดิฟเฟอเรนเชียลพัลส์แอนโอดิกสทริปปิงโวลแทมเมตรี และ 0.02 และ 0.01 ไมโครกรัมต่อลิตร ด้วยสแควร์เวฟแอนโอดิกสทริปปิงโวลแทมเมตรี ผลการทดลองแสดงว่าดิฟเฟอเรนเชียลพัลส์แอนโอดิกสทริปปิงโวลแทมเมตรีและสแควร์เวฟแอนโอดิกสทริปปิงโวลแทมเมตรีที่ขั้วไฟฟ้าคาร์บอนในตัวรับรู้แบบไมโครโพลาร์ร่วมกับระบบการไหลแบบอัตโนมัติมีประสิทธิภาพดีในการตรวจวัดไอออนของโลหะหนัก

นอกจากนี้ได้ออกแบบและสร้างโพลาร์เซลล์เชิงไฟฟ้าเคมีแบบไหลผ่านสำหรับขั้วไฟฟ้าคาร์บอนเพสต์สำหรับการตรวจวัดโลหะหนักที่มีสภาพไวสูงโดยการวิเคราะห์การไหลแบบอัตโนมัติร่วมกับสแควร์เวฟแอนโอดิกสทริปปิงโวลแทมเมตรี สภาพไวของโพลาร์เซลล์ที่สร้างขึ้นสำหรับตรวจวัดไอออนของแคดเมียมและตะกั่วดีขึ้นเมื่อใช้ช่องการไหลขนาดเล็ก ภายใต้ภาวะทดลองที่เหมาะสม จิตจำกัดการตรวจวัดไอออนของแคดเมียมและตะกั่วด้วยโพลาร์เซลล์ที่สร้างขึ้น (0.08 และ 0.07 ไมโครกรัมต่อลิตร ตามลำดับ) ต่ำกว่าเมื่อใช้โพลาร์เซลล์ที่มีจำหน่าย (1.1 และ 0.8 ไมโครกรัมต่อลิตร ตามลำดับ) 13.8- และ 11.4-เท่า นอกจากนี้ในการทดสอบกับตัวอย่างน้ำ ร้อยละการคืนกลับของแคดเมียมและตะกั่วที่ได้จากโพลาร์เซลล์ที่สร้างขึ้นสูงกว่าค่าที่ได้จากโพลาร์เซลล์ที่มีจำหน่ายและอยู่ในช่วงที่ยอมรับได้

สุดท้ายได้พัฒนาขั้วไฟฟ้าคาร์บอนเพสต์คัดแปรด้วยแกรฟีนที่เป็นมิตรกับสิ่งแวดล้อมสำหรับการหาปริมาณของแคดเมียมและตะกั่วด้วยระบบการไหลอัตโนมัติ ได้ศึกษาพฤติกรรมของขั้วไฟฟ้าที่พัฒนาขึ้นด้วยไซคลิกโวลแทมเมตรีและสแควร์เวฟแอนโอดิกสทริปปิงโวลแทมเมตรี ขั้วไฟฟ้าแกรฟีนคาร์บอนเพสต์คัดแปรด้วยบิสมันท์แสดงอิเล็กโทรออกซิเดชันของแคดเมียมและตะกั่วที่ดีเยี่ยมในระบบการไหลแบบอัตโนมัติโดยให้สัญญาณกระแสไฟฟ้าสูงกว่าเมื่อเทียบกับขั้วไฟฟ้าคาร์บอนเพสต์ที่ไม่ได้คัดแปร จิตจำกัดการตรวจวัดคือ 0.07 และ 0.04 ไมโครกรัมต่อลิตร สำหรับแคดเมียมและตะกั่ว ตามลำดับ เมื่อนำขั้วไฟฟ้านี้ไปตรวจวัดไอออนของแคดเมียมและตะกั่วในตัวอย่างที่มีเมทริกซ์น้อย (น้ำประปา) และตัวอย่างที่มีเมทริกซ์มาก (ปลากระพง และหอยลาย) โดยสแควร์เวฟแอนโอดิกสทริปปิงโวลแทมเมตรีในระบบการไหลอัตโนมัติ ร้อยละการคืนกลับอยู่ในช่วงที่ยอมรับได้จาก 70.4-120 สำหรับแคดเมียม และ 65.8-113.5 สำหรับตะกั่ว.

ภาควิชา.....เคมี.....ลายมือชื่อนิสิต.....

สาขาวิชา.....เคมี.....ลายมือชื่อ อ.ที่ปริกษาวิทยานิพนธ์หลัก.....

ปีการศึกษา.....2554.....ลายมือชื่อ อ.ที่ปริกษาวิทยานิพนธ์ร่วม

507 39272 23 : MAJOR CHEMISTRY

KEYWORDS : FLOW ANALYSIS / CARBON ELECTRODE / GRAPHENE / LEAD / CADMIUM

WANIDA WONGSAWAT: METHOD DEVELOPMENT OF AUTOMATED FLOW ANALYSIS COUPLED WITH ANODIC STRIPPING VOLTAMMETRY FOR DETERMINATION OF HEAVY METALS. ADVISOR: ASSOC. PROF. ORAWON CHAILAPAKUL, Ph.D., CO-ADVISOR: ASSIST. PROF. SUCHADA CHUANUWATANAKUL, Ph.D., 150 pp.

In this research, automated flow analysis procedures for trace heavy metal determination by a differential pulse anodic stripping voltammetry (DPASV) and square wave anodic stripping voltammetry (SWASV) were developed. A micro-flow sensor consisted of preconcentration membrane and three-electrode electrochemical part with a carbon working electrode was used as a detector. Detection limits (DL) of Cd^{2+} and Pb^{2+} were 2.37 and 0.15 $\mu\text{g L}^{-1}$ by DPASV and 0.02 and 0.01 $\mu\text{g L}^{-1}$ by SWASV. The results indicated that DPASV and SWASV at the carbon electrode in micro-flow sensor coupled with on-line automated flow system have a good efficiency for the heavy metal ion determination.

Furthermore, a low-cost electrochemical flow-through cell based on a carbon paste electrode (CPE) was designed and constructed for the highly sensitive determination of heavy metals by automated flow analysis coupled with SWASV. The sensitivity of the proposed flow-through cell for Cd^{2+} and Pb^{2+} ion detection was improved by using the small channel height. Under the optimum conditions, the DL of Cd^{2+} and Pb^{2+} ions (0.08 and 0.07 $\mu\text{g L}^{-1}$, respectively) were 13.8- and 11.4-fold lower than that of a commercial flow cell (1.1 and 0.8 $\mu\text{g L}^{-1}$, respectively). Moreover, the percentage recoveries of Cd^{2+} and Pb^{2+} for the in-house designed flow-through cell were higher than those for the commercially available flow cell in all tested water samples, and within the acceptable range.

Finally, an environmentally friendly graphene-modified carbon paste electrode (GCPE) for determination of Cd^{2+} and Pb^{2+} levels in an automated flow system was successfully developed. The electrochemical behavior of the developed electrode was studied by cyclic voltammetry and SWASV. The *in situ* bismuth-modified graphene carbon paste electrode (Bi-GCPE) exhibited excellent electrooxidation of Cd^{2+} and Pb^{2+} in the automated flow system with a significantly higher peak current for both metal ions compared with the unmodified CPE. The DLs were 0.07 and 0.04 $\mu\text{g L}^{-1}$ for Cd^{2+} and Pb^{2+} , respectively. The Bi-GCPE was also applied for the determination of Cd^{2+} and Pb^{2+} in low- (tap water) and high- (sea bass fish and undulated surf clam tissues) matrix complexity samples by SWASV in the automated flow system. The recoveries were acceptable and ranged from 70.4 to 120% for Cd^{2+} and 65.8 to 113.5% for Pb^{2+} .

Department : CHEMISTRY Student's Signature

Field of Study : CHEMISTRY Advisor's Signature

Academic Year : 2011 Co-advisor's Signature

ACKNOWLEDGEMENTS

First of all, I would like to express my deepest gratitude and sincerest appreciation to my advisor, Assoc. Prof. Dr. Orawon Chailapakul and my co-advisor, Assist. Prof. Dr. Suchada Chuanuwatanakul, who always gives the great opportunity for my research throughout four and half years. They have consistently provided me with invaluable guidance, profound assistance and forbearance discerning suggestion, critical proof reading, encouragement and especially sincere forgiveness for my mistakes throughout the research. They have also supported moral principles, knowledge and various experiences to me, until I obtain great successful science education today. In addition, I would like to thank my committee members, Assist. Prof. Dr. Warinthorn Chavasiri, Assoc. Prof. Dr. Nattaya Ngamrojanavanich, Assist. Prof. Dr. Pakorn Varanusupakul, Dr. Passapol Ngamukot and Dr. Weena Siangproh, who give helpful comments and advices in my dissertation.

Special thanks are also extended to my oversea supervisor, Professor Dr. Shoji Motomizu (Okayama University, Japan) for his challenging ideas, kindness, financial support, advice, and suggestions over the year of conducting research and valuable experience and provision in Japan.

I am especially grateful for all the financial support from the Commission on Higher Education, Ministry of Education, Thailand, under the Higher Educational Strategic Scholarships for Frontier Research Network Project, Japan Student Services Organization under JASSO-Short-Term Student Exchange Promotion Program (Inbound) Scholarship, the Center of Excellence for Petroleum, Petrochemicals and Advanced Materials, Chulalongkorn University, the 90th Anniversary of Chulalongkorn University Fund (Ratchadaphiseksomphot Endowment Fund), and Chulalongkorn University. The Publication Counseling Unit, Faculty of Science, is also acknowledged for suggestions and English corrections. I am grateful to the Department of Chemistry, Faculty of Science, Chulalongkorn University, for providing chemicals and laboratory facilities. Moral supports and encouragement of my friends and all members of the electroanalytical chemistry research group of Chulalongkorn University are truly appreciated. Special thanks go to Mr. Eakkasit Punrat and Dr. Wijitar Dungchai for their suggestion.

Finally, I am affectionately thankful to my parents and family for their heartfelt unlimited support, enthusiasm support, stand by for my success and best understanding throughout my study.

CONTENTS

	PAGE
ABSTRACT IN THAI.....	iv
ABSTRACT IN ENGLISH.....	v
ACKNOWLEDGEMENTS.....	vi
CONTENTS.....	vii
LIST OF TABLES.....	xiii
LIST OF FIGURES.....	xv
LIST OF ABBREVIATIONS.....	xxii
CHAPTER I INTRODUCTION.....	1
1.1 Introduction.....	1
1.2 Objectives of the research.....	3
CHAPTER II THEORY AND LITERATURE SURVEY.....	4
2.1 Principles of electrochemistry.....	4
2.1.1 Electrochemical technique.....	4
2.1.2 Voltammetry technique.....	8
2.1.3 Electrodes.....	17
2.1.4 Electrochemical cell.....	22
2.1.5 Electrochemical flow-through cell.....	22
2.2 Flow based technique.....	26
2.2.1 Flow injection analysis.....	27
2.2.2 Sequential injection analysis.....	28
2.3 Heavy metal.....	32
2.4 Literature survey.....	34
2.4.1 Part I: Electrochemical characterization of carbon electrode in micro-flow sensor by on-line automated flow system.....	34

	PAGE
2.4.2 Part II: Highly sensitive determination of Cd ²⁺ and Pb ²⁺ using a low-cost electrochemical flow-through cell based on a carbon paste electrode.....	35
2.4.3 Part III: Graphene-modified carbon paste electrode for Cd ²⁺ and Pb ²⁺ monitoring with flow based system	38
CHAPTER III EXPERIMENTAL	41
Part I: Electrochemical characterization of carbon electrode in micro-flow sensor by on-line automated flow system.....	41
3.1 Instruments and apparatus.....	41
3.2 Chemicals and reagents.....	42
3.3 Chemical preparations.....	42
3.3.1 Carrier solution.....	42
3.3.2 Stock standard solution.....	42
3.3.3 Cleaning solution.....	43
3.3.4 Reference electrode filling solution.....	43
3.4 Experimental procedures.....	43
3.4.1 Long-term stability and reproducibility of the carbon electrode in the micro-flow sensor.....	45
3.4.2 Study of the differential pulse anodic stripping voltammetric parameters.....	46
3.4.3 Study of the square wave anodic stripping voltammetric parameters..	46
3.5 Analytical performance.....	46
Part II: Highly sensitive determination of Cd ²⁺ and Pb ²⁺ using a low-cost electrochemical flow-through cell based on a carbon paste electrode.....	47
3.6 Instruments and apparatus.....	47
3.7 Chemicals and reagents.....	48
3.8 Chemicals preparations.....	49
3.8.1 Design and characterization of flow cell.....	49
3.8.2 Characterization of in-housed thin layer flow cell using	

	PAGE
amperometric method.....	49
3.8.3 Reagent used in sequential injection analysis.....	49
3.9 Electrode preparation.....	50
3.9.1 Carbon paste electrode preparation.....	50
3.9.2 Preparation of Bi-film modified electrode.....	51
3.10 Sample preparation.....	51
3.10.1 Water sample.....	51
3.11 Experimental procedure for Bi-CPE.....	52
3.11.1 Optimization in-house designed flow cell.....	52
3.11.2 Characterization of a thin layer flow cell with amperometric detection.....	53
3.11.3 The study of the Bi ³⁺ modified method with SIA system.....	53
3.11.4 Characterization of Bi-film electrode.....	54
3.11.5 Study of the electrode stability.....	55
3.11.6 Optimization of SIA-SWASV parameters.....	56
3.12 Applications.....	58
3.12.1 Application of Bi-CPE.....	58
Part III: Graphene-modified carbon paste electrode for Cd ²⁺ and Pb ²⁺ monitoring with flow based system.....	59
3.13 Instruments and apparatus.....	59
3.14 Chemicals and reagents.....	60
3.15 Chemical and reagents preparation.....	61
3.15.1 Preparation of 5000 µg L ⁻¹ of Cd ²⁺ and Pb ²⁺ in 0.05 M HCl.....	61
3.15.2 Preparation of 0.5 mM K ₃ Fe(CN) ₆ and K ₄ Fe(CN) ₆ .3H ₂ O.....	61
3.15.3 Working standard solutions.....	61
3.15.4 Carrier solution	61
3.15.5 Cleaning solution.....	61
3.15.6 Bi-plating solution.....	61

	PAGE
3.16 Electrode preparation.....	62
3.16.1 Graphene/Carbon paste electrode (GCPE) preparation.....	62
3.16.2 <i>In-situ</i> modification from Bi ³⁺ plating solution.....	62
3.17 Sample preparation.....	62
3.17.1 Non-complicated matrix: Water sample.....	62
3.17.2 Complicated matrix: Undulated surf clams tissues and sea bass fish tissue.....	62
3.18 Experimental procedure for Bi-GCPE.....	63
3.18.1 Solvent dispersion.....	63
3.18.2 The graphene and graphite mass ratio	63
3.18.3 Prepared Bi ³⁺ modified GCPE.....	64
3.18.4 Optimization of SIA-SWASV with Bi-GCPE.....	64
3.19 Analytical performance.....	65
3.19.1 Analytical performance from Bi-CPE.....	65
3.19.2 Analytical performance from Bi-GCPE.....	65
3.20 Applications.....	66
3.20.1 Application of Bi-GCPE.....	66
3.21 Control of the analytical performance of the proposed method.....	66
 CHAPTER IV RESULTS AND DISCUSSION.....	 68
 Part I: Electrochemical characterization of carbon electrode in micro-flow sensor by on-line automated flow system.....	 68
4.1 The study of long-term stability and reproducibility of the carbon electrode in the micro-flow.....	68
4.2 Study of the DPASV parameters.....	70
4.2.1 Effect of the deposition potential.....	70
4.2.2 Effect of the pulse time and the pulse potential.....	71

	PAGE
4.3 Study of the SWASV parameters.....	73
4.3.1 The effect of deposition potential.....	73
4.3.2 The effect of the square wave frequency.....	74
4.3.3 Effect of the potential step.....	75
4.3.4 Effect of the potential amplitude.....	76
4.4 Analytical performance.....	79
Part II: Highly sensitive determination of Cd ²⁺ and Pb ²⁺ using a low-cost electrochemical flow-through cell based on a carbon paste electrode.....	83
4.5 Design and characterization of the in-house thin-layer flow cell.....	83
4.5.1 Optimization of the channel height on the in-house thin-layer flow cell.....	83
4.5.2 Characterization of the in-house thin-layer flow cell.....	84
4.6 Study of Bi ³⁺ modification method.....	85
4.6.1 <i>In-situ</i> modification from Bi ³⁺ plating solution.....	85
4.6.2 <i>In-situ</i> modification from Bi ₂ O ₃ nanopowder (BiNP).....	86
4.7 Characterization Bi-film electrode.....	87
4.7.1 Study of the redox behavior.....	87
4.7.2 Study of the mass transfer process.....	88
4.8 Study of the electrode stability.....	89
4.9 Optimization of the condition for Cd ²⁺ and Pb ²⁺ analysis.....	90
4.9.1 Effect of Bi ³⁺ concentration.....	90
4.9.2 Optimization of the condition for Cd ²⁺ and Pb ²⁺ analysis using in-house thin layer flow cell and commercial flow cell	91
4.9.3 Study of the SWASV parameter for Cd ²⁺ and Pb ²⁺ analysis using in-house thin layer flow cell and commercial flow cell	93
4.10 Calibration data.....	101

	PAGE
4.11 Applications.....	105
Part III: Graphene-modified carbon paste electrode for Cd ²⁺ and Pb ²⁺ monitoring with flow based system.....	107
4.12 Structural characterization of graphene and carbon powder.....	107
4.13 Electrochemical behavior of graphene –carbon paste electrode (GCPE)...	108
4.14 Effect of the parameters on the GCPE measurement.....	109
4.14.1 Effect of mass ration of graphene/carbon paste electrode.....	109
4.14.2 The optimal Bi ³⁺ concentration used to modify the GCPE.....	110
4.14.3 Effect of HCl oncentration.....	112
4.14.4 Optimization of Bi-GCPE electrochemical parameters electrode...	114
4.15 Calibration data.....	118
4.15.1 Linearity.....	118
4.15.2 Limit of detection (LOD) and limit of quantification (LOQ).....	119
4.16 Applications.....	120
4.16.1 Non-complicated matrix sample: Tap water sample.....	120
4.16.2 Complicated matrix sample: Undulate surf clams and sea bass fish.....	121
4.17 Control of the analytical performance of the proposed method.....	123
CHAPTER V CONCLUSION AND FURTHER WORKS.....	125
REFERENCES.....	128
APPENDICES.....	144
APPENDIX A.....	145
VITAE.....	150

LIST OF TABLES

TABLE		PAGE
2.1	Some important flow-through voltammetric electrode designs and limiting current characteristics.....	25
3.1	The instruments and apparatus.....	41
3.2	The chemicals and reagents used in this research.....	42
3.3	Step sequence and time necessary for each step.....	44
3.4	The instruments and apparatus.....	47
3.5	The chemicals and reagents used in this research.....	48
3.6	The instruments and apparatus.....	59
3.7	The chemicals and reagents used in this research.....	60
4.1	Stripping currents and reproducibility for $50 \mu\text{g L}^{-1}$ Cd^{2+} and Pb^{2+} in 1.0 M HCl measured in micro-flow system (intra-day analysis: $n = 10$).....	69
4.2	Comparison of the stripping currents and the reproducibility between days for $50 \mu\text{g L}^{-1}$ of Cd^{2+} and Pb^{2+} in 1.0 M HCl using micro-flow system.....	69
4.3	The optimized experimental parameters for the on-line DPASV and SWASV determination of Cd^{2+} and Pb^{2+} using the carbon electrode in micro-flow sensor coupled with SIA operating system.....	77
4.4	The peak currents of $50 \mu\text{g L}^{-1}$ of Cd^{2+} and Pb^{2+} in 1.0 M HCl obtained by DPASV and SWASV at the carbon electrode in the micro-flow sensor coupled with the SIA operating system under the optimum conditions.....	78
4.5	The DPASV peak current of Cd^{2+} and Pb^{2+} at various concentrations	79
4.6	The SWASV peak current of Cd^{2+} and Pb^{2+} at various concentrations	80
4.7	Analytical performance of the on-line DPASV and SWASV method for Cd^{2+} and Pb^{2+} on the unmodified carbon electrode in micro-flow sensor coupled with an SIA operating system at the optimal condition.....	82

TABLE		PAGE
4.8	Slope and linear range of the current vs. concentration plot of Cd ²⁺ and Pb ²⁺ ions at the Bi-film modified CPE using thin-layer flow cells with a 1.6, 2.0 or 2.5 mm channel height.....	83
4.9	The average peak current for 150 µg L ⁻¹ Cd ²⁺ and Pb ²⁺ detected by SWASV at CPE, 100 µg L ⁻¹ Cd ²⁺ and Pb ²⁺ at the Bi-film CPE modified from the Bi ³⁺ plating solution (Bi-CPE) and the Bi-film CPE modified from Bi ₂ O ₃ nanopowder (BiNP-CPE).....	86
4.10	Summary of the optimum conditions in the in-house and commercial flow cells.....	100
4.11	Summary of the analytical performance for the detection of Cd ²⁺ and Pb ²⁺ ions by the commercial and the in-house designed thin-layer flow cells.....	101
4.12	Determination of the Cd ²⁺ and Pb ²⁺ ion levels in water samples (N=3).....	106
4.13	Optimization of HCl concentration (N=3).....	113
4.14	Summary of the optimum conditions for determination of Cd ²⁺ and Pb ²⁺ by Bi-GCPE.....	116
4.15	The summarization of the calibration data and r ² values obtained from the difference concentration of metal ions.....	120
4.16	Determination of (spiked) Cd ²⁺ and Pb ²⁺ levels in a non-complicated (tap water) or complicated (sea bass fish and undulated surf clam tissues) matrix with the Bi-GCPE under SWASV (n = 4).....	123
4.17	Results for the determination of Cd ²⁺ and Pb ²⁺ in a complicated matrix sample (undulated surf clams and sea bass fish); (N= 3, P = 0.95, t _{critical} = 4.30).....	124

LIST OF FIGURES

FIGURE		PAGE
2.1	The schematic showing the migration movement of the ions in the solution	5
2.2	The schematic of convection movement of the ions in the solution.....	5
2.3	The schematic of diffusion movement of the ion in the solution.....	6
2.4	The concentration distance profile during the diffusion controlled reaction of $A + e^- \longrightarrow P$	7
2.5	Excitation signal waveform of cyclic voltammetry.....	9
2.6	Cyclic voltammogram for reversible reaction.....	10
2.7	Square-wave excitation waveform.....	12
2.8	Proposed model of the double-layer region.....	15
2.9	Voltammetric curves: 1) Deposition or preconcentration step; 2) Stripping step.....	17
2.10	Schematic of silver/silver chloride reference electrode.....	20
2.11	The schematic of the electrochemical cell.....	21
2.12	Flow patterns, (a) is turbulent flow and (b) is laminar flow...	23
2.13	Simple FIA manifold.....	27
2.14	The analog output is in the form of a peak, with the recording starting at S (time of injection). H is the peak height, W is the peak width at a selected level, and A is the peak area. T is the residence time corresponding to the peak height measurement, and t_b is the peak width at the baseline.....	28
2.15	Basic scheme of a SIA manifold.....	29
2.16	A sample and reagent zones stacked in the holding coil.....	29
2.17	Merging of sequenced zones of sample and reagent in the holding coil on flow reversal to give a zone of detectable product.....	30
2.18	Comparison of simple FIA and SIA manifold.....	31

FIGURE		PAGE
2.19	The dispersion profile in FIA and SIA: (1) is the sample injection point in FIA and during the flow reversal in SIA, (2) is the carrier started to move toward the detector in FIA and SIA.....	31
3.1	Schematic diagram of instrument set up for the determination of metal ions by on-line anodic stripping voltammetry on micro-flow sensor. A1 = 0.5 M HNO ₃ ; A2 = 1.0 M HCl; R = 0.1 M KCl; M = Metal ion solution; F = preconcentration membrane; and W = waste.....	44
3.2	Carbon paste electrode (CPE).....	51
3.3	A) A schematic diagram of the in-house designed thin-layer flow-through electrochemical cell seen from the side view and the top view; (a) counter electrode and outlet port, (b) reference electrode port, (c) working electrode port, and (d) inlet port. B) In-house designed flow cell with (a) a stainless steel tube as a counter electrode as well as an outlet of the flow cell, (b) a Ag/AgCl reference electrode, (c) CPE as a working electrode.....	53
3.4	The electrochemical cell for cyclic voltammetry experiment..	55
3.5	The SIA manifold for the determination of Cd ²⁺ and Pb ²⁺ by SWASV with Bi-CPE; HC is a holding coil.....	56
4.1	Effect of the deposition potential on the DPASV peak currents for a solution containing 50 µg L ⁻¹ of Cd ²⁺ and Pb ²⁺ in 1.0 M HCl using the carbon electrodes in the micro-flow sensor coupled with SIA operating system. Conditions: deposition time, 180 s; step potential, 0.005 V; conditioning potential, -1.00 V; scan rate, 0.005 V s ⁻¹ ; equilibration time, 10 s.....	71
4.2	The effect of the pulse time on the DPASV peak currents for a solution containing 50 µg L ⁻¹ of Cd ²⁺ and Pb ²⁺ in 1.0 M HCl using the carbon electrode in the micro-flow sensor coupled with SIA operating system. Conditions: deposition potential, -1.2 V; deposition time, 180 s; step potential, 0.005 V; conditioning potential, -1.00 V; scan rate, 0.005 V s ⁻¹ ; quiet time, 10 s	72

FIGURE		PAGE
4.3	Effect of the pulse potential on the DPASV peak currents for a solution containing $50 \mu\text{g L}^{-1}$ of Cd^{2+} and Pb^{2+} in 1.0 M HCl using the carbon electrode in the micro-flow sensor coupled with SIA operating system. Conditions: deposition potential, -1.2 V; deposition time, 180 s; step potential, 0.005 V; conditioning potential, -1.00 V; scan rate, 0.005 V s^{-1} ; quiet time, 10 s.....	73
4.4	Effect of the deposition potential on the SWASV peak heights for a solution containing $50 \mu\text{g L}^{-1}$ of Cd^{2+} and Pb^{2+} in 0.1 M HCl on the carbon electrode in the micro-flow sensor coupled with the SIA operating system.....	74
4.5	The effect of the square wave frequency on the SWASV peak currents for a solution containing $50 \mu\text{g L}^{-1}$ of Cd^{2+} and Pb^{2+} in 1.0 M HCl using the carbon electrode in the micro-flow sensor coupled with the SIA operating system.....	75
4.6	Effect of the potential step on the SWASV peak currents for a solution containing $50 \mu\text{g L}^{-1}$ of Cd^{2+} and Pb^{2+} in 1.0 M HCl using the carbon electrode in the micro-flow sensor coupled with SIA operating system.....	76
4.7	The effect of the potential amplitude on the SWASV peak currents for a solution containing $50 \mu\text{g L}^{-1}$ of Cd^{2+} and Pb^{2+} in 1.0 M HCl on the carbon electrode in the micro-flow sensor coupled with the SIA operating system.....	77
4.8	Voltammograms of a solution containing $50 \mu\text{g L}^{-1}$ of Cd^{2+} and Pb^{2+} in 1.0 M HCl by (a) DPASV and (b) SWASV on the carbon electrode in the micro-flow sensor coupled with SIA operating system under the optimum conditions.....	78
4.9	Calibration plots of Cd^{2+} and Pb^{2+} obtained from DPASV ...	80
4.10	Calibration plots of Cd^{2+} and Pb^{2+} obtained from SWASV...	81
4.11	The voltammograms of $50 \mu\text{g dm}^{-3}$ Cd^{2+} and Pb^{2+} using the in-house designed thin-layer flow cell with a channel height of (A) 1.6 mm, (B) 2.0 mm and (C) 2.5 mm. Voltammograms shown are representative of those seen from five independent repeats.....	84
4.12	The relationship between the current of $0.1 \text{ M Fe (CN)}_6^{3-}$ / Fe(CN)_6^{4-} in 0.1 M KCl and the cube root of the flow rate....	85

FIGURE		PAGE
4.13	The voltammograms of 150 mg dm ⁻³ Cd ²⁺ and Pb ²⁺ at the CPE (a: dash line), 100 mg dm ⁻³ Cd ²⁺ and Pb ²⁺ at Bi ₂ O ₃ nanopowder-modified CPE (b: dot line), and the Bi ³⁺ plating solution modified CPEs (c: solid line). Voltammograms shown are representative of those seen from three independent repeats.....	87
4.14	Cyclic voltammogram of 0.5 mM Fe(CN) ₆ ³⁻ /Fe(CN) ₆ ⁴⁻ solution in 0.1 M KCl at a potential range of -0.25 to 0.80 V and a 0.025 V s ⁻¹ scan rate. Cyclic voltammograms shown are representative of those seen from three independent repeats.....	88
4.15	The linear relationship of the cathodic current; <i>i</i> _{pc} (a) and the anodic current; <i>i</i> _{ac} (b) versus scan rate (<i>v</i> ^{1/2}) of 0.05 mM Fe(CN) ₆ ³⁻ /Fe(CN) ₆ ⁴⁻ solution in 0.1 M KCl. The data is shown as the mean ± SD, and is derived from three independent repeats.....	89
4.16	The plot of the measurement number and the anodic current of 5 µg L ⁻¹ Cd ²⁺ and Pb ²⁺ solution in 0.1 M HCl.....	90
4.17	Effect of Bi ³⁺ concentration on the ASV peak currents of 10 µg L ⁻¹ Cd ²⁺ and Pb ²⁺ in 0.1 M HCl at a deposition potential of -1.2 V for 140 s. The data are shown as the mean ± SD, and are derived from three independent repeats.....	91
4.18	Dependence of the average current on the HCl concentration for in-house designed thin-layer flow cell. Conditions: 10 µg L ⁻¹ Cd ²⁺ and 50 µg L ⁻¹ Pb ²⁺ solution in HCl, 500 mg L ⁻¹ Bi ³⁺ , deposition time of 140 s and -1.2 V deposition potential. The data is shown as the mean ± SD, and is derived from three independent repeats.....	92
4.19	Effect of the deposition potential on the SWASV peak currents of 10 µg L ⁻¹ Cd ²⁺ and Pb ²⁺ in 0.1 M HCl using the in-house flow cell at a deposition potential of -1.2 V for 140 s; The data is shown as the mean ± SD, and is derived from three independent repeats.....	93
4.20	The effect of the deposition potential on the ASV peak currents of 100 µg L ⁻¹ Cd ²⁺ and 50 µg L ⁻¹ Pb ²⁺ in 0.5 M HCl at a deposition potential of -1.2 V for 140 s; The data is shown as the mean ± SD, and is derived from three independent repeats.....	94

FIGURE	PAGE	
4.21	The effect of the square wave frequency on the ASV peak currents of $10 \mu\text{g L}^{-1} \text{Cd}^{2+}$ and Pb^{2+} in 0.1 M HCl using the in-house thin layer flow cell at a deposition potential of -1.2 V for 140 s; The data is shown as the mean \pm SD, and is derived from three independent repeats.....	95
4.22	The effect of the square wave frequency on the ASV peak currents of $100 \mu\text{g L}^{-1} \text{Cd}^{2+}$ and $50 \mu\text{g L}^{-1} \text{Pb}^{2+}$ in 0.5 M HCl using the commercial flow cell at a deposition potential of -1.2 V for 140 s; The data is shown as the mean \pm SD, and is derived from three independent repeats.....	96
4.23	The effect of the step potential on the ASV peak currents of $10 \mu\text{g L}^{-1} \text{Cd}^{2+}$ and Pb^{2+} in 0.1 M HCl using the in-house thin layer flow cell at a deposition potential of -1.2 V for 140 s; The data is shown as the mean \pm SD, and is derived from three independent repeats.....	97
4.24	The effect of the step potential on the ASV peak currents of $100 \mu\text{g L}^{-1} \text{Cd}^{2+}$ and $50 \mu\text{g L}^{-1} \text{Pb}^{2+}$ in 0.5 M HCl using the commercial flow cell at a deposition potential of -1.2 V for 140 s; the in-set is the voltammograms of $100 \mu\text{g L}^{-1} \text{Cd}^{2+}$ and $50 \mu\text{g L}^{-1} \text{Pb}^{2+}$ in 0.5 M HCl at various step potential; The data is shown as the mean \pm SD, and is derived from three independent repeats.....	98
4.25	The effect of the potential amplitude on the ASV peak currents of $10 \mu\text{g L}^{-1} \text{Cd}^{2+}$ and Pb^{2+} in 0.1 M HCl using the in-house thin layer flow cell at a deposition potential of -1.2 V for 140 s; The data is shown as the mean \pm SD, and is derived from three independent repeats.....	99
4.26	The effect of the potential amplitude on the ASV peak currents of $100 \mu\text{g L}^{-1} \text{Cd}^{2+}$ and $50 \mu\text{g L}^{-1} \text{Pb}^{2+}$ in 0.5 M HCl using the commercial flow cell at a deposition potential of -1.2 V for 140 s, The data is shown as the mean \pm SD, and is derived from three independent repeats.....	100
4.27	The square wave anodic stripping voltammogram for an increasing concentration level of 0.5 - $100 \mu\text{g L}^{-1} \text{Cd}^{2+}$ and 0.25 - $250 \mu\text{g L}^{-1} \text{Pb}^{2+}$ together with background response recorded in <i>in-situ</i> Bi-film modified CPE using the in-house designed flow cell. Voltammograms shown are representative of those seen from three independent repeats.....	102

FIGURE	PAGE
4.28	Calibration curve of Cd^{2+} by SWASV using <i>in-situ</i> Bi-film modified CPE in the in-house designed flow cell..... 103
4.29	Calibration curve of Pb^{2+} by SWASV using <i>in-situ</i> Bi-film modified CPE in the in-house designed flow cell..... 103
4.30	Calibration curve of Cd^{2+} by SWASV using <i>in-situ</i> Bi-film modified CPE in a commercial flow cell..... 104
4.31	Calibration curve of Pb^{2+} by SWASV using <i>in-situ</i> Bi-film modified CPE in a commercial flow cell..... 104
4.32	FT-IR spectrum of the as-used (a) graphite and (b) graphene samples..... 107
4.33	Cyclic voltammograms of 0.5 mM $\text{K}_3\text{Fe}(\text{CN})_6/\text{K}_4\text{Fe}(\text{CN})_6$ in 0.1 M HCl on bare CPE and GCPE (The weight ratio of the carbon powder toward graphene powder is 1 : 5). The scan rate is 50 mV s^{-1} . The voltammograms shown are representative of those seen from three independent repeats... 109
4.34	The relationship between current responses towards the amount of graphene in the GCPE registered with SWASV of 10 $\mu\text{g L}^{-1}$ Pb^{2+} and Cd^{2+} in 0.1 M HCl. The data is shown as the mean \pm SD, and is derived from four independent repeats. 110
4.35	The effect of the Bi^{3+} concentration in the plating solution on the current obtained for a 10 $\mu\text{g L}^{-1}$ of Cd^{2+} and Pb^{2+} . The data is shown as the mean \pm SD, and is derived from four independent repeats. 112
4.36	The relationship between the peak current and the HCl concentration of a 10 $\mu\text{g L}^{-1}$ Cd^{2+} and Pb^{2+} ; The data is shown as the mean \pm SD, and is derived from four independent repeats 113
4.37	The influence of the deposition potential on the current obtained for a 10 $\mu\text{g L}^{-1}$ of Cd^{2+} and Pb^{2+} . The data is shown as the mean \pm SD, and is derived from four independent repeats 114
4.38	The influence of the SW frequency on the current obtained for a 10 $\mu\text{g L}^{-1}$ of Cd^{2+} and Pb^{2+} . The data is shown as the mean \pm SD, and is derived from four independent repeats ... 115
4.39	The influence of the step potential on the current obtained for a 10 $\mu\text{g L}^{-1}$ of Cd^{2+} and Pb^{2+} . The data is shown as the mean \pm SD, and is derived from four independent repeats 116

FIGURE		PAGE
4.40	Square wave anodic stripping voltammograms obtained from (A) CPE, (B) GCPE, (C) Bi-CPE, and (D) Bi-GCPE with a $10 \mu\text{g L}^{-1}$ of Cd^{2+} and Pb^{2+} . Voltammograms shown are representative of those seen from four independent repeats..	117
4.41	Voltammograms of Cd^{2+} and Pb^{2+} in a linear concentration range of $0.1 - 50 \mu\text{g L}^{-1}$ measured under the optimum conditions and (In-set) the plot of the relationship between the anodic current peak height and the heavy metal ion concentration. Voltammograms shown are representative of those seen from four independent repeats.....	119
4.42	An overlay square wave anodic stripping voltammogram for consecutive additions of $5 \mu\text{g L}^{-1}$ Cd^{2+} and Pb^{2+} in 0.05 M HCl , deposition potential at $-1.2 \text{ V vs. Ag/AgCl}$ for 140 s. ..	122

LIST OF ABBREVIATIONS

PVC	Polyvinyl chloride
Hg	Mercury
CPE	Carbon paste electrode
SIA	Sequential injection analysis
Bi-GCPE	Bismuth-film graphene carbon paste electrode
Bi-CPE	Bismuth-film carbon paste electrode
DPASV	Differential pulse anodic stripping voltammetry
SWASV	Square wave anodic stripping voltammetry
CV	Cyclic voltammetry
C	Counter electrode
W	Working electrode
R	Reference electrode
μm	Micrometer
i	Current
n	Number of the electron transfer
F	Faraday constant (96,495 C/eq)
A	Electrode area
J	Flux
$\partial C(x, t)/\partial x$	Concentration gradient (at distance x and time; t)
D	Diffusion coefficient
E	Potential (V)
t	Time (s)
R	Gas constant ($8.3144 \text{ J mol}^{-1} \text{ K}^{-1}$)
T	Absolute temperature (K)

E°	Standard potential
E_p	Peak potential
E_{pa}	Anodic peak potential
E_{pc}	Cathodic peak potential
i_{pa}	Anodic peak current
i_{pc}	Cathodic peak current
i_p	Peak current
C	Concentration (mol L ⁻¹)
v	Potential scan rate (V s ⁻¹)
i_{net}	Net current
f	Square-wave frequency
CSV	Cathodic stripping voltammetry
AdSV	Adsorptive stripping voltammetry
δ	Diffusion layer thickness
U	Convection rate
α	Electrode geometry
a_{Cl}	Activities of chloride ion
I_{lim}	Limiting current
K	equilibrium constant
i_l	Limiting current
t_d	Deposition time
V_{Hg}	Volume of the mercury electrode or working electrode
M	Molar
μM	Micromolar
μg	Microgram
mg	Milligram

mL	Milliliter
mM	Millimolar
mV	Millivolt
mm	Millimeter
nm	Nanometer
CNT	Carbon nanotube
i.d	Inner diameter
°C	Degree Celsius
s	Second
ICP-OES	Inductively coupled plasma - optical emission spectrometer
P	product
R	Reduced form
O	Oxidized form
RSD	Relative standard deviation
SPE	Screen printed electrode
DMF	Dimethyl formamide
IPA	Isopropanol
V	volt

CHAPTER I

INTRODUCTION

1.1 Introduction

The contamination of heavy metals such as cadmium (Cd^{2+}) and lead (Pb^{2+}) in environmental water is a critical worldwide problem because it can be incorporated into various food chains. The widespread utilization of heavy metals in various sources includes the industrial and agricultural processes. There are hundreds of the products in our daily lives that contain heavy metals such as Cd^{2+} and Pb^{2+} . The most significant use of Cd^{2+} is in batteries such as a rechargeable power source because it provides a high output, long life, low maintenance and high tolerance to physical and electrical stress. In addition, the applications of Cd^{2+} coating in food container, marine products, food containers and aerospace engines to protect against corrosion are widely used. For other uses of Cd^{2+} , it is contained in pigments, stabilizer for PVCs, alloys and electronic components, petroleum products and also in cigarette smoke. The general population is contaminated with Pb^{2+} , mainly due to the combustion processes from the transportation and industry. Both Cd^{2+} and Pb^{2+} have been extensively studied because of their effects on the human health. They are released to the environment and tend to accumulate especially in the lakes, marine sediments, natural water sources and soil. They also can be transported from one environmental compartment to another. In the human body, heavy metals are accumulated in organisms as a result of intake through respiration and food. Effect of the health caused by Cd^{2+} and Pb^{2+} are kidney and bone damage, carcinogenic agents and also Itai itai disease. Exposure to Pb^{2+} can produce neurotoxic effects, reduce blood levels and cause lung cancer. The toxicity of heavy metals depends on various factors such as exposure levels and exposure time. The critical level of heavy metal has been debated. Furthermore, the detection methods have been developed to protect the human health.

The electrochemical anodic stripping techniques have been widely used to determine trace of heavy metals. As is well known, they possessed many advantages compared to other techniques. They provide high sensitivity depending on the selection technique and type of working electrode, rapid analysis, easy integration with other techniques and portable analyzer.

One alternative to obtain the high sensitivity is the integration of the electrochemical technique with sequential injection analysis (SIA). This system is currently raised methodologies in terms of low reagent consumption, robustness, simplicity of sample and reagent manipulation, manifold versatility, and system automation. A powerful automated technique for accurate handling in a micro-scale volume of the solution through the analytical part with desired sequence of reagent or analyte can be carried out with SIA system. The operation of SIA is based on the syringe pump and several modes of operation such as unidirectional flow, bi-directional flow, multi-bi-directional flow and stopped-flow are potentially feasible. It was demonstrated to be a feasible tool for anodic stripping voltammetry. Therefore, SIA coupled with ASV was selected for the determination of heavy metal ions in this research.

Carbon materials are generally used as the working electrode in the electrochemical technique because they provide a wide anodic potential region and a low background current. In this research, the carbon electrode in a micro-flow sensor was used for on-line electrochemical analysis of heavy metal ions. Furthermore, a carbon paste electrode (CPE) made from carbon nanopowder was used as the working electrode because of its ease of fabrication, modification and surface renewal as well as its ability to enhance the electron transfer and conductivity. The bismuth (Bi)-film was chosen for the modification of CPE because it has several advantages over the mercury (Hg)-film electrode. The main reason for using the Bi-film electrode is it is insensitive to dissolve oxygen in the solution. In addition, the sensitivity of the electrode can be increased by incorporating nanomaterial into CPE before modifying with Bi-film. Graphene, a high electrical conductivity carbon material, has been beneficially utilized in many areas especially in electro-catalytic nanoparticles and electrochemical sensors. Thus, bismuth-film graphene modified carbon paste

electrode (Bi-GCPE) was also used as a working electrode for trace heavy metal ions determination in this research.

There are three parts in this research. In part I, a micro-flow sensor consisted of a preconcentration membrane and a three-electrode system for electrochemical detection was used as a detector in conjunction with SIA system. The characterization of carbon working electrode such as life time, reproducibility and sensitivity for determination of model heavy metal ions (Cd^{2+} and Pb^{2+}) were performed. Analytical characteristics for the quantitative determination of Cd^{2+} and Pb^{2+} ions by the differential pulse anodic stripping voltammetry (DPASV) and square wave anodic stripping voltammetry (SWASV) were investigated. In part II, the low-cost thin-layer electrochemical flow-through cell was in-house designed, fabricated and characterized for use with CPE. The model heavy metal ions (Cd^{2+} and Pb^{2+}) were determined by SIA-ASV using Bi-CPE in the designed flow cell. The developed method was applied for three kinds of water sample which were tap water, pond water and drinking water using the calibration method. Finally, part III describes the use of Bi-GCPE in the in-house designed flow cell for the determination of the same model heavy metal ions by SIA-ASV. For the application, the amount of Cd^{2+} and Pb^{2+} in two kinds of complicated matrix samples including undulated surf clams and sea bass fish tissue as well as a non-complicated matrix sample (tap water) were studied.

1.2 Objectives of the research

This research consists of two targets for development and improvement.

1. To develop the method for the determination of heavy metals by automated flow analysis coupled with electrochemical detection.
2. To apply the proposed method for the determination of heavy metals in the environmental samples

CHAPTER II

THEORY AND LITERATURE SURVEY

This chapter is concerned with the theoretical electrochemistry and flow based analysis which is used in this work. The modification of the working electrode with Bi-film and Bi-film graphene carbon paste electrode were considered. Moreover, the importance of the heavy metals in the environment and food analysis were described. Finally, the associated literatures were considered to develop the proposed method.

2.1 Principles of Electrochemistry

Electrochemistry is claimed by many researcher to be that it have a powerful, simple and sensitive analytical tool for the determination of the heavy metals for both qualitative and quantitative analysis. Numerous electrochemical methods are categorized according to potentiometry, coulometry and voltammetry.

2.1.1 Electrochemical techniques [1-5]

The electrochemical techniques are described in this research involved the technique that was used in this research. In all electrochemical methods, the rates of oxidation and reduction reaction depend on mass transport of the electroactive species reaching the electrode surface from the bulk solution and the electrode kinetics.

In the solution, the movements of the chemical species also called mass transfer processes are classified into three processes comprised of migration, convection, and diffusion, respectively.

The migration is the movement of charged particle due to the attraction force of the electric field that generated by the electrode towards ion which have opposite charges and also the repulsion force of the ion which have the same charges as the electrode, as described in Figure 2.1.

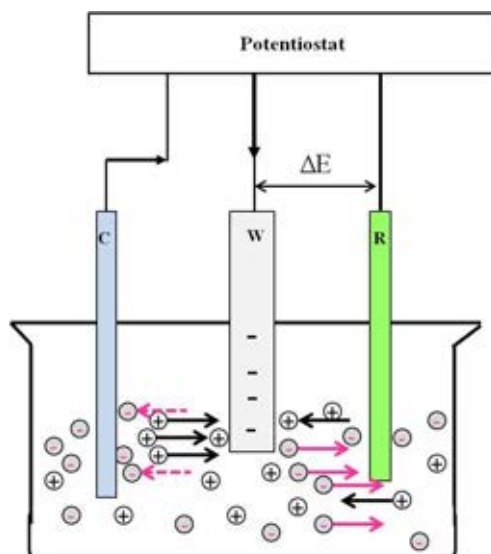


Figure 2.1 The schematic showing the migration movement of the ions in the solution

The convection is the motion of the species due to stirring the solution by some form of mechanical movement of the solution or the electrode such as stirred solution, rotating or vibrating the electrode. In this case, the molecules of the solvent and the analytes move with a more motion that becomes more laminar in the vicinity of the electrode surface (Figure 2.2). Moreover, it is more efficient than diffusion and migration to obtain higher current for a given concentration which mean greater analytical sensitivity.

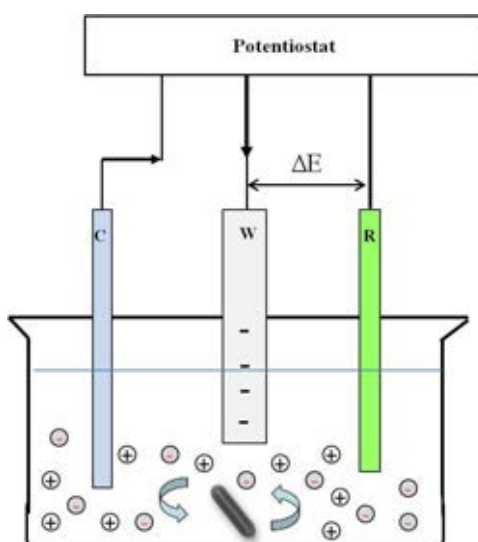


Figure 2.2 The schematic of the convection movement of the ions in the solution

Lastly, the diffusion process (Figure 2.3) is the spontaneous movement of the species due to the concentration gradient, from a high concentration to low concentration region. This region called the diffusion layer in which the process of a thin layer-form of the solution is occurs in the near-electrode surface. The layer thickness of the diffusion layer is 10 – 100 μm in the stirred solution and 500 μm in a quiescent solution. The electroactive species in the diffusion layer is shows only diffusion movement. Then, the diffusion speed of the analyte which reaches to the electrode is directly proportional to the concentration gradient and to the concentration of the electroactive species in the solution. Moreover, the intensity of the obtained faradic current is limited by the velocity of the electroactive species from bulk solution reaching to the diffusion layer.

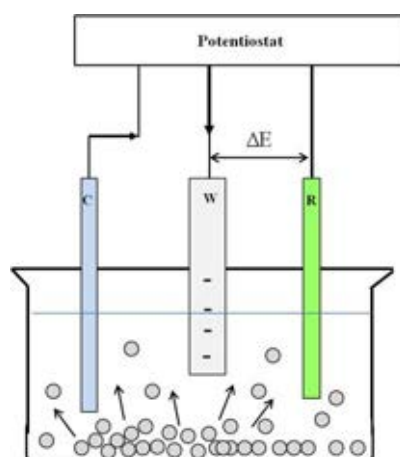


Figure 2.3 The schematic of the diffusion movement of the ion in the solution

From the three above phenomena, the case of migration and convection are undesirable modes. In the case of migration, a 100 fold excess of an electrochemically inert electrolyte was added to reduce the migration of the analyte. In convection, the transport of the analyte to the electrode is eliminated or controlled by the physical movement or external mechanical energy such as stirring the solution, rotating the electrode, and flowing the solution. Voltammetry is a versatile method for measurement of only the diffusion of the electroactive species from the bulk solution to the electrode surface. The current (i) in the electrochemical method is directly

proportional with the flux and the electrode surface area (A), as indicated in Equation 1.

$$i = -nFAJ \quad \text{-----} \rightarrow \quad \text{Equation 2.1}$$

Among the diffusion process, rate of diffusion is described by Fick's first law (Equation 2) that flux from the diffusion is directly proportional to the slope of the concentration gradient.

$$J = -D \partial C(x,t)/\partial x \quad \text{-----} \rightarrow \quad \text{Equation 2.2}$$

J is the flux, D is the diffusion coefficient (cm^2/s), and $\partial C(x, t)/\partial x$ is the concentration gradient (at distance x and time; t)

From the combination of Equation 1 and Equation 2, the faradaic current resulting from the redox reaction process is related to the flux at the interface of the electrode and is proportional to the gradient of electroactive concentration at any time. Then, Fick's second law describes that the rate of concentration changed with time of the concentration, as shown in Figure 2.4.

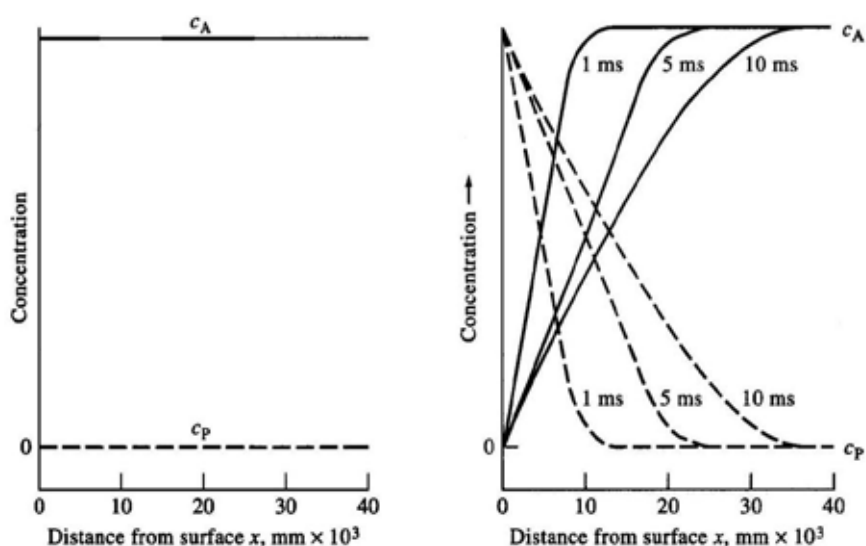


Figure 2.4 The concentration distance profile during the diffusion controlled reaction of $A + e^- \rightarrow P$

2.1.2 Voltammetry technique

The characteristic of voltammetry is an analytical technique based on the application of a potential (E) to an electrode dipped in a solution containing electro-active species and measuring the current (i) flowing through an electrode. In some cases, the applied potential is varied and the current over a period of time (t) is monitored. The advantage of voltammetric methods are excellent sensitivity for organic and inorganic compounds, rapid analysis time, simultaneous determination and being able to determine kinetic parameters. It is also the most important application for trace heavy metal quantitative analysis.

In voltammetry, the applied potential controls the concentration of the electroactive species on the electrode surface. The rate of electroactive species diffused to the electrode surface is described by the Nernst equations.

$$E = E^{\circ} - \frac{RT}{nF} \ln \frac{C_R}{C_O} \quad \text{-----} \blacktriangleright \text{Equation 2.3}$$

Where R is the molar gas constant ($8.3144 \text{ J mol}^{-1}\text{K}^{-1}$), T is the absolute temperature (K), n is the number of electrons transferred, F is the Faraday constant ($96,485 \text{ C/eq}$), and E° is the standard reduction potential for redox couple in the case of diffusion control.

2.1.2.1 Cyclic voltammetry

Cyclic voltammetry (CV) is the most widely used electrochemical technique for the study of the redox processes, for the investigation of the reaction intermediates, for obtaining stability of the reaction production, and for the qualitative data of the electrochemical reaction. Cyclic voltammetry is performed in the first step when the electrochemical technique is applied.

This technique is based on linear scanned potential with the time of the working electrode in both forward and reverse directions within the

potential range of the working electrode using a triangular potential wave form in a quiescent solution while monitoring current (Figure 2.5). The resulting faradaic current – potential curve is called cyclic voltammogram. The cyclic voltammograms provide the information on the overall rate of the processes occurring at the working surface.

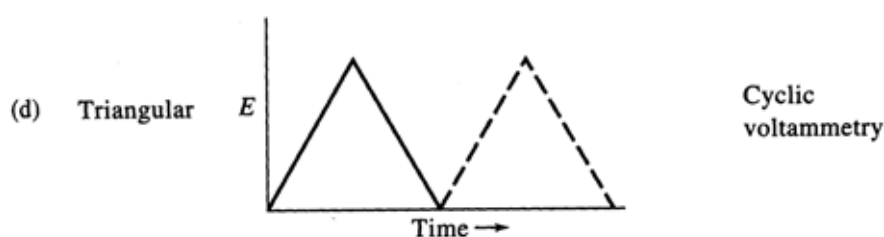


Figure 2.5 Excitation signal waveform of cyclic voltammetry

Consider the following reversible reaction: $O + e^- \rightleftharpoons R$. A typical voltammogram of a reversible redox couple during a single potential cycle is shown in Figure 2.6. It is assumed that only the oxidized form O to R form is present initially. In Figure 2.6, the forward scanning potential starts from a positive potential to a negative potential direction to cause a reduction. In Figure 2.6, the reduction process occurs from (a) the initial potential to (d) the switching potential. The cathodic current (i_{pc}) begins to increase when the potential applied approached to the characteristic E^0 for the redox process until a peak is reached. The extreme potential (d) called the switching potential is the point where the voltage is sufficient enough to have caused an oxidation or reduction of an analyte. The corresponding peak potential occurring at (c) is called the cathodic peak potential (E_{pc}). After that, the reverse scanning potential (positive direction) occurs from (d) to (g), in which the oxidation process takes place. During the reverse scan, R molecules are reoxidized to O obtaining in an anodic peak. This results in anodic current (i_{pa}) and oxidation to occur. The peak potential at (f) is called the anodic peak potential (E_{pa}), and is reached when all of the substrates at the surface of the electrode have been oxidized.

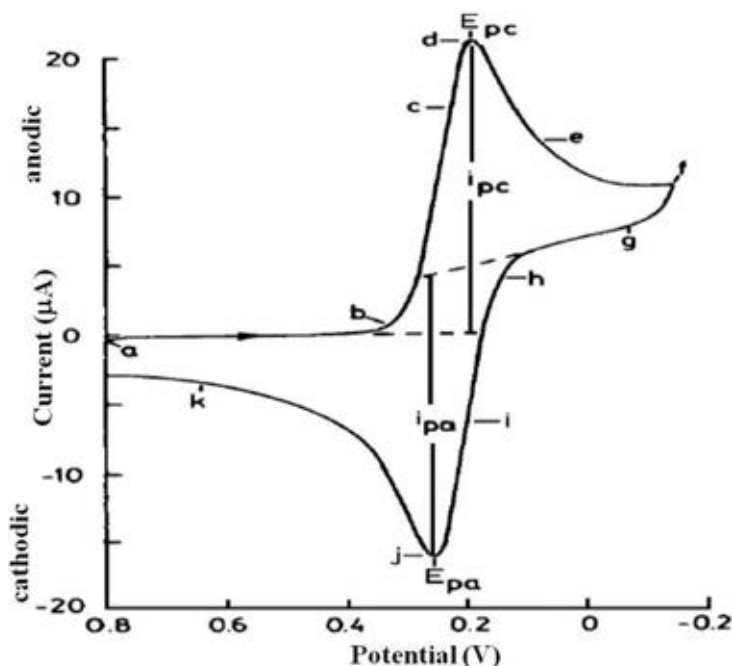


Figure 2.6 Cyclic voltammogram for a reversible reaction

The important parameters in cyclic voltammetry are peak potential (E_{pa} and E_{pc}) and peak current (i_{pa} and i_{pc}) of the anodic and cathodic peak, respectively. In the reversible systems, a fast electron transfer process occurs. The current in the reversible reaction at the electrode surface is described by Randles-Sevcik equation.

$$i_p = (2.69 \times 10^5) n^{3/2} A C D^{1/2} \nu^{1/2} \quad \text{-----} \rightarrow \quad \text{Equation 2.4}$$

Where n is the number of the electrons, A the electrode area (cm^2), C the concentration (mol cm^3), D the diffusion coefficient ($\text{cm}^2 \text{s}^{-1}$), and ν the potential scan rate (V s^{-1}). From the equation, the current is directly proportional to the concentration and increases with the square root of the scan rate. From the reason, it is indicated that the electrode reaction is controlled by the diffusion process. The ratio of the reverse and forward current is unity for simple reversible reaction ($i_{pc}/i_{pa} = 1$). In addition, the formal potential (E^0) of the redox reaction is centered between the E_{pa} and E_{pc} position:

$$E^0 = (E_{pa} + E_{pc})/2 \quad \text{-----} \rightarrow \quad \text{Equation 2.5}$$

The peak separation is given by following equation.

$$\Delta E_p \text{ (V)} = E_{pa} - E_{pc} = 2.303 RT/nF = 0.059/n \quad \text{---} \rightarrow \text{Equation 2.6}$$

Thus, the peak separation, ΔE_p (V), should be $0.0592/n$ or about 60 mV for one electron transfer.

For the irreversible system, a slow electron transfer rate occurs. The wide peak separation (than 70mV) is obtained. In the quasi-reversible system, the current is controlled by both the charge transfer and diffusion transport. The voltammograms of a quasi-reversible system are more drawn out and exhibit a larger separation in the peak potential compared to a reversible system. Then, the potential scan-rate is use as the diagnostic tool- the rate of reagent transport is proportional to square root of the scan rate – to distinguish between the reversible (diffusion-controlled) and irreversible (charge-transfer controlled) kinetics of the electrode surface.

2.1.2.2 Square wave voltammetry

In order to increase speed and sensitivity, many forms of pulse voltammetric techniques have been tried over the years. One of pulse techniques, shown in Figure 2.7, is widely used. The various types of pulse voltammetry are based on sampled current/ potential-step experiment. The excitation waveform and the current sampling regime differ in various types of pulse methods. After the stepped potential, the charging current decays rapidly to a negligible value, while the faradaic current decays more slowly. Thus, an effective discrimination against the charging current is achieved by sampling the current late in the pulse life.

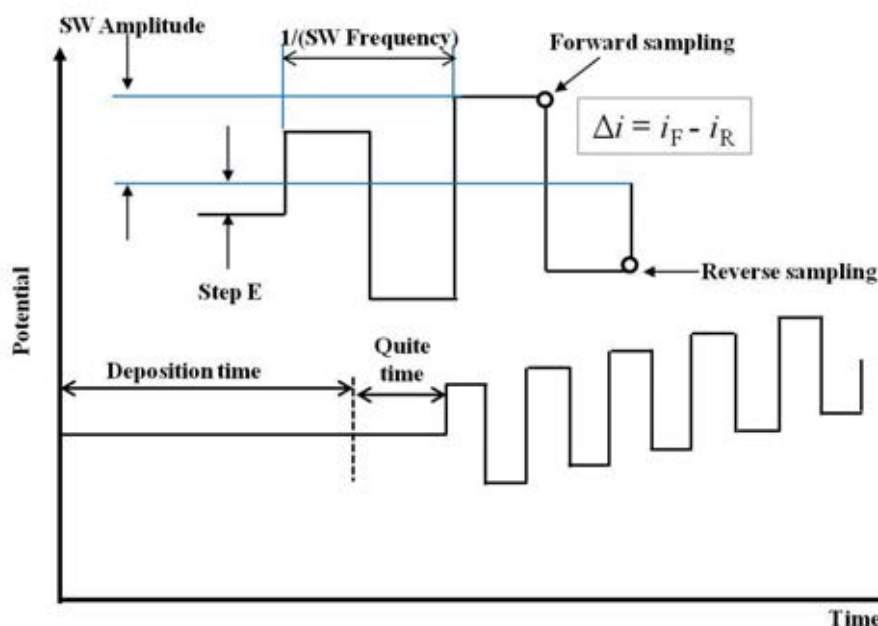


Figure 2.7 Square-wave excitation waveform

Square wave voltammetry is the excitation signal which consisted of a symmetrical square-wave waveform of a large-amplitude differential technique. It involves the superposition of a small step height potential (ΔE) superimposed on a staircase waveform applied to the working electrode. The current is sampled twice during each square wave cycle, once at the end of the forward and once at the end of reverse pulse. Since the square-wave modulation amplitude is very large, the reverse pulses cause the reverse reaction of the product of the forward pulse. The difference between the forward and reverse currents obtained the net current (i_{net}), is plotted versus the potential. The peak height is directly proportional to the concentration of the electroactive species. Excellent sensitivity accrues from the fact that the net current is larger than either the forward or reverse components. From the effective discrimination against the charging background current, the detection limits as low as $10^{-8} \text{ mol L}^{-1}$ can be obtained.

Square-wave voltammetry has several advantages. The major advantage is its speed. This speed, coupled with computer control and signal averaging, allows for experiments to be performed repetitively and increases the signal to- noise ratio. The effective scan rate is given by $f\Delta E_s$. The term f is the

square-wave frequency (Hz) and ΔE_s is the step height. The frequencies of 1-100 cycles per second permit the use of extremely fast potential scan rate. Example, if $\Delta E_s = 10$ mV and $f = 50$ Hz, then the effective scan rate is 0.5 V s^{-1} . From the result, the analysis time is dramatically reduced and a voltammogram can be recorded within a few seconds. Then, the inherent speed of square-wave voltammetric method can greatly increase sample throughputs both in batch and flow analytical systems.

Applications of square-wave voltammetry include the study of electrode kinetics with regards to preceding, following, or catalytic homogeneous chemical reactions, determination of some species at trace levels, and its use with electrochemical detection in flow based analysis such as HPLC, flow injection analysis (FIA), and sequential injection analysis (SIA).

2.1.2.3 Anodic stripping voltammetry

The stripping technique is an extremely sensitive electroanalytical technique for lowest limits of detection in trace metal analysis. The three most commonly used stripping forms are anodic stripping voltammetry (ASV), cathodic stripping voltammetry (CSV), and adsorptive stripping voltammetry (AdSV). The stripping analysis consists of a two-step technique. First, the deposition step involves the electrolytic deposition of a small portion of the metal ion in the solution accumulated on the working electrode for the preconcentrated the metals. The deposition step is carried out by controlled-potential electrolysis for a definite time under reproducible hydrodynamic (convection transport) conditions in the solution. Anodic stripping voltammetry is most widely used form of the stripping analysis. In this case, the preconcentration is done by cathodic deposition at a controlled time and potential. The deposition potential is more negative than E^0 to completely and easily reduce the metal ions in 100-1000 times the concentration of the ion in the solution. The shift from E^0 of the deposition potential is two or three times $(0.059/n)$ V as predicted by the Nernst equation (n is the number of the electron in the reaction). The metal ions reach the working electrode by diffusion and convection, where they are reduced and concentrated as amalgams or alloys. In the following equation, the mercury working electrode is represented.



For any working electrode and convection transport used in stripping analysis, the same general deposition theory applies. The concentration of the metal in the amalgam, C_{Hg} , is given by Faraday's law:

$$C_{Hg} = \frac{i_l t_d}{nFV_{Hg}} \quad \text{-----} \rightarrow \quad \text{Equation 2.7}$$

where i_l is the limiting current for the deposition of the metal, t_d is the time of deposition period, F is the Faraday constant, and V_{Hg} is the volume of the mercury electrode or working electrode. The deposition current is related to the flux of the metal ion at the surface.

For inert material electrodes, the concentration in moles of metal ion deposited on the electrode is possible to calculate by following equation:

$$C_M = i_l t_d / nF \quad \text{-----} \rightarrow \quad \text{Equation 2.8}$$

Under the forced convection condition, both diffusion and convection provide to the deposition current. This phenomenon produces the solution of the corresponding hydrodynamic equation. When applied the potential, the concentration of ion close to the electrode surface becomes zero. According to Nernst diffusion layer model as shown in Figure 2.8, the concentration of metal ion considered from the distance between the bulk solutions up to the certain distance from the electrode, δ (the diffusion layer thickness), is uniform due to the convection force. At the diffusion layer region, ions are move toward the electrode surface by the diffusion process. The rate of ion moving is proportional to the concentration difference. Accordingly, the deposition current is proportional to the slope of the concentration profile at the electrode surface, as described by:

$$i_l = \frac{nFADC_b}{\delta} \quad \text{-----} \rightarrow \quad \text{Equation 2.9}$$

From the equation, the parameters that reduce the value of δ will increase the deposition current. Moreover, the δ is related to the convection rate by:

$$\delta = \frac{K}{U^\alpha} \quad \text{-----} \rightarrow \text{Equation 2.10}$$

where U is the convection rate, K and α are constants dependent on the flow regime and electrode geometry. From the equation, the diffusion layer thickness decreases with the convection rate increase.

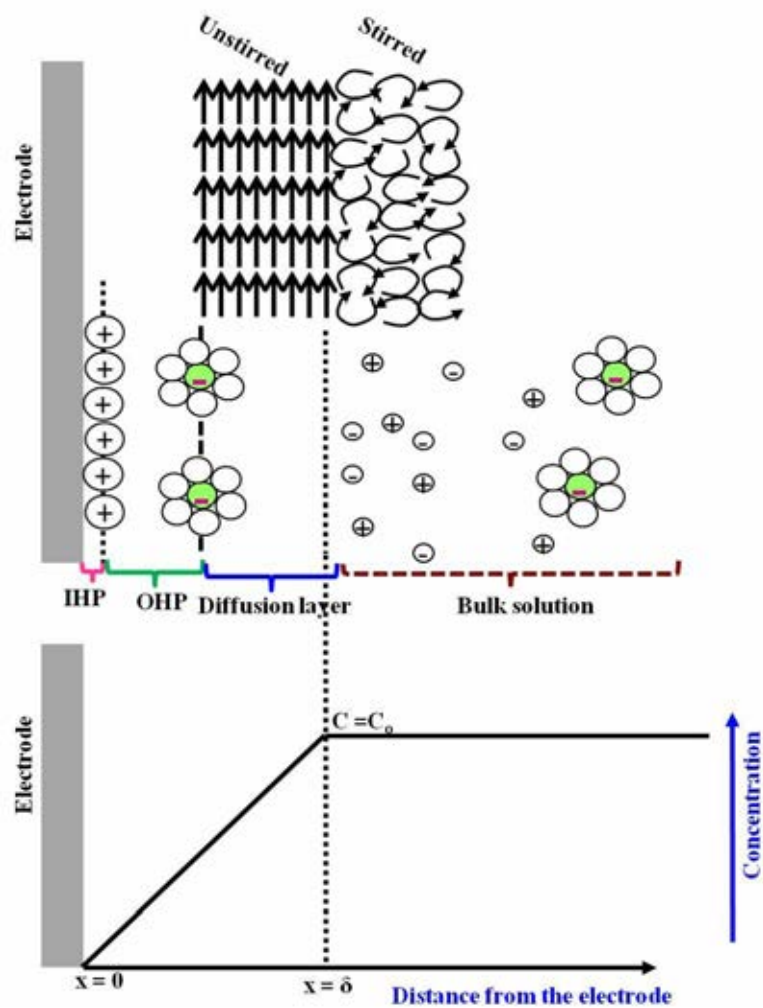


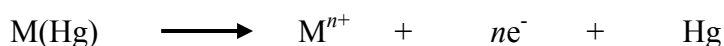
Figure 2.8 Proposed model of the double-layer region

The deposition time, t_d , must be controlled carefully because the longer deposition time is the larger amounts of the analyte at the electrode. Generally, the deposition time of 12 and 2 min are sufficient for the determination of 10^{-9} and 10^{-7} mol L⁻¹ metal ion solution with differential pulse mode, respectively. Normally, the amount of metal plate is proportional to the deposition time. Then, the plot of the resulting peak current (i_d) against the deposition time is a straight line. In a long deposition time, the deviations from the theoretical predictions may result from the interference of the intermetallic formation or saturation on the working electrode and bulk depletion of the metal ion in conjunction with a small sample volume.

Before starting with the stripping step, a rest period or equilibrate time is employed between the depositions and stripping step to stop the forced convection, rapidly establish a uniform concentration distribution, and insure that the solution is in a quiescent solution before the stripping step.

The subsequent step is the stripping step or measurement step which related with the dissolution or stripping of deposit. There are various types of potential waveforms used for the stripping step. The most widely used of the potential waveforms are the differential pulse and the square wave due to the discrimination against the charging current.

After the deposition step, the forced convection is stopped. The stripping step is started with the scanned potential in the anodic direction. During the anodic scan, the amalgamated metals are reoxidized when the potential reaches the standard potential of the metal, stripped out of the electrode surface, as shown in the following equation.



The peak potential positions are arranged in order of each metal standard potential. The peaks potential serve to identify the metal in the sample. The stripping peak current is proportional to the concentration of the metal. The peak current depends on various parameters of the deposition and stripping steps, as well as on the

characteristics of the metal ion and electrode geometry. Then, the method is applicable for simultaneous detection of several metal ions. Figure 2.9 summarizes both deposition or preconcentration and stripping step in anodic voltammetry.

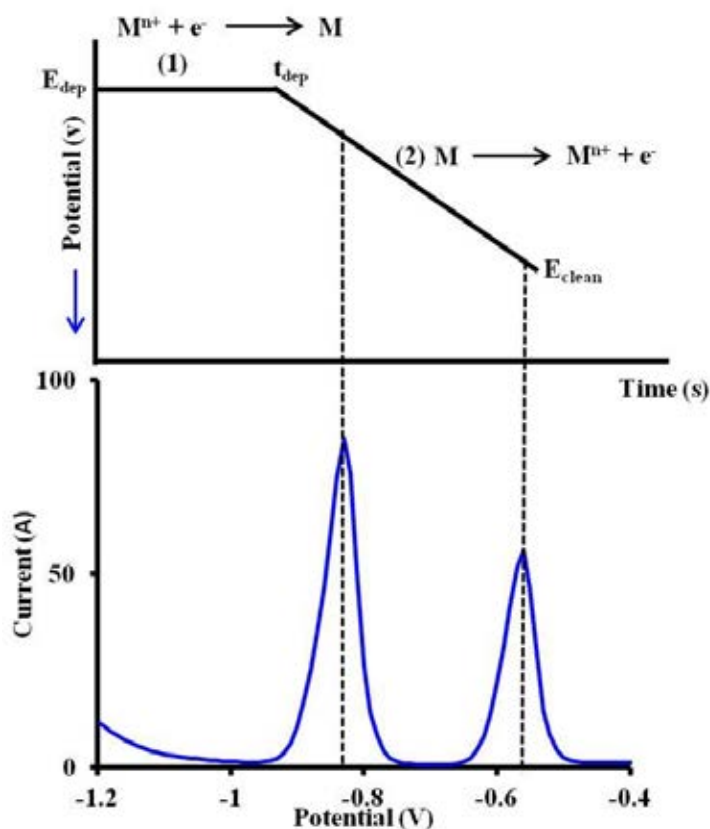


Figure 2.9 Voltammetric curves: 1) Deposition or preconcentration step; 2) Stripping step

The major interferences in anodic stripping voltammetry procedure are overlapping the stripping peak caused by a similarity in the oxidation potential.

2.1.3 Electrodes [6]

2.1.3.1 Working electrode

The working electrode is the electrode at which the interesting reaction occurs. In the voltammetric method, the small surface area of the working

electrode is used for enhanced polarization and to minimize depletion of the analyte. The performance of the stripping voltammetry is strongly influenced by the working electrode material. The ideal working electrode should provide a high signal- to- noise ratio of the interested analyte, low background current over the potential region required, a reproducible surface, a wide potential window, high electrical conductivity, cost, toxicity, and availability. The widely used metal electrodes are mercury, platinum, gold, and various forms of carbon. Solid metals are typically fashioned into disks surrounded by a chemically inert shroud made from Teflon, glass, or epoxy. In the stripping measurement, mercury electrode and inert solid electrode are most popularly used. Disadvantages of the mercury electrode are limited in the anodic range and toxicity. The widespread use of material are carbon based material because broad potential window, low background current, rich surface area, low cost, chemical inert, and easy to modify for various sensing or various applications. The most popular form of carbon materials are glassy carbon, carbon paste, carbon fiber, carbon screen-printed, and carbon film.

Carbon electrodes allow scans to more negative potentials than platinum or gold electrode in the anodic potential window. In contrast, the rate of the electron transfer on the carbon surface electrode is slower than on the metal electrodes. Therefore, the cleaning of the electrode surface, the pretreatment of the electrode, and type of carbon electrode such as glassy carbon, carbon fiber, screen-printed carbon, carbon film, and carbon paste electrode have been proposed to increase the electron transfer rate.

2.1.3.1.1 Glassy Carbon Electrode (GCE)

GCE has been a popular electrode because of its excellent electrical properties. The structure of GCE involves thin, tangled ribbons of cross-linked graphite-like sheets. The pretreatment of the electrode surface is usually operated to create active surface, to obtain reproducible signal, and to enhance the analytical performance. The pretreatment is performed by polishing with alumina particles to obtain a shiny electrode surface. Then, the electrode is rinsed with water before use.

2.1.3.1.2 Carbon paste electrode (CPE)

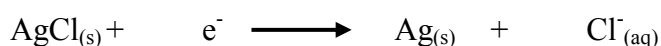
CPE was introduced by Ralph Noeman Adams from the University of Kansas. CPE is a mixture of carbon or graphite powder mix and a binder (pasting liquid). It offers an easily renewable and modified surface, low cost, and low background current. Powdered carbon or graphite is the main component of the electrode. The appropriate properties of carbon material comprised low micrometric scale of the particle size, uniform distribution of the particles, high chemical purity, and low adsorption capabilities which are an important factor in making the electrochemical sensor. The most often selected carbon powder is spectroscopic carbon or graphite. So far, other carbonaceous material such as charcoal, acetylene black, glassy carbon powder with globular particles, porous carbon, carbon microspheres, and carbon nanotubes have also used for the preparation of carbon paste mixtures. In order to lower adsorption capabilities of carbon or graphite, the adsorbed oxygen is removed by heating in the vacuum with subsequent stabilization by impregnating with a ceresin wax. In case of binder, the suitable properties are immiscibility with organic solvents, minimal solubility in aqueous solutions, high viscosity and low volatility, and chemical inertness and electroinactivity. The most popular binding agents used for carbon pastes are mineral (paraffin) oils; namely Nujol or similar trade-mark products and a solvent for spectroscopy. Other frequently used binders are aliphatic or aromatic hydrocarbons, halogenated derivatives, silicone oils, greases, organic ester of the organophosphate, and ionic liquids. A distinct advantage of CPE is their very low ohmic resistance. Thus, modified CPE with appropriate material such as metallic film, organic compound and nanomaterial is used to improve the problem.

2.1.3.2 Reference electrode

The potential applied to the working electrode is measured within the context of a known potential, which is in turn obtained from the reference electrode. This electrode acts as a reference point along the potential axis by which the oxidizing or reducing power of the working electrode is judged. Ideally, the reference electrode must provide a stable potential and temperature independent. In

addition, the ideal reference electrode should be easy to make and to use. The most widely used is the silver/ silver chloride reference electrode because it is simple, inexpensive, very stable and non-toxic.

The redox reaction of the electrode is based on the redox coupled between AgCl and Ag:



A silver/silver chloride electrode is shown in Figure 2.10. This electrode consists of a silver wire, the end of which is coated with thin film of AgCl. The wire is immersed in a solution containing chloride ions such as desired concentration of KCl or NaCl. The porous (vycor frit) plug serves as the salt bridge or the junction between the reference electrode solution and the sample solution. **Figure 2.10** Schematic of silver/silver chloride reference electrode

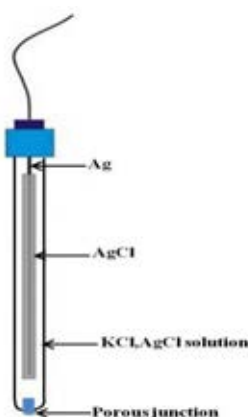


Figure 2.10 Schematic of silver/silver chloride reference electrode

The Nernst equation for the determination of the potential of the silver/silver chloride electrode is shown in the following equation:

$$E = E^{\circ} + \frac{RT}{nF} \ln \frac{1}{a_{\text{Cl}}} \quad \text{-----} \rightarrow \text{Equation 2.11}$$

where a_{Cl} is the activities of chloride ion. From the equations, it is shown that variations in the chloride ion concentration in the electrode change the redox

potential. Since there is generally a large chloride concentration gradient across the reference electrode frit, there is slow diffusion of chloride ions from the reference electrode solution into the sample solution; that is, the reference potential will gradually change when used.

The Ag/AgCl electrode prepared using a saturated solution of KCl has a potential of +0.197 V at 25 °C. The common Ag/AgCl electrode used a solution of 3.5 M KCl and has a potential of +0.205 V at 25 °C.

There are some precautions that can be taken to minimize the reference potential drift. The reference electrode should also be removed from the electrochemical cell and stored in this solution between experiments (this is particularly important when using non-aqueous solvent systems). Occasionally, air bubbles will form in the solution next to the Vycor frit; these should be removed by gently flicking the end of the electrode.

2.1.3.3 Counter or Auxiliary electrode

The auxiliary (counter) electrode usually is employed to minimize errors from cell resistance in controlling the potential of the working electrode. The auxiliary electrode is made of a chemically inert conducting material with large surface area. Platinum wire or graphite rods are the most common auxiliary electrode in the stripping analysis.

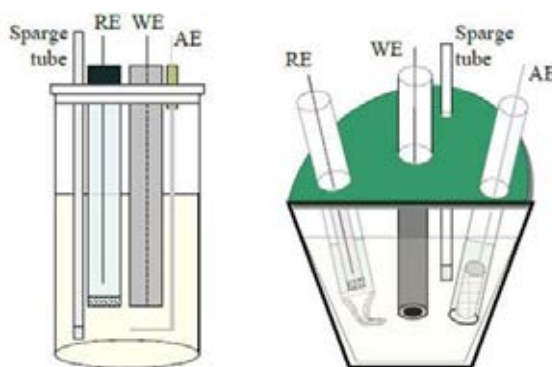


Figure 2.11 The schematic of the electrochemical cell [7]

2.1.4 Electrochemical cell

The redox process is carried out in the cell that consists of the working electrode, reference electrode, and counter electrode which are immersed in an electrolyte solution containing the analyte compound. This part is called the electrochemical cell, as shown in Figure 2.11.

The importance of the electrode position is considered for minimization of the solution resistance. The three electrodes are kept as close together as feasible. The critical of the electrode position is closed between the reference and working electrode. The solution resistance between these electrodes lead to an iR drop that manifests itself as an error in the measured potential difference between them. A second important consideration involves the shape and size of the auxiliary electrode relative to the working electrode. The auxiliary should be at least as large in area as the working electrode and positioned symmetrically with respect to the working electrode so that the current density and potential experienced along its entire length is constant.

2.1.5 Electrochemical flow-through cell

Most of the known electroanalytical techniques such as potentiometry, voltammetry including pulsed amperometry, coulometry, and conductometry are available for detection in flow analytical methods. A flow-through electrochemical detector consists of a detection cell and the electronic circuitry required for the cell operation and for monitoring, recording, and processing the detector signal. The detector signal depends on the electroanalytical technique selected for detection. The flow-through cell monitors the concentration of the analyte in the flow system.

There are several types of flow-through cells. Each type is characterized by parameters such as the length, diameter, and shape of its detection channel, which determines the character of the liquid flow under the given experimental conditions (laminar or turbulent, as described by the Reynolds number)

and the predominant mode of the mass transport within the cell (diffusion or convection).

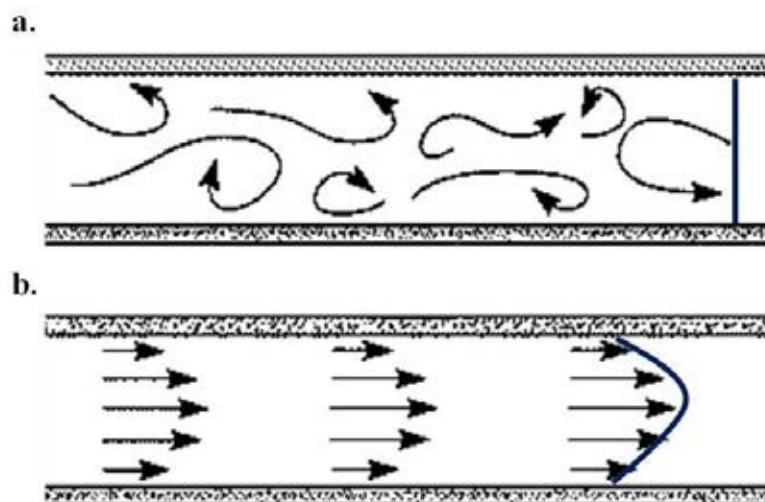


Figure 2.12 Flow patterns, (a) is turbulent flow and (b) is laminar flow [8]

2.1.5.1 Flow patterns [1]

2.1.5.1.1 Turbulent flow

Turbulent flow occurs at high flow velocities and has fluctuating motion, irregular motion or moves randomly in Zigzag manner randomly. The flow is not the greatest at the centre. In the electrochemical method, the turbulent flow is generated by stirring the solution, letting the solution flow or by using the rotating disk electrode.

2.1.5.1.2 Laminar flow

Laminar flow occurs at low flow velocities and has a smooth and regular motion. The flow occurs in parallel layers and the flow is greatest at the centre and decreases towards the periphery as shown in Figure 2.12b.

The design of the flow-through cell influences the overall performance characteristics of the detector. The flow cell design is the first part of the optimization in the flow system for a given sensitive analytical signal. The

optimized flow cells provide a high sample throughput, reduced sample volumes and reagent consumption, high precision and accuracy, high sensitivity, are easy to operate, and low costs, etc.

2.1.5.2 Factors influencing sensitivity and detection limits [9]

The detection limit is determined by the signal-to-noise (S/N) ratio. The S/N ratio of electroanalytical techniques can be improved electronically and hydrodynamically.

In voltammetry, the waveform of the excitation signal and the sampling pattern of the measured current determine the sensitivity and detection limit. The different potential pulse techniques typically improve the detection limit of the electroanalytical detection by reducing the noise.

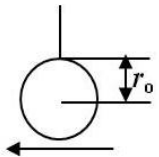
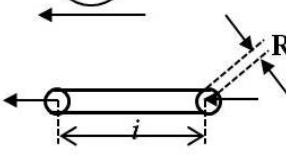
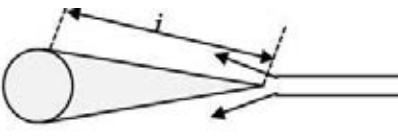
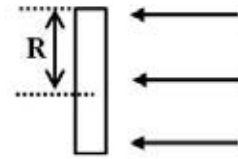
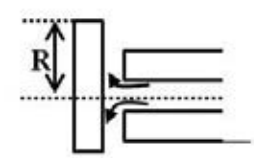
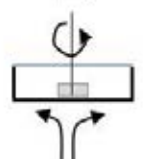
In flow-through voltammetric methods, the S/N ratio is increased and the detection limit is improved through the increased mass transfer rates. It is called the *hydrodynamic approach* for improving the S/N ratio. For example, the faradic current signal increases with an increased flow rate, while the minimal change of the background current is observed, which is the result of the flow-independent.

Moreover, the electrode geometries in the flow-through electrochemical cells also differ. In common arrangements, the flow is either parallel to the electrode surface (e.g., thin-layer cells), perpendicular to the electrode surface (e.g., wall-jet cells) or the liquid passes through a tubular, annular, or porous electrode cell.

2.1.5.3 Flow cell design [9,10]

Electrochemical detection based on voltammetry is most important and widely applied in flow analysis. The design of the most common voltammetric electrodes used in flow-through electrochemical detectors and the relationship between signals vs. concentrations are shown in Table 2.1

Table 2.1 Some important flow-through voltammetric electrode designs and limiting current characteristics.

Electrode shape	Electrode design	Limiting current
	Spherical	$I_{\text{lim}}=0.85nFAD^{2/3}\nu^{-1/6}\nu^{1/2}l^{1/2}$
	Tubular	$I_{\text{lim}}=2.01nFD^{2/3}\nu^{1/2}l^{1/2}R^{2/3}C$
	Conical	$I_{\text{lim}}=0.77nFAD^{2/33}\nu^{-1/6}\nu^{1/2}l^{1/2}C$
	Disk with perpendicular	$I_{\text{lim}}=knFD^{2/3}\nu^{-1/6}\nu^{1/2}l^{1/2}RC$
	Wall-jet	$I_{\text{lim}}=1.38nFD^{2/3}\nu^{-5/2}F_m^{3/4}d^{1/2}R^{3/4}C$
	Rotating disk	$I_{\text{lim}}=0.62nFACD^{2/3}\nu^{-1/6}\omega^{1/2}$

2.1.5.4 Special features of electrochemical detectors for flow analysis

An electrochemical detection under hydrodynamically controlled conditions shows the following characteristic features:

1. The shear forces of the flowing liquid continuously clean the surface of the working electrode. Consequently, the electrochemical and/or mechanical regeneration of the working electrode surface in the flow system with intensive washing, solution or solvent switching, potential cycling, etc. are generally not important when compared to the batch analysis.
2. The continuously streaming carrier solution removes reaction products from the voltammetric working electrodes.
3. The convective transport of an analyte and/or a reactant reduces response time and improves the detection limit compared to batch measurements.
4. The reference electrode can be located downstream with respect to the working electrode; it gives great flexibility in the reference electrode selection and design as well as the salt bridge composition.
5. Microelectrodes and microelectrode arrays bring about additional advantages for flow measurements, such as the ability to operate in low conductivity solutions, suppressed signal dependence on the liquid flow rate due to a high mass transport rate generated by efficient spherical or semispherical and nonlinear diffusion, fast establishment of a steady-state signal which permits the use of rapid-scan voltammetric techniques in the combination with flow analytical techniques, and continuous replenishment of the diffusion layer with analytes during the passage of the solution over a microelectrode array as the increasing of detectability.

2.2 Flow based Technique

Flow analysis techniques are based on the introduction, processing, and detection of liquid samples in the flow media. The processing may involve the sample transport under diffusion and/or convection dispersion conditions.

2.2.1 Flow injection analysis (FIA)

FIA is a simple and versatile analytical tool for automating chemical analysis. FIA is based on the physical and chemical manipulation of a dispersed liquid analyte and/ or reagent zone formed from an injection into a non-segmented flowing carrier stream and detection downstream. This continuous flow analysis was defined by Ruzicka and Hansen (in 1975) and Stewart, Beecher, and Hare (in 1976).

A typical FIA manifold illustrated in Figure 2.13 is comprised of a pump which is used to propel the carrier stream to the narrow tubing, injection valve which is used to introduce the small sample volume into the carrier stream in a reproducible manner, micro reactor or reaction coil which is the sample zone dispersed and reacted with the components in the carrier solution detector to form a detectable species, and tubing manifold. This species is sensed by the detector as a transient peak (in Figure 2.14). The height and the area of peak are proportional to the analyte concentration.

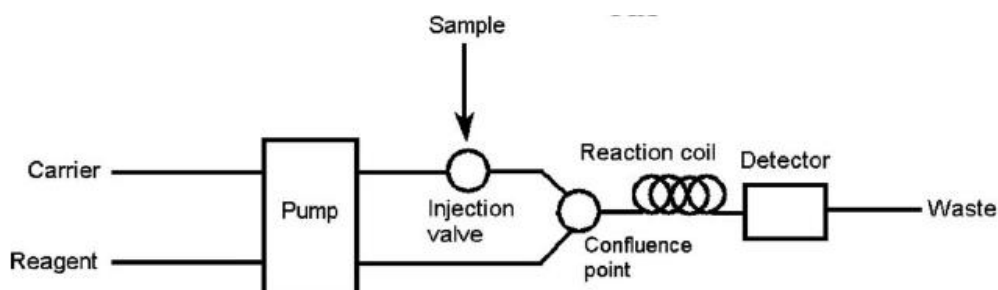


Figure 2.13 Simple FIA manifold [11]

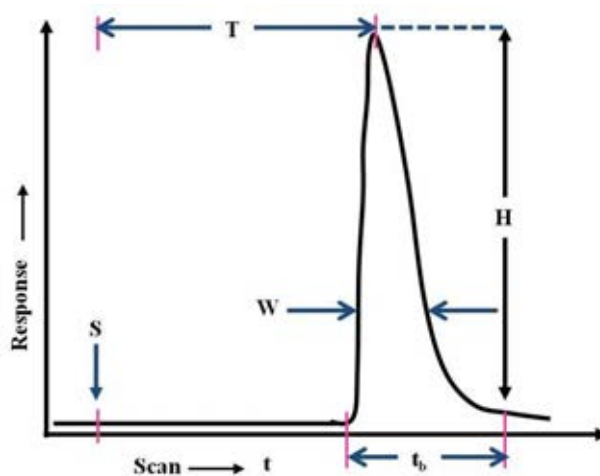


Figure 2.14 The analog output is in the form of a peak, with the recording starting at S (time of injection). H is the peak height, W is the peak width at a selected level, and A is the peak area. T is the residence time corresponding to the peak height measurement, and t_b is the peak width at the baseline.

2.2.2 Sequential injection analysis (SIA) [11-16]

SIA is an important analytical tool in the area of continuous flow methods. This method was first reported by Ruzicka and Marshall from the University of Washington in 1990. A diagram of a basic SIA instrument includes a bi-directional pump used to draw up small samples and reagents in forward and reverse direction, a multi position selection valve used to select fluid (substituting the injection valve in FIA), reaction or holding coil, pump tubes, and a detector flow cell. Again, the process causes a mixing of the sample and reagent segments leading to the chemistry that forms a detectable species before reaching the detector in the same way as the FIA. The system is controlled by computer.

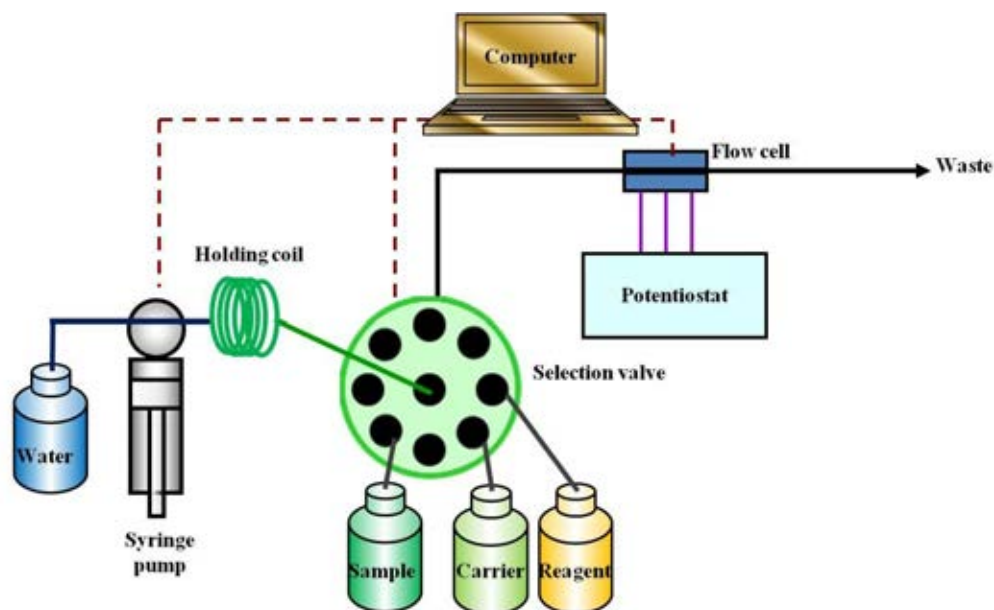


Figure 2.15 Basic scheme of a SIA manifold [17]

From Figure 2.15, the ports of the multi position selection valve are connected to a sample reservoir. Aliquots of sample and reagent are sequentially aspirated into a holding coil connected to the common port of the multi position selection valve by operating the pump in the reverse mode. After the steps of sequential aspiration, the sample and reagents zones are stacked in the holding coil (Figure 2.16). Between these aspiration steps the propulsion device is stopped to avoid an increase in the pressure.

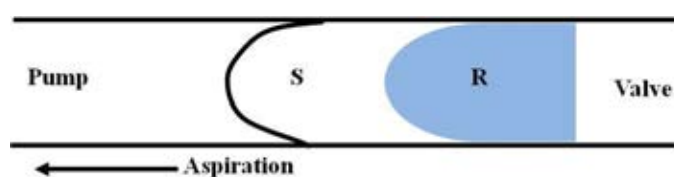


Figure 2.16 Sample and reagent zones stacked in the holding coil

The flow reversal by the selection valve is switched to the detector port. This procedure leads to the mixing of the sample and reagent zones in the holding coil forming the detectable product (Figure 2.17)

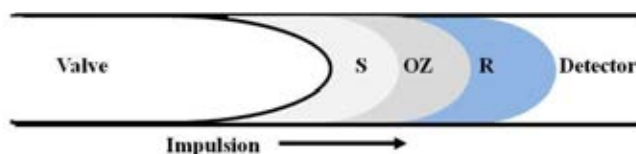


Figure 2.17 Merging of sequenced zones of sample and reagent in the holding coil on flow reversal to give a zone of detectable product.

The order in which the sample and reagent zones are stacked depends on the chemistry being used; additional zones of reagent or diluents may also be aspirated. On-line dilutions and modification of the chemical reaction may be achieved by aspiration of additional diluents and reagent zones. The volumes of sample and reagent used are controlled by the aspiration time.

2.2.2.1 Comparison of FIA and SIA

From the simple FIA manifold shown below (Figure 2.18), a sample is injected into the injection loop of a two-position injection valve and the carrier flows constantly through the detector usually by peristaltic pump. The length of the injection loop determines the volume of the sample injected. When the sample in the injection loop is loaded, the valve is switched and the sample is introduced into a flowing carrier stream. The carrier carries the sample through the reactor (usually a reaction coil) to the detector. The sample reacts with the reagent to form a detectable species passes through the flow cell detector to produce a peak.

For SIA (Figure 2.18), the injection valve is replaced with a multi-position selection valve. The peristaltic pump is replaced with a syringe pump and the holding coil is added. To achieve the same measurement as in FIA, the syringe is filled with the carrier solution containing the reagent. Then the selection valve is advanced to a port that is connected to the sample line for drawing up the small sample volume into the holding coil by pump. The selection valve is then advanced to a port that is connected to the detector, and the carrier transports the sample through the reactor to the flow cell of the detector. Again, a detectable species is formed and is registered as a peak by the detector.

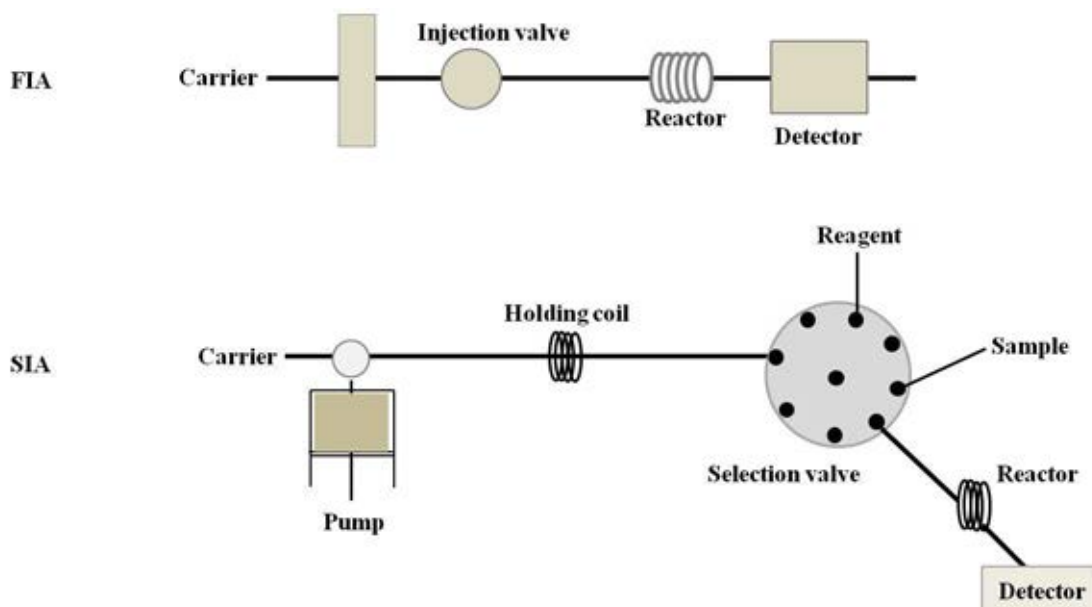


Figure 2.18 Comparison of simple FIA and SIA manifold

In FIA, an undispersed plug of sample is introduced into the carrier stream whereas in the SIA, the sample dispersion begins to take place whilst aspirating the sample into the holding coil and the flow reversal when the sample moves to the detector flow cell. In Figure 2.19, the graphic dispersion in FIA and SIA are compared. This phenomenon may cause an SIA peak to look slightly different to an FIA peak. As long as there has been good mixing between sample and reagent, this will not affect the quantification because samples and standards are treated alike. In fact, it has been shown that the flow reversal contributes significantly to the mixing of zones.

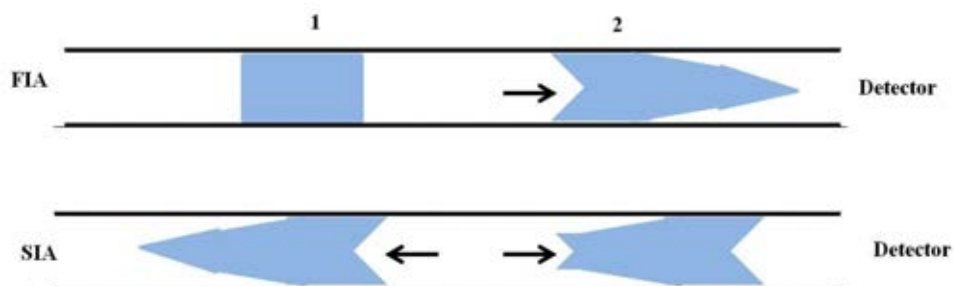


Figure 2.19 The dispersion profile in FIA and SIA: (1) is the sample injection point in FIA and during the flow reversal in SIA, (2) is the carrier starting to move towards the detector in FIA and SIA.

2.2.2.2 The advantages of SIA

SIA has several advantages over FIA shown in the list

- The sample and reagent consumptions are dramatically reduced (mL level in FIA and μL level in SIA).
- An accurate handling of sample and reagent zones are controlled with a computer, so automation becomes essential.
- From above, the flow manifolds are simple and robust and the same manifold can be use for different chemistries or a wide range of assays by changing the flow program.

Moreover, the popularity of the electrochemical detectors in SIA systems has dramatically grown in the recent years due to the advantageous characteristics consisting of

- Ideally suited to electrochemical stripping methods that use a preconcentration step of the analyte on the working electrode surface before the measurement.
- The coupling of the highly sensitive amperometric detection with the selectivity of biosensors or immunosensors can be automatically assayed and perform rapidly in food, biological and pharmaceutical samples.
- The simple automated procedures could be implements on the selectivity of the analyte.
- SIA provides the possibility for simultaneous determination in electrochemical detectors with high precision and good accuracy.

2.3 Heavy metal [18, 19]

Heavy metal is defined as the metal with the elemental densities above 5 g cm^{-3} . They can be found in the Earth's crust and also small amounts of some heavy metals are found in the human body. In human, low concentration of some heavy metals are involved in the metabolisms which are called essential elements. The poisoning of heavy metals is caused by exceeding the acceptable level in the body.

The presence of heavy metals in the environment and food chain are the main effected which increase the bioaccumulation of heavy metals in the biological organism which caused of health effects.

In this research, Cadmium (Cd^{2+}) and Lead (Pb^{2+}) are considered for the monitoring in the environment and food product. Both Cd^{2+} and Pb^{2+} are non-essential metal elements for both plants and animals.

The International Agency for Research on Cancer has classified Cd^{2+} as a human carcinogen. Cd^{2+} enters the human body mainly from food, for example mushrooms, mussels, cocoa powder, and marine products (seaweed and shellfish). Other high Cd^{2+} levels occur from tobacco smoke, industries (refinery industry, batteries industry or batteries product), pigments or color, PVC and electronic products. Firstly, it is transported to the liver through the blood and it is bonds with proteins to from complexes molecules before being transported to the kidneys. In particular, it replaces the role of zinc (Zn) in the enzymes and accumulates in bone, kidney, and liver leading to failure after a long exposure.

Pb^{2+} can occur naturally in the environment as a rare Earth element. However, the toxicity of Pb^{2+} because of exposure of high concentration that found in the environment as a result from human activities. The main sources of contamination are smelting work, alloy, batteries, a painting or coloring agents in ceramics and candles, cables, solders, lead crystal glassware, ammunition, and the glass of computer and television screens. After the applications of Pb^{2+} from human activities are generated large amount drop to the ground immediately and pollute soils or surface waters. The smaller particles travel long distances through air and remain in the atmosphere. Some of it will fall back to the earth when it rains. It can enter through the human body by uptake of food (fruit, vegetables, meats, grains, seafood, wine, and soft drink), water, and air. Several unwanted health effects from Pb^{2+} poisoning are disrupted biosynthesis of haemoglobin may caused anemia, raised blood pressure, damaged kidney, brain, nervous system, and learning abilities of children. These effects are the main reason has caused lead pollution has become a worldwide issue.

2.4 Literature survey

2.4.1 Part I: Electrochemical characterization of carbon electrode in μ -flow sensor by on-line automated flow system

Heavy metal ions such as lead and cadmium in the environment can be toxic to human beings, even at very low concentrations [20]. Therefore, it is very important to analyze the contamination of heavy metal ions in environmental pollution monitoring. These demands have led to increasing efforts aimed at developing new analytical tools for the simultaneous measurement of metal ions. There are several accepted analytical methods currently available for the measurement of metals in environmental samples. These include atomic absorption spectrometry (AAS) [21], electrothermal atomic absorption spectrometry (ETAAS) [22], flame atomic absorption spectrometry (FAAS) [23], and on-line micro-column preconcentration coupled with inductively coupled plasma optical emission spectrometry (ICP-OES) [24]. However, these methods require comparatively expensive equipment and they are not readily amenable to portable instrumentation. Electrochemical stripping analyses have the potential to overcome some of the problem experienced by spectroscopic techniques. These techniques provide the sensitivity needed for measuring trace metals. Stripping voltammetry has been adapted to the flow system with the advantages conferred by on-line analysis that provide lower sample consumption and on-line mixing of the sample and the reagents [25,26]. The development of automated flow systems with highly sensitive detection was tried because of the time-saving benefit especially in sample preconcentration step, being convenient for field analysis, as well as reducing sample, solvents and reagents consumption. Most of the interest in these devices arises from the potential of incorporating sample- processing steps, such as sample pretreatment, dilution, calibration, separation, derivatization, and detection onto a cm-dimensioned “chip” [27].

2.4.2 Part II: Highly sensitive determination of Cd²⁺ and Pb²⁺ using a low-cost electrochemical flow-through cell based on a carbon paste electrode

The importances of flow analysis in analytical chemistry have been briefed by G.D. Christian [28]. A growing trend in analytical chemistry of flow methods continuously arise because it provided rapid, precise, and automated analysis, low reagent and sample consumption that meant the goal of green chemistry was developed. Electrochemical on-line monitoring of metal is preferable because it provides a convenient and effective means to determine heavy metal in aqueous effluent streams [29]. A flow-through electrochemical cell has been attempted for development in situ heavy metal determination [30-33]. The new designed electrochemical cell with dual-band electrode as a generator-collector was used to eliminate error and improve the precision of the classical titration method [34].

Several forms of carbon electrode materials are widely used in electroanalysis. In particular, carbon paste (CP) which is the most popularly used disposable electrode. The great featured advantages of carbon paste are the anodic potential region widely used, ease of fabrication, regenerated, modification and renewable, very low background current and inexpensive [35-38]. From all of the advantages, the first published article about the carbon paste electrode (CPE) was presented by Ralph Norman Adams [39-42]. Recently, there have been several reports about the characteristics and application of the carbon paste electrode. For example, the investigation of carbon-to-binder ratio in CPE that changes the ohmic resistance [42], an improved electron transfer and enhanced conductivity of the CPE by the use of a conducting binder to replace a non-conducting binder[43] and the versatile room temperature ionic liquid (RTIL) [44], good features of CP micro-electrode applied to measure dopamine, ascorbic acid, lead and cadmium [39], and the electroactivity comparison between conventional CPE and commercially screen-printed CPE by the adsorption of oxidation product of indigo carmine on the electrode surface [38,45] were studied. The use of various modifiers are often being applied to carbon paste electrodes due to their providing the way to immobilize with cofactors, activators and additives. Therefore, the electrochemical reaction and analytical

performance of CP based sensors have improved, especially in pharmaceutical and biological analysis. The most popular electrochemical technique is amperometric biosensors for drug analysis such as, cobalt-5 nitrosalophen [46], ruthenium (III) piperidinedithiocarbamate complex [47], horseradish peroxidase [48], enzyme immobilisation [49], polyethylene glycol (PEG) [50], and also complicated molecules of DNA mixing with carbon nano tube (CNT) modified CP. An ionic liquid (ILs) modified CPE [51, 52] are developed for square wave voltammetric sensors. Differential pulse adsorption voltammetry for determination of procaine hydrochloride in a urine sample was investigated using pumice as a modifier on CPE [53]. In amperometric immunosensors, the immobilisation of antibodies on very versatile magnetic nanoparticles of CdFe_2O_3 surface was developed by Zhi-Min Lui and et.al. [54]. Moreover, the combination of pharmaceutical amperometric sensor and utilizable flow systems have been developed. Flow injection analysis (FIA) coupled with amperometric sensors when the modifier is used, D-lactase dehydrogenase and alanine aminotransferase enzyme [55], D-fructose dehydrogenase [56], biocomposite of 5% enzyme [57], nujol-graphite and diphenylether-graphite [58], yeast alcohol dehydrogenase (ADH) [59]. Sequential injection analysis (SIA) was also constructed in amperometric HIV drug [60]. The application of modified CPE for simultaneous determination of sugar and ascorbic acid by capillary zone electrophoresis with amperometric detection was reported [61]. In general, enantioselective analysis of chiral compounds based on electrochemical detection was very difficult. Therefore, the main advantages of modified CPE coupled with SIA over other techniques are easy, fast and selective method for a simultaneous enantiomeric assay [62-65]. Nowadays, real-time amperometric monitoring of oxygen in brain tissue was characterized by using CPE [66].

Furthermore, a modified CPE electrode for the determination of trace heavy metal was applied for copper ion [67], mercury ion [68], cadmium ion [69], and molybdenum ion [70]. Among the applications, the integration of flow systems with modified CPE can rarely be found in trace amounts of heavy metal ion analysis. The feasibility of the established system was demonstrated for copper ion [71], and lead ion [26,72].

One alternative of all modifiers that has shown promising performance for monitoring trace heavy metal ion with stripping voltammetry is the bismuth modifier electrode [73]. Bi-film electrode has electrochemical properties similar to mercury (Hg) [74]. The main attraction of Bi-film electrodes: they are environmentally friendly, have high hydrogen evolution, highly reproducible response, wide accessible potential window, insensitive electrode to dissolved oxygen, well-defined stripping signals for metal, etc. [75-85]. Therefore, Bi-film modified electrode was chosen for the experiment.

Square wave anodic stripping voltammetry (SWASV) is one of favorable techniques for measuring traces heavy metals [86-89] including Cd^{2+} and Pb^{2+} [90,91]. This technique presents a significant sensitivity depending on the ability of the preconcentrate target species during the accumulation step on the working electrode [92,93]. Moreover, stripping voltammetry also has traditionally been used because of their advantages, such as high sensitivity, reproducibility, purity of the surface, high hydrogen overpotential, easy to operate, able to analyse the element speciation, and the possibility of amalgam formation [77, 94, 95].

Recently, the increasing demand for monitoring heavy metal ion levels such as Cd^{2+} and Pb^{2+} in water is essential for human life. There are toxicological substance due to exposure to the excessive lead and cadmium resulting in health problems such as which causes serious brain and nervous system damage [96,97], while cadmium leads to human carcinogens [86-92]. There are various analytical methods applied for the determination of Cd^{2+} and Pb^{2+} , including electrothermal atomic absorption spectrometry, atomic absorption spectrometry, inductively coupled plasma mass spectrometry [98], etc., but the wide utilization of these methods is limited by the expensive equipment. Among of them, the square wave anodic stripping voltammetric method was very suitable for measuring of Cd^{2+} and Pb^{2+} because it provided high sensitivity, relative instrumental simplicity, minimum sample pretreatment prior to analysis and low equipment and maintenance costs [99].

2.4.3 Part III: Graphene-modified carbon paste electrode for Cd²⁺ and Pb²⁺ monitoring with flow based system

A new class of promising carbon-material, graphene, is of vast interest. Graphene is a two-dimensional (2D) material comprising a planar monolayer of sp² carbon atom bonding in a hexagonal configuration [100]. The unit cell of graphene contains two carbon atoms with the inter-atomic length of 0.142 nm. In addition, it exhibits good electrical conductivity and optical properties, lightweight, large specific surface area and chemical stability. From these properties, a widespread application of novel materials [101, 102] have been generated in various fields including biomedical sensor, nanoelectronic devices, transparent electrodes, photodetectors, hydrogen storage, solar cells, fuel cells, electrical batteries [103-107] and supercapacitors[108]. Furthermore, graphene provides the advantages over CNTs such as low cost and low metallic contaminating [109,110]. Therefore, graphene is exploited an alternative choice for electrical sensors, especially fabrication of electrochemical-sensing with graphene [111]. The first electrochemical sensor reported by Papakonstantinou and co-workers [112]. Moreover, the metal-graphene nanocomposite to improve the sensitivity such as mercury (Hg) [113], gold (Au) [114, 115], Co [116], Pd [117, 118], Pt [118, 119], Ag [120], Cu [120] has been widely reported. Another example, Shuo Wu et al. [121] used β -cyclodextrin-graphene modified glassy carbon electrodes for the ultra-high sensitive detection of methyl parathion with the detection limit of 0.05 $\mu\text{g L}^{-1}$. The dopamine sensing fabricated from graphene-modified glassy carbon electrode (graphene-GCE) is provided the selective of dopamine in the presence of ascorbic acid with the linear relationship from 5.0 to 200 $\mu\text{mol L}^{-1}$ [91]. The determination of ascorbic acid (AA) [70] with graphene-CPE was obtained the detection limit of 10 $\mu\text{g L}^{-1}$. For diagnosis, a graphene-based immunosensor was reported for quantification of phosphorylated p53 on serine 15 as well-known as the tumor suppressor protein [122] with the detection limit of 0.1 ng mL^{-1} . The sensitive detection of glucose and hydrogen peroxide (H₂O₂) as the important mediator in food, pharmaceuticals, clinical analysis, industry and environmental monitoring was successfully to developed on the graphene oxide/Prussian blue hybrid film modified GCE [123]. The amperometric response

showed the detection limit of 0.343 (glucose) and 0.122 (H_2O_2) $\mu\text{mol L}^{-1}$. The graphene has been shown to be beneficial in many kinds of drugs such as the successfully used room temperature ionic liquid (IL)–graphene composite modified GCE for determining azithromycin that is used as an antibiotic for humans with the detection limit of 0.19 $\mu\text{g mL}^{-1}$ [124], antitumor herbal drug aloe-emodin analysis with graphene-nafion modified GCE [118] obtained the detection limit of 2 nmol L^{-1} , and the carbamazepine as an anticonvulsant analysis with graphene-gold nanoparticles modified gold electrode obtained the detection limit of 0.30 $\mu\text{mol L}^{-1}$ [125].

For heavy metals, the analysis of transition of heavy metals, especially cadmium (Cd^{2+}) and lead (Pb^{2+}), in affected health sample of human is considerable interest because Cd^{2+} and Pb^{2+} can accumulate in kidney, liver, lung and central nervous [126-128]. There are also carcinogenic agents mentioned WHO International Agency for Research on cancer. An increased risk of cancer is attributed to the distribution of metal in the environment, exposure time and the concentration levels. Moreover, long-term exposure to low level concentration is also affects the health. Cd^{2+} and Pb^{2+} are released to soil and air and finally accumulate in the water source which is dangerous because it can affect to the quality of water, it can be ingested by marine products such as fish and crab, and can affect agricultural and food products. Thus, the careful monitoring with fast analysis and low concentration monitoring are crucial topics for on-site metal screening.

The electrochemical method has been developed for the determination of Cd^{2+} and Pb^{2+} because it requires inexpensive equipment. It also provides high specificity and sensitivity, and simplicity. In recent years, various types of modified electrodes were developed to overcome the problems of trace metal contamination. Carbon nanotubes (CNTs)-modified electrodes have been investigated in order to enhance the signal of target analyte metal because the capability to increase the electron-transfer kinetics and to reduce the over-potential, towards many electrochemical processes of analytical significance, and anti-fouling capability of the electrode surface are important properties of CNTs-modified electrodes that are widely used in electroanalysis [129, 130]. For example, the multi-wall (MW) CNTs used for

determination of Cd^{2+} and Pb^{2+} from environmental water was reported with the LOD of $0.60 \mu\text{g L}^{-1}$ (Cd^{2+}) and $0.83 \mu\text{g L}^{-1}$ (Pb^{2+}) [94]. Next, the determination of Cd^{2+} and Pb^{2+} in herbal medicines [131] was published with the LOD of $0.80 \mu\text{g L}^{-1}$ (Cd^{2+}) and $0.2 \mu\text{g L}^{-1}$ (Pb^{2+}). From the report, a lower limit of detection compared to another kind of the electrode was obtained. Recently, highly sensitive Bi-Nafion-graphene electrode for the determination Cd^{2+} and Pb^{2+} has been successfully reported by Li J. *et al.* [101]. The LOD was $0.02 \mu\text{g L}^{-1}$ for both metals. In the next two year, the graphene nanosheet was fabricated by Bin W. *et al.* for high sensitivity in detecting Cu^{2+} , Cd^{2+} and Pb^{2+} [132]. In this case, the detection limits of 0.11 (Cd^{2+}), 0.027 (Pb^{2+}), and 0.63 (Cu^{2+}) $\mu\text{g L}^{-1}$ were obtained. These results showed a much lower value when compared with the obtained results from CNTs modified electrode. Then, graphene has especially fascinated in the electroanalytical field because it provided high electrical conductivity and a large surface area.

Recently, the quality control both in the environment and food has become very crucial. Hence, an extensive development of flow-automation in chemical analysis is stimulated by the need for rapid analysis with high sample throughput, for simultaneous determination, for the continuous monitoring, and flexible systems. Sequential injection analysis (SIA) was chosen for this research. Besides automation that is controlled with a computer, it offers is fast, simple, minimizes the reagent consumption and flexible enough to employ the stopped flow method. Therefore, the SIA system incorporated with voltammetric technique is suitable for Cd^{2+} and Pb^{2+} analysis. To date, only one publication demonstrated the graphene/nafion hybrid electrode for amperometric glucose biosensor in flow-injection analysis [109] was published. Since, the graphene-related research in electrochemical method for heavy metal analysis still in it modified electrode material applied in batch system.

CHAPTER III

EXPERIMENTAL

For the research, all chemicals, instruments, preparation and modification of the electrode are explained in this chapter.

Part I: Electrochemical characterization of carbon electrode in micro-flow sensor by an on-line automated flow system

3.1 Instruments and Apparatus

The instruments and apparatus used in this part of the research are listed in the Table 3.1

Table 3.1 The instruments and apparatus

Instruments and Apparatus	Suppliers
PalmSens BV	Palm Instruments BV, The Netherlands
Micro-flow sensor, consisting of preconcentration membrane and three-electrode system with a carbon working electrode, a Ag/AgCl reference electrode and a carbon counter electrode	Sekisui Chemical, Kyoto, Japan
pH meter	Metrohm 744 pH meter, Switzerland
Analytical balance	AT 200, Mettler, Switzerland
Sequential analysis system (2.5 mL syringe pump)	MGC, Japan
PTFE tubing (ϕ 0.8 and 1.5 mm)	Upchurch
Flanged Nut/washer 1/16"	Upchurch
Milli-Q water system ($R \geq 18.3 \text{ M}\Omega$)	Nihon Millipore, Japan
Micro balance(AB204s)	Mettler-Toledo AG, Switzerland

3.2 Chemicals and Reagents

The chemicals and reagents used in this research were analytical grade and were used without further any purification. The list of chemicals and reagents are shown in Table 3. 2.

Table 3.2 The chemicals and reagents used in this research.

Chemicals	Suppliers
Bismuth (Bi^{3+}) atomic absorption analysis standard solution $1,000 \text{ mg L}^{-1}$	Kanto Chemical, Japan
Lead (Pb^{2+}) atomic absorption analysis standard solution $1,000 \text{ mg L}^{-1}$	Kanto Chemical, Japan
Cadmium (Cd^{2+}) atomic absorption analysis standard solution $1,000 \text{ mg L}^{-1}$	Kanto Chemical, Japan
Hydrochloric acid (HCl), electronic grade, 36%, 1.18 g mL^{-1}	Mitsubishi Chemicals, Japan
Nitric acid (HNO_3)	Wako Pure Chemical Industries, Japan
Potassium chloride	Kanto Chemical, Japan

3.3 Chemical preparations

3.3.1 Carrier solution: 1.0 M HCl

The carrier solution was prepared from 30% HCl ultrapure electronic reagent grade diluted with Milli-Q water to 1.0 M.

3.3.2 Stock standard solution: Cd^{2+} and Pb^{2+}

Stock standard solution of $10 \text{ mg L}^{-1} \text{ Cd}^{2+}$ was diluted from $1000 \text{ mg L}^{-1} \text{ Cd}^{2+}$ (AAS grade) in 1.0 M HCl

Stock standard solution of $10 \text{ mg L}^{-1} \text{ Pb}^{2+}$ was prepared by diluting AAS standard solution with 1.0 M HCl .

3.3.3 Cleaning solution: 0.5 M HNO_3

The cleaning solution, 0.5 M HNO_3 , was prepared by diluting 69 \%v/v HNO_3 with milli-Q water.

3.3.4 Reference electrode filling solution: 0.1 M KCl

The reference electrode filling solution, 0.1 M KCl , was prepared by dissolving 7.455 g potassium chloride and diluting to 100 mL with Milli-Q water.

3.4 Experimental procedures

The micro-flow sensor was connected to the SIA system and potentiostat as shown in Figure 3.1. The performance of the on-line method was tested with Cd^{2+} and Pb^{2+} standard solution before applying to the real samples. The on-line operating step and time necessary for the determination of Cd^{2+} and Pb^{2+} are listed in Table 3.3.

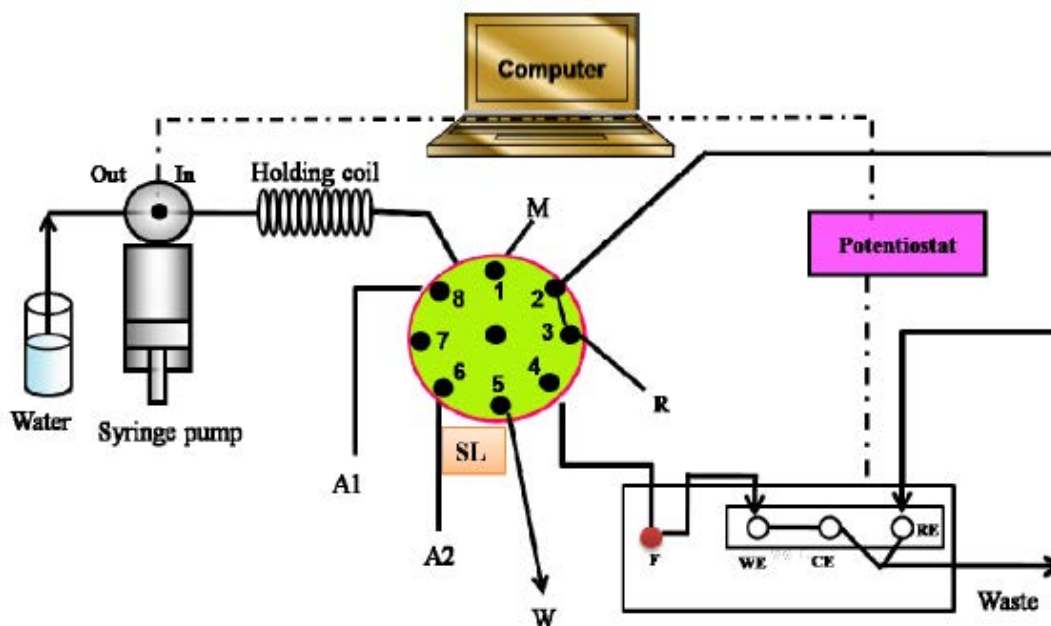


Figure 3.1 Schematic diagram of instrument set up for the determination of metal ions by on-line anodic stripping voltammetry on micro-flow sensor. A1 = 0.5 M HNO_3 ; A2 = 1.0 M HCl ; R = 0.1 M KCl ; M = Metal ion solution; F = pre-concentration membrane; and W = waste.

Table 3.3 Step sequence and time necessary for each step

Step	Methodology	Time per step
A. Filling the line	Fill the solution into the tubing in the SIA system	150s
B. Sensor washing: H_2O	Wash the sensor with water	150s
C. Sensor washing: Acid	Wash the sensor with 0.5 M HNO_3 and 1.0 M HCl	215s
D. Electrode filling	Fill 0.1 M KCl for reference electrode	66s
E. Electrode conditioning	Conditioning the carbon electrode with 1.0 M HCl for 300 s	300s
F. Background analysis	Anodic stripping voltammetric determination of the supporting electrode, 1.0 M HCl , 3-5 times or until the background current was stable	684 s

Table 3.3 (continued) Step sequence and time necessary for each step

Step	Methodology	Time per step
G. Sample analysis	Cd ²⁺ and Pb ²⁺ determination	684 s
H. Electrode cleaning	Wash sensor with 0.5 M HNO ₃ and 1.0 M HCl	215 s

Before use, the reference electrode was filled with 0.1 M KCl solution. The carbon working electrode of the micro-flow sensor was washed with water and conditioned with 1.0 M HCl supporting electrolyte at -1.40 V for 300 s to obtain stable background current. Anodic stripping voltammetric measurements were performed with a bare carbon electrode in a solution of 1.0 M HCl containing 50 µg L⁻¹ Cd²⁺ and Pb²⁺ and applying a deposition potential of -1.40 V (unless otherwise stated) for a defined period of time (usually 180 s) under flowing conditions.

Following the deposition step, the flowing was stopped for 10 s. The voltammogram was recorded by applying a positive going voltammetric potential scan. The scan was terminated at +0.80 V. Prior to each measurement, one “cleaning” scan from -1.40 to +0.80 V was performed without the deposition step, followed by a 10 s conditioning step (with flowing 0.5 M HNO₃ solution) at +0.80 V in order to clean and remove the target metals from the electrode surface. All experiments were performed at room temperature with untreated carbon electrode.

3.4.1 Long-term stability and reproducibility of the carbon electrode in the micro-flow sensor

Long-term stability and reproducibility of the carbon electrode was studied by monitoring the current signal of Cd²⁺ and Pb²⁺ for a period of time. The experimental conditions for the differential pulse anodic stripping voltammetry were investigated with 50 µg L⁻¹ Cd²⁺ and Pb²⁺ in 1.0 M HCl. A preconcentration potential of -1.20 V was applied to the working electrode under flow conditions for 180 s. After the accumulation, an equilibration period of 10 s at the stopped-flow system and an anodic stripping voltammetric scan (initial potential -1.20 V; final potential 0.60 V;

step potential 5 mV; conditioning time 5 s) were applied to the working electrode and the voltammogram was recorded. The experimental sequence for on-line stripping voltammetry was based on the procedure in Table 3.3. The electrode was found to be stable, even after 10 voltammetric scans. The inter- and intra-day reproducibility of the electrode was determined by 10 replicate measurements during three operating days.

3.4.2 Study of the differential pulse anodic stripping voltammetric (DPASV) parameters

The parameters of DPASV consisted of deposition potential, effect of pulse time, and pulse potential. The DPASV were studied with $50 \mu\text{g L}^{-1}$ Cd^{2+} and Pb^{2+} in 1.0 M HCl in on-line Auto-Pret system.

3.4.3 Study of the square wave anodic stripping voltammetric (SWASV) parameters

The parameters of SWASV consisted of deposition potential, effect of square wave frequency, potential step, and potential amplitude. The SWASV were studied with $50 \mu\text{g L}^{-1}$ Cd^{2+} and Pb^{2+} in 1.0 M HCl in on-line Auto-Pret system.

3.5 Analytical performance

From the optimum condition of each method (DPASV and SWASV), the electrochemical performance of on-line Auto-Pret system in micro-flow sensor were examined.

Part II: Highly sensitive determination of Cd²⁺ and Pb²⁺ using a low-cost electrochemical flow-through cell based on a bismuth-carbon paste electrode

3.6 Instruments and Apparatus

The instruments and apparatus used in this research are listed in Table 3.4.

Table 3.4 The instruments and apparatus.

Instruments and Apparatus	Suppliers
PalmSens BV	Palm Instruments BV, The Netherlands
Ag/AgCl reference electrode	BAS, Japan
Platinum wire for counter electrode	Goodfellow, USA
Carbon pasted electrode block	Home made
Carbon paste electrode for designed flow cell	Home made
Electrical wire	Bangkok cable
A thin layer cross flow cell	BAS, Japan
Designed flow cell	Home made
pH meter	Metrohm 744 pH meter, Switzerland
Analytical balance	AT 200, Mettler, Switzerland
Sequential analysis system (2.5 mL syringe pump)	MGC, Japan
PTFE tubing (ϕ 0.8 and 1.5 mm)	Upchurch
Flanged Nut/washer 1/16"	Upchurch
Milli-Q water system ($R \geq 18.3 \text{ M}\Omega$)	Millipore, Bedford, MA, USA
Rheodyne injection valve (20 μL , 0.5 mm i.d., injection loop)	Model 5100, Altech
Agate Mortar & Pestle Sets (01441-AB)	SPI Supplies / Structure Probe, USA
Filter papers (Cat No 1001 125, ϕ 125mm)	Whatman, General Electric
Micro balance (AB204s)	Mettler-Toledo AG, Switzerland
Thermometer	West-Germany
Sonicator	A006651, USA

Instruments and Apparatus	Suppliers
Memmert Oven (Model 100-800)	Memmert, Germany
Centrifuge (Universal 320R)	Hettich, Germany

3.7 Chemicals and Reagents

The chemicals and reagents used in this research were analytical grade and were used as received without any further purification. The list of chemicals and reagents are shown in Table 3. 5.

Table 3.5 The chemicals and reagents used in this research.

Chemicals	Suppliers
Bismuth (Bi^{3+}) standard solution 1,000 mg L ⁻¹	BDH, England
Lead (Pb^{2+}) standard solution 1,000 mg L ⁻¹	BDH, England
Cadmium (Cd^{2+}) standard solution 1,000 mg L ⁻¹	BDH, England
Hydrochloric acid (HCl)	Merck, Germany
Nitric acid (HNO_3)	Merck, Germany
Potassium ferricyanide ($\text{K}_3\text{Fe}(\text{CN})_6$)	Sigma-aldrich, USA
potassium ferrocyanide trihydrate ($\text{K}_4\text{Fe}(\text{CN})_6 \cdot 3\text{H}_2\text{O}$)	A.C.S.
Potassium chloride (KCl)	Ajax Finechem, New Zealand
Epoxy	Royal adhesives & sealants, USA
Mineral oil	Sigma-aldrich, USA
Carbon powder (particle size < 20 μm)	Sigma-aldrich, USA
Bismuth oxide nanoparticle (Bi_2O_3 ; 90-210 nm)	Sigma-aldrich

3.8 Chemicals preparations

3.8.1 Design and Characterization of flow cell

3.8.1.1 Preparation of 50 $\mu\text{g L}^{-1}$ of Cd^{2+} and Pb^{2+}

The stock solution of Cd^{2+} and Pb^{2+} were diluted with 0.1 M HCl as the supporting electrolyte to the desired volume.

3.8.2 Characterization of in-house flow-through cell using the amperometric method

3.8.2.1 Preparation of 0.1 M KCl

The solution of 0.1 M potassium chloride was prepared by dissolving 1.86 g of potassium chloride with Milli-Q water and adjusting the volume to 250 mL. The solution was used as a supporting electrolyte. After that, the solution was stored at 4°C for one week.

3.8.2.2 Preparation of 0.5 mM $\text{K}_3\text{Fe}(\text{CN})_6$ and $\text{K}_4\text{Fe}(\text{CN})_6 \cdot 3\text{H}_2\text{O}$

The mixture solution of 0.5 mM $\text{K}_3\text{Fe}(\text{CN})_6$ and $\text{K}_4\text{Fe}(\text{CN})_6 \cdot 3\text{H}_2\text{O}$ was prepared by mixing 8.23 mg $\text{K}_3\text{Fe}(\text{CN})_6$ and 10.56 mg $\text{K}_4\text{Fe}(\text{CN})_6 \cdot 3\text{H}_2\text{O}$ and made up to 50 mL with 0.1 M KCl.

3.8.3 Reagent used in Sequential Injection Analysis

3.8.3.1 Stock solution

Cadmium(II) solution (5000 $\mu\text{g L}^{-1}$)

A stock solution of 5000 $\mu\text{g L}^{-1}$ Cd^{2+} was prepared by dilution of 1000 mg L^{-1} Cd^{2+} standard solution with 1.0 M HCl and kept for a month.

Lead(II) solution (5000 $\mu\text{g L}^{-1}$)

A stock solution of 5000 $\mu\text{g L}^{-1}$ Pb^{2+} was prepared by dilution of 1000 mg L^{-1} Pb^{2+} standard solution with 1.0 M HCl and kept for a month.

3.8.3.2 Working standard solutions

The working standard solutions of Cd^{2+} and Pb^{2+} were prepared daily by diluting from the stock solution in 0.1 M HCl for the use of Bi-CPE

The plating solution was obtained by diluting Bi^{3+} standard solution in 0.1 M HCl for studying with Bi-CPE to the appropriated concentration.

3.8.3.3 Carrier solution

A HCl solution was prepared daily by diluting 37% HCl to 500 mL with Milli-Q water to the appropriate concentration.

3.8.3.4 Cleaning solution

A concentration of 0.5 M HNO_3 used for cleaning solution was prepared by diluting 65% HNO_3 with Milli-Q water.

3.9 Electrode preparation

3.9.1 Carbon paste electrode (CPE) preparation

The carbon paste electrode was prepared by mixing 0.5 mg graphite powder with 0.33 mg mineral oil (60:40% (wt/wt) ratio) using a mortar and pestle into a homogeneous carbon paste. The resulting paste was packed into the end of each electrode holder. The flanged nut was used as the electrode holder. Next, the electrical contact was made by inserting the copper wire into the carbon paste. Prior to use, the redundant paste was remove from the electrode surface and polished with weighing paper without any further electrochemical pretreatment. Figure 3.2 shows CPE that is described above.



Figure 3.2 Carbon paste electrode (CPE)

3.9.2 Preparation of Bi-film modified electrode

3.9.2.1 Used of Bi₂O₃ nanopowder

Modified CPE with Bi₂O₃ nanopowder was prepared by 1.0 mg Bi₂O₃ nanopowder, 1.0 mg graphite powder, and 1.5 mL mineral oil thoroughly mixed until obtaining a uniformly damp paste. The graphite powder and Bi₂O₃ nanopowder ratio was obtained from the optimum ratio that was reported by G-H.,Hwang and *et al.*[133]. The mixture was packed into the end of a flanged nut. Electrical contact with the carbon paste was made using a copper wire. The carbon paste was smoothed onto the weighing paper until it had a shiny appearance and was used directly for voltammetric measurements without preconditioning requirements.

3.9.2.2 Use of Bi-plating solution

In order to prepare the Bi-film electrode from Bi-plating solution, the appropriate volume of bismuth standard solution was diluted with 0.1 M HCl for Bi-CPE. The Bi-film modified CPE was obtained by simultaneously depositing a Bi³⁺ plating solution with the target metal ions onto the surface of CPE with anodic stripping voltammetric technique.

3.10 Sample Preparation

3.10.1 Water sample

The three kinds of water samples, such as tap water, drinking water, and pond water were employed to evaluate the ability of in-house flow cell with Bi-CPE. Prior to detection, a 1.00 cm³ portion of the water sample was added to 4.00 cm³

electrolyte. To demonstrate the recovery and precision, water samples were spiked with 5 and 25 $\mu\text{g dm}^{-3}$ of Cd^{2+} and Pb^{2+} .

3.11 Experimental Procedure for Bi-CPE

3.11.1 Optimization in-house designed flow cell

The flow cell was fabricated from Plexiglass as shown in Figure 3.3. It consists of an inlet hole, working electrode, reference electrode and counter electrode position. Each position was effected by the analytical signal; the working electrode is placed close to the reference electrode to reduce the ohmic drop and is placed the working electrode next to the inlet hole in order to improve the sensitivity and to prevent a side reaction from another electrode or undesired species. The solution was aspirated to inlet at the bottom of the in-house designed flow cell and passed through the working electrode, reference electrode, to flow out from the flow cell at the top through the outlet channel that was also used as a counter electrode. The channel height of the in-house flow cell was fabricated from various sizes (1.6, 2.0 and 2.5mm.); the optimization of the channel height was examined by use of a sequential injection system coupled with the anodic stripping current of Cd^{2+} and Pb^{2+} calibration curve at various concentrations to compare the slope or sensitivity of the channel height.

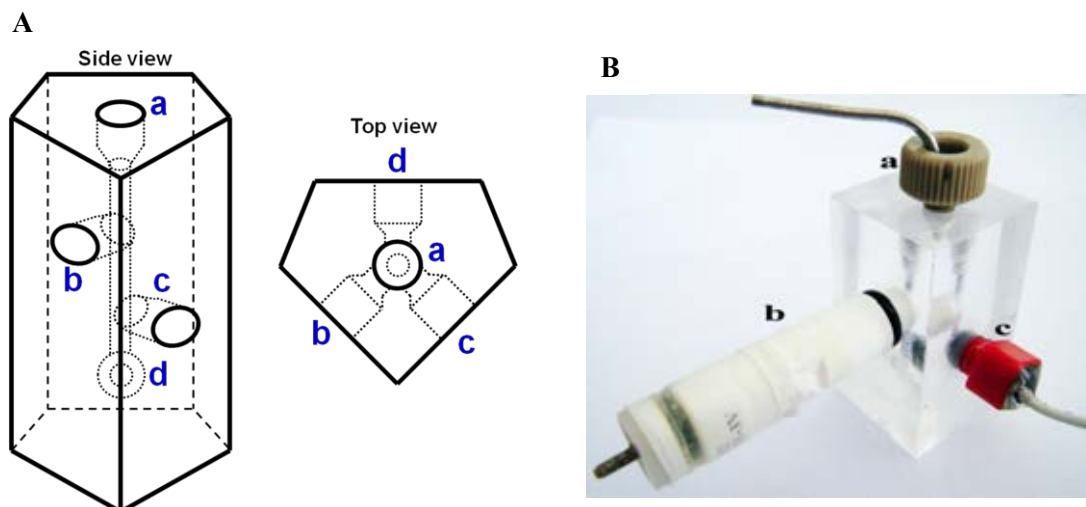


Figure 3.3 A) A schematic diagram of the in-house designed flow-through electrochemical cell seen from the side view and the top view; (a) counter electrode and outlet port, (b) reference electrode port, (c) working electrode port, and (d) inlet port. B) In-house designed flow cell with (a) a stainless steel tube as a counter electrode as well as an outlet of the flow cell, (b) a Ag/AgCl reference electrode, (c) CPE as a working electrode

3.11.2 Characterization of a thin layer flow cell with amperometric detection

To improve the thin-layer flow cell, the flow injection analysis with amperometric detection of $0.1 \text{ M Fe(CN)}_6^{3-}/\text{Fe(CN)}_6^{4-}$ was performed. The effect of the flow rate (ν) on the limiting current (i) in the thin-layer geometry was studied. The results were in a linear plot between the current and root of the flow rate.

3.11.3 The study of the Bi^{3+} modified method with the SIA system

In this research, two critical ways of the modification method to construct the Bi-film on the CPE were investigated.

3.11.3.1 *In-situ* modification from Bi^{3+} plating solution

The Bi^{3+} ions were prepared to the optimum concentration by diluting from the Bi^{3+} standard solution with an appropriate concentration of supporting electrolyte. Next, the Bi^{3+} plating solution was directed in a continuous flow to the in-house thin-layer flow cell with the analytes ions solution. Then, the Bi-film was electrodeposited on the electrode simultaneously with the analytes ions.

3.11.3.2 *In-situ* modification from Bi_2O_3 nanopowder

After preparing the Bi_2O_3 -carbon paste electrode from the previous description (3.4.3.1), the deposition potential of -1.2 V was applied to the electrode. The carbon paste electrode which contained Bi_2O_3 nanopowder was simultaneously reduced to the Bi-film at the surface of CPE with the analytes ions.

3.11.4 Characterization of Bi-film electrode

3.11.4.1 The investigation of the redox behavior

The cyclic voltammetry were performed in a single compartment electrochemical glass cell as show in Figure 3.4. The cyclic voltammetry cell consists of Bi-film CPE, Ag/AgCl with a salt bridge and platinum wire were used as the working, reference and counter electrodes, respectively. The electrochemical behavior of the Bi-film CPE for the reversible reaction of 0.5 mM $\text{Fe}(\text{CN})_6^{3-}/\text{Fe}(\text{CN})_6^{4-}$ in 0.1 M KCl was studied. The potential range of -0.25 to 0.80 V s^{-1} and a 0.025 Vs^{-1} scan rate was applied to a 0.5 mM $\text{Fe}(\text{CN})_6^{3-}/\text{Fe}(\text{CN})_6^{4-}$ solution in 0.1 M KCl.



Figure 3.4 The electrochemical cell for cyclic voltammetry experiment.

3.11.4.2 The investigation of the reaction process

The experiments were carried out in the same way as described above (3.6.4.1). For the reaction process on the surface of the electrode, the rate of electron transfer was investigated. The scan rate varied from 0.005 to 0.10 V s^{-1} in 0.5 mM $\text{Fe}(\text{CN})_6^{3-}/\text{Fe}(\text{CN})_6^{4-}$ solution in 0.1 M KCl. The peak currents obtained from the experiment at each scan rate were plotted as a function of the square root of the scan rate.

All of cyclic voltammetric experiments were carried out at room temperature and housed in a faraday cage.

3.11.5 Study of the electrode stability

The stability of the Bi-film CPE was studied with anodic stripping voltammetry of $5 \mu\text{g L}^{-1}$ Cd^{2+} and Pb^{2+} mixed solution in 0.1 M HCl using the in-house designed flow cell. The plots between the current signal and number of the analysis cycle were obtained.

3.11.6 Optimization of SIA-SWASV parameters

The important parameters that influence the obtained current were studied. The sequential injection components were arranged as shown schematically in Figure 3.5. The SIA system consisted of a 2.5 mL syringe pump, an eight port selection valve, an in-house thin layer flow cell, and PalmSens BV (potentiostat). All tubing connecting the different component of flow system is made from PTFE with the inner diameter of 0.8 mm.

3.11.6.1 The effect of Bi^{3+} concentration

In the case of the in situ plated Bi-film, the Bi^{3+} concentration is an important parameter that can affect the stripping peak response and preconcentration time [78,134]. In the in-house designed thin-layer flow cell, the effect of the Bi^{3+} concentration was evaluated in the range of 0.01 to 10.0 M.

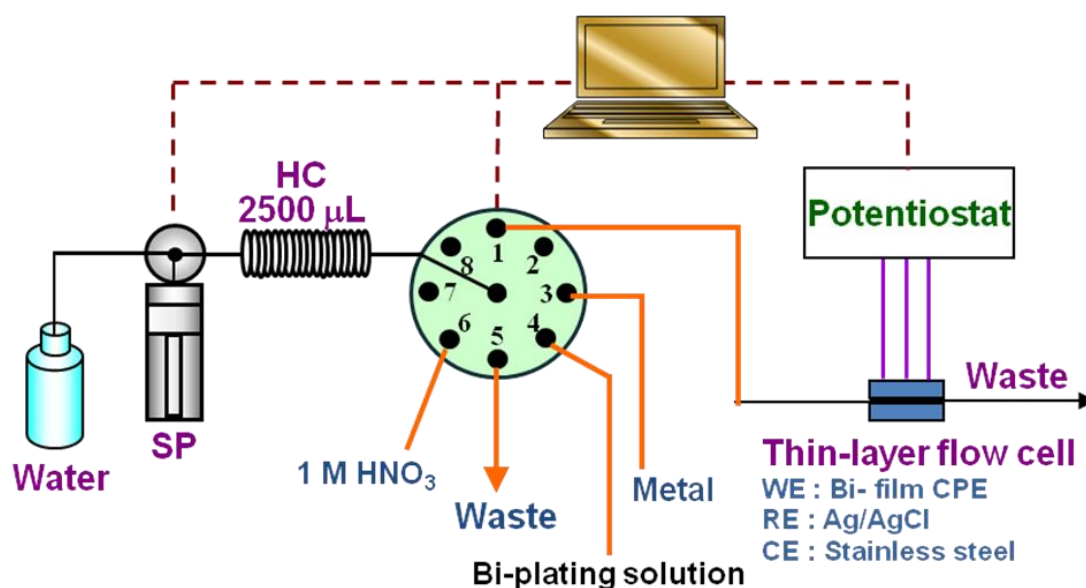


Figure 3.5 The SIA manifold for the determination of Cd^{2+} and Pb^{2+} by SWASV with Bi-CPE; HC is a holding coil.

3.11.6.2 The effect of HCl concentration

HCl acid was used as the supporting electrolyte in the research. The concentration of 0.1 to 2.0 M HCl was studied. The signal currents were measured for each concentration and the results were compared.

3.11.6.3 Optimum accumulation potential or deposition potential

In order to obtain the optimal accumulation potential for high specification and high sensitivity in Cd^{2+} and Pb^{2+} determination with SWASV, the investigation was performed by varying the accumulation potential from -0.8 to -1.4 V vs Ag/AgCl. Then, the average peak current obtained from the measurements were plotted as the function of the accumulation potential.

3.11.6.4 Effect of square wave (SW) frequency, step potential and pulse height on SWASV performance

The peak current obtained from SWASV is also dependent on various instrument parameters such as frequency, step potential or amplitude and pulse height. Then, the effect of the pulse frequency was studied in the range of 10 - 100 Hz. The current and applied frequency was plotted to find the optimum best peak heights.

The other variable studied was the step potential in the SWASV, which corresponds to the scan rate. When the step potential is changed, the scan rate is automatically changed. The dependence of the response on the step potential was investigated from 0.0025 to 0.025 V. The optimum step potential was obtained from the graph between the current and applied step potential.

Lastly, the influence of the SW-pulse height variation on the analyte peak currents, within the range of 0.005 to 0.075 V, was evaluated. Therefore, the optimum value was chosen from the relation between the plot of the current signal and SW-pulse height.

3.11.6.5 Analytical performance from Bi-CPE

The calibration plots for the simultaneous determination of Cd^{2+} and Pb^{2+} ion levels by SI-ASV, using the commercial and the in-house flow cells, were generated under the optimum conditions of each flow cell.

A series of stripping voltammetry measurements of Cd^{2+} and Pb^{2+} in the concentration range of either 0.5 to 75 $\mu\text{g L}^{-1}$ in the commercial flow cell or 0.25 to 500 $\mu\text{g L}^{-1}$ in the in-house designed thin-layer flow cell were investigated by diluting the standard solution stock. The current response at the Bi-film CPE in the commercial and in the in-house designed thin-layer flow cells were plotted against the Cd^{2+} and Pb^{2+} concentrations.

The detection limit (LOD, the concentration corresponding to three times the standard deviation of the response obtained from the blank solution) and the quantification limit (LOQ, the concentration corresponding to ten times the standard deviation of the response obtained from blank solution), were also studied.

3.12 Applications

3.12.1 Application of Bi-CPE

The calibration method was used for the determination of Cd^{2+} and Pb^{2+} in the water sample. Both the commercial and the in-house designed electrochemical thin-layer flow-through cells, based on the Bi-film modified CPE, were applied to test three types of water, including a high organic matter containing pond water, and the same samples after spiking with 5 or 25 $\mu\text{g L}^{-1}$ of Cd^{2+} and Pb^{2+} .

Part III: Graphene-modified carbon paste electrode for Cd²⁺ and Pb²⁺ monitoring with a flow based system

3.13 Instruments and Apparatus

The instruments and apparatus used in this research were listed in Table 3.6.

Table 3.6 The instruments and apparatus.

Instruments and Apparatus	Suppliers
PalmSens BV	Palm Instruments BV, The Netherlands
Ag/AgCl reference electrode	BAS, Japan
Platinum wire for counter electrode	Goodfellow, USA
Carbon pasted electrode block	Home made
Carbon paste electrode for designed flow cell	Home made
Electrical wire	Bangkok cable
A thin layer cross flow cell	BAS, Japan
Designed flow cell	Home made
pH meter	Metrohm 744 pH meter, Switzerland
Analytical balance	AT 200, Mettler, Switzerland
Sequential analysis system (2.5 mL, syringe pump)	MGC, Japan
PTFE tubing (ϕ 0.8 and 1.5 mm)	Upchurch
Flanged Nut/washer 1/16"	Upchurch
Milli-Q water system ($R \geq 18.3 \text{ M}\Omega$)	Millipore, Bedford, MA, USA
A Rhedynne injection valve (20 μL , 0.5 mm i.d., injection loop)	Model 5100, Altech
Agate Mortar & Pestle Sets (01441-AB)	SPI Supplies/Structure Probe, USA
Filter papers (Cat No 1001 125, ϕ 125mm)	Whatman, General Electric
Micro balance (AB204s)	Mettler-Toledo AG, Switzerland
Thermometer	West-Germany

Instruments and Apparatus	Suppliers
Sonicator	A006651,USA
ICP spectrometer (iCAP 6000 Series)	Thermo scientific
Memmert Oven (Model 100-800)	Memmert, Germany
Centrifuge (Universal 320R)	Hettich, Germany

3.14 Chemicals and Reagents

The chemicals and reagents used in this research were analytical grade and were used as received without any further purification. The listed of chemicals and reagents were showed in Table 3. 7.

Table 3.7 The chemicals and reagents used in this pasrt.

Chemicals	Suppliers
Bismuth (Bi^{3+}) standard solution 1,000 mg L ⁻¹	BDH, England
Lead (Pb^{2+}) standard solution 1,000 mg L ⁻¹	BDH, England
Cadmium (Cd^{2+}) standard solution 1,000 mg L ⁻¹	BDH, England
Hydrochloric acid (HCl)	Merck, Germany
Nitric acid (HNO_3)	Merck, Germany
Potassium ferricyanide ($\text{K}_3\text{Fe}(\text{CN})_6$)	Sigma-aldrich, USA
potassium ferrocyanide trihydrate ($\text{K}_4\text{Fe}(\text{CN})_6 \cdot 3\text{H}_2\text{O}$)	A.C.S.
Epoxy	Royal adhesives & sealants, USA
Mineral oil	Sigma-aldrich, USA
Carbon powder (particle size < 20 μm)	Sigma-aldrich, USA
Bismuth oxide nanoparticle (Bi_2O_3 ; 90-210 nm)	Sigma-aldrich
Graphene	SkySpring Nanomaterials, USA
Perchloric acid (HClO_4)	Merck, Germany
2-Propanal	Merck, Germany
Dimethylformamide (DMF)	BDH, France

3.15 Chemicals and reagents preparation

3.15.1 Preparation of 5000 $\mu\text{g L}^{-1}$ of Cd^{2+} and Pb^{2+} in 0.05 M HCl

The stock solution of Cd^{2+} and Pb^{2+} were prepared by diluting 1000 mg L⁻¹ of the standard solution of Cd^{2+} and Pb^{2+} with 0.05 M HCl and storing them for a month.

3.15.2 Preparation of 0.5 mM $\text{K}_3\text{Fe}(\text{CN})_6$ and $\text{K}_4\text{Fe}(\text{CN})_6 \cdot 3\text{H}_2\text{O}$

The mixture solution of 0.5 mM $\text{K}_3\text{Fe}(\text{CN})_6$ and $\text{K}_4\text{Fe}(\text{CN})_6 \cdot 3\text{H}_2\text{O}$ was prepared by mixing 8.23 mg $\text{K}_3\text{Fe}(\text{CN})_6$ and 10.56 mg $\text{K}_4\text{Fe}(\text{CN})_6 \cdot 3\text{H}_2\text{O}$ and made up to 50 mL with 0.1 M KCl.

3.15.3 Working standard solutions

The working standard solutions of Cd^{2+} and Pb^{2+} were prepared daily by diluting from the stock solution in 0.05 M HCl for the use of Bi-GCPE

3.15.4 Carrier solution: 0.05 M HCl

A HCl solution was prepared daily by diluting 37% HCl to 500 mL with Milli-Q water to the appropriate concentration.

3.15.5 Cleaning solution

A concentration of 0.5 M HNO_3 used as the cleaning solution was prepared by diluting 65% HNO_3 with Milli-Q water.

3.15.6 Bi-plating solution

In order to prepare the Bi-film electrode from Bi-plating solution, the appropriate volume of bismuth standard solution was diluted with 0.05 M HCl for Bi-GCPE. The Bi-film modified GCPE was obtained by simultaneously depositing a Bi^{3+} plating solution with the target metal ions onto the surface of GCPE using the anodic stripping voltammetric technique.

3.16 Electrode preparation

3.16.1 Graphene/Carbon paste electrode (GCPE) preparation

Appropriate graphene powder was dispersed in optimum solvent with the aid of ultrasonication for 120 min. The dispersion of graphene was evaporated in a vacuum oven at 60 °C for 30 minutes. Then, GCPE was prepared by mixing graphene powder and graphite powder with mineral oil (60:40 %wt/wt, respectively) in an agate mortar to form a homogeneous paste [135-137]. The electrode-holder was filled with the, and a copper wire was inserted into the opposite end as the electrical connector. A fresh electrode surface and a smooth surface were obtained by polished with weighing paper prior to use.

3.16.2 *In-situ* modification from Bi³⁺ plating solution

The Bi³⁺ ions were prepared to the optimum concentration by diluting the Bi³⁺ standard solution with the appropriate concentration of supporting electrolytes. Next, the Bi³⁺ plating solution flowed directly and continuously to the thin-layer flow cell with the analytes ions solution. Then, the Bi-film was electrodeposited on the electrode simultaneously with the analytes ions.

3.17 Sample preparation

3.17.1 Non-complicated matrix: Water sample

The water sample prepared using 1.00 mL portion of each water sample was added to 4.00 mL carrier solution. The recovery and precision of the method were evaluated by the calibration method for the analysis of water samples following spiking with both metal ions at final concentrations of 7 or 20 µg L⁻¹ each.

3.17.2 Complicated matrix: Undulated surf clams tissue and sea bass fish tissue

Sea bass fish and undulated surf clam samples were also investigated by mincing the tissue into small pieces and then grinding for a few minutes in a

blender machine. After that, known amounts of Cd^{2+} and Pb^{2+} were spiked into a portion of the homogenized sample tissue. Then, 1.0 mL of $13.42 \text{ mol L}^{-1} \text{ HNO}_3$ and 2.0 mL of $11.87 \text{ mol L}^{-1} \text{ HClO}_4$ were added to 1.0 g of this sample homogenate [138], and the sample was heated at $100 \text{ }^\circ\text{C}$ for 5 h. Next, the solid residue was filtered with filter paper, and the resulting solution was clear. The pH was then adjusted with NaOH and HCl close to pH of the supporting electrolyte before being diluted with the supporting electrolyte to a final volume of 25 mL. The complex matrix samples (sea bass fish tissues and undulated surf clam) were evaluated after spiking with both metal ions at 1.0 and $5.0 \text{ } \mu\text{g L}^{-1}$ prior to extraction by the standard addition method.

3.18 Experimental Procedure for Bi-GCPE

3.18.1 Solvent dispersion

The graphene-induced aggregation is crucial for the electrochemical signal [139]. Due to the small size and flat shape of graphene, graphene nanopowder is sensitive to van der Waal's interactions and conglomerates in the dry state, leading to poor electrical conductivity [116, 119, 122, 140-142]. Therefore, to obtain the unique and desired properties of graphene-based electrodes, the prevention of graphene aggregation is an important process [143]. Then, dispersion in optimum solvent is a good way to improve it. The amounts of graphene are directly dispersed into IPA, 15% IPA, and DMF at the concentration of 0.1 mg L^{-1} . A well-dispersed graphene suspension was prepared by ultrasonic dispersing for 120 minutes to give a more homogeneously dispersed graphene suspension. The well-dispersed graphene suspension was dried by evaporation of solvent in a vacuum oven at $60 \text{ }^\circ\text{C}$ for 30 minutes. The dried graphene was used to prepare the GCPE in the following step.

3.18.2 The graphene and graphite mass ratio

The amount of graphene mixed with the carbon paste electrode has an effect on the electrical conductivity [70, 136, 144]. The weight fraction of graphene in the GCPE was evaluated by a varying weight of graphene composited from 0.5 to 5.0 mg in constant weight of carbon nanopowder. The electrochemical response of 10

$\mu\text{g L}^{-1}$ Cd^{2+} and Pb^{2+} was chosen to characterize the electrical conductivity of the different amounts of graphene in CPE.

3.18.3 Prepared Bi^{3+} modified GCPE

The Bi^{3+} modified GCPE was prepared with a suitable concentration of Bi^{3+} diluted with an appropriate concentration of the HCl as the supporting electrolyte. The film was prepared by *in-situ* plating method with Cd^{2+} and Pb^{2+} solution.

3.18.4 Optimization of SIA-SWASV with Bi-GCPE

3.18.4.1 Effect of the Bi^{3+} concentration in the plating solution

The thickness of Bi-film in Bi-GCPE was studied because it also influenced the current response. The influence of the Bi^{3+} concentration was examined from 1.0 to 5.0 mg L^{-1} . The optimum concentration was obtained from the plots of the peak current and the Bi^{3+} concentration.

3.18.4.2 The effect of the HCl concentration

Hydrochloric acid (HCl) has been widely recommended as the electrolyte solution for the determination of several metals by anodic stripping voltammetry. The concentration of HCl was verified from 0.01 to 1.0 $\mu\text{g L}^{-1}$; the corresponding peaks for Cd^{2+} and Pb^{2+} were collected. The anodic peak current behavior of Cd^{2+} and Pb^{2+} in various concentrations of HCl was achieved from the plotting of the current and the HCl concentration.

3.18.4.3 Effect of SW-parameters

The parameters such as deposition potential, SW frequency, and the step potential, are general trends to examine. First of all parameters, the influence of deposition potential or accumulation potential was performed in the range of -1.3 to -0.9 V. The highest current response was obtained from the plotting of the current with the accumulation potential.

The next important parameter is the square wave frequency that related to the scan rate of the method. The effect of the square wave frequency was studied between the range of 30 to 90 Hz.

The last electrochemical parameter, the effect of the step potential was investigated. Step potential was varied in the range 5.0 to 20 mV. All of the SWASV-parameters were investigated with $10 \mu\text{g L}^{-1}$ of Cd^{2+} and Pb^{2+} .

3.19 Analytical performance

3.19.1 Analytical performance from Bi-CPE

The calibration plots for the simultaneous determination of Cd^{2+} and Pb^{2+} ion levels by SI-ASV, using the commercial and the in-house thin-layer flow cells, were generated under the optimum conditions of each flow cell.

A series of stripping voltammetry measurements of Cd^{2+} and Pb^{2+} in the concentration range of either 0.5 to $75 \mu\text{g L}^{-1}$ in the commercial flow cell or 0.25 to $500 \mu\text{g L}^{-1}$ in the in-house designed thin-layer flow cell were investigated by diluting from the stock standard solution. The current response at the Bi-film CPE in the commercial and in the in-house designed thin-layer flow cells were plotted against the Cd^{2+} and Pb^{2+} concentrations.

The detection limit (LOD, the concentration corresponding to three times the standard deviation of the response obtained from the blank solution) and the quantification limit (LOQ, the concentration corresponding to ten times the standard deviation of the response obtained from the blank solution), were also studied.

3.19.2 Analytical performance from Bi-GCPE

Under the optimum analytical conditions, the calibration data of Cd^{2+} and Pb^{2+} peak current related with different concentrations was carried out. The analytical concentration ranges of analytes were 0.1 to $100 \mu\text{g L}^{-1}$ for both metal ions. The detection limits (LOD) were set as the concentration that gives a response equivalent to three times the standard deviation (SD) of the blank ($n = 10$), while the

quantification limits (LOQ) were calculated as the concentration that gives a response equivalent to ten times the SD of the blank, respectively. The precision of the procedure, expressed by the relative standard deviation for three measurements of each metal, was also calculated.

3.20 Applications

3.20.1 Application of Bi-GCPE

3.20.1.1 Tap water sample

The concentration of Cd^{2+} and Pb^{2+} in the tap water sample was collected by the calibration method without pretreatment and filtration. The spike concentration level at 7.0 and 20.0 $\mu\text{g L}^{-1}$ of the Cd^{2+} and Pb^{2+} stock standard solution were added into the tap water sample. The average found concentration and the recovery of Cd^{2+} and Pb^{2+} in the tap water sample were studied.

3.20.1.2 Application in undulated surf clams and sea bass fish tissue

After the digestion, the concentration of trace Cd^{2+} and Pb^{2+} in undulated surf clams and sea bass fish under optimum investigation were carried out using the standard addition method. This method was favorably used in the sample in which the matrix effects influenced the analytical method. The accuracy of the stripping voltammetric procedure with Bi-GCPE was evaluated by the recovery assay at the concentration of part per million levels. The recovery of Cd^{2+} and Pb^{2+} were tested by the addition of 25.0 and 125.0 $\mu\text{g Kg}^{-1}$ standard stock solutions into the undulated surf clams and sea bass fish tissue before starting the digestion process. The obtained results were done based on four repetitions ($N=4$) of the analysis.

3.21 Control of the analytical performance of the proposed method

The proposed method for determination of Cd^{2+} and Pb^{2+} in complicated matrix sample (sea bass fish and undulated surf clam) was compared with the ICP-

OES method. The spiked concentration of 125.0 and 250.0 $\mu\text{g Kg}^{-1}$ of Cd^{2+} and Pb^{2+} were prepared by the method that described in the section 3.17.2. The experiments were carried out by three consecutive of the spiked sample. The results were used to plot the standard addition curve. A paired t -test at the 95% confidence level was applied, and the $t_{\text{calculated}}$ compared with t_{critical} was used for data analysis between the two methods.

CHAPTER IV

RESULTS AND DISCUSSION

This chapter is divided into three parts. The first part is the results, discussion and application from using Bi-CPE for the determination of Cd^{2+} and Pb^{2+} in the micro-flow sensor. The second part details the results, discussion and application on the development of the in-house thin layer flow cell for CPE with the in-situ modification of Bi-film. Lastly, the third part is the results, discussion and application from using Bi-GCPE also for the determination of Cd^{2+} and Pb^{2+} in the in-house thin layer flow cell. All of the results were obtained from SWASV technique coupled with the SIA.

Part I: Electrochemical characterization of carbon electrodes in the μ -flow sensor by an on-line automated flow system

In this part, the sensitive results were compared between two voltammetric methods which comprised of the differential pulse and square wave anodic stripping voltammetry using the micro-flow sensor. Several advantages of HCl as a suitable supporting electrolyte for the determination of Cd^{2+} and Pb^{2+} have been reported in the literature. Then, the first part of the research used 1.0 M HCl as the supporting electrolyte [145]. The study proposed that the μ -flow sensor could provide an adequate sensitivity for analysis of Cd^{2+} and Pb^{2+} in an environmental samples.

4.1 The study of long-term stability and reproducibility of the carbon electrode in the μ -flow sensor

The long-term stability of the carbon electrode was investigated by the monitoring of the current signal of Cd^{2+} and Pb^{2+} for a period of time. From the results, the electrode was found to be stable, even after 10 voltammetric scans. The corresponding voltammograms of the inter- and intra-day reproducibility test of the electrode were analyzed and data is presented in Table 4.1 and Table 4.2 in terms of average peak heights.

Table 4.1 Stripping currents and reproducibility for 50 $\mu\text{g L}^{-1}$ of Cd^{2+} and Pb^{2+} in 1.0 M HCl measured in the micro-flow system (intra-day analysis: N = 10)

N	Average current (μA)					
	Cd^{2+}			Pb^{2+}		
	A	B	C	A	B	C
1	0.75	0.72	0.70	0.66	0.65	0.61
2	0.64	0.89	0.91	0.62	0.65	0.61
3	0.57	0.71	0.68	0.65	0.65	0.60
4	0.64	0.88	0.71	0.64	0.59	0.68
5	0.65	0.89	0.79	0.70	0.59	0.69
6	0.56	0.74	0.75	0.64	0.69	0.61
7	0.56	0.75	0.70	0.64	0.60	0.61
8	0.62	0.76	0.68	0.60	0.65	0.59
9	0.60	0.83	0.68	0.69	0.63	0.58
10	0.59	0.82	0.78	0.67	0.67	0.55
Average	0.62	0.80	0.74	0.65	0.64	0.61
SD	0.06	0.07	0.07	0.03	0.03	0.04
%RSD	9.44	9.13	9.86	4.74	5.50	6.75

Table 4.2 Comparison of the stripping currents and the reproducibility between days for 50 $\mu\text{g L}^{-1}$ of Cd^{2+} and Pb^{2+} in 1.0 M HCl using the micro-flow system

μ -flow sensor	Date measured	Cd^{2+}		Pb^{2+}	
		Average current \pm SD (μA)	%RSD	Average current \pm SD (μA)	%RSD
1	8-Oct	0.70 \pm 0.07	10.44	0.55 \pm 0.03	6.08
	10-Oct	0.70 \pm 0.07	10.16	0.55 \pm 0.04	7.43
	14-Oct	0.72 \pm 0.07	9.55	0.48 \pm 0.32	6.54
2	24-Oct	0.62 \pm 0.06	9.44	0.65 \pm 0.03	4.74
	25-Oct	0.80 \pm 0.07	9.13	0.64 \pm 0.03	5.5
	29-Oct	0.74 \pm 0.07	9.86	0.61 \pm 0.04	6.75
3	30-Oct	0.77 \pm 0.08	10.06	0.56 \pm 0.03	4.85
	31-Oct	0.71 \pm 0.07	10.52	0.54 \pm 0.01	1.45
	3-Nov	0.78 \pm 0.08	10.06	0.55 \pm 0.03	4.92

The results in Table 4.1 and 4.2 show a good reproducibility of the carbon electrode in the micro-flow system with a relative standard deviation (RSD) of less

than 10 %. From the data in Table 4.2, the average stripping peak current in each measurement within a day ($N = 10$ per day) was obtained in a range of 0.62 to 0.80 μA for Cd^{2+} and in a range of 0.61 to 0.65 μA for Pb^{2+} . The analysis time was 11.2 min, including aspiration and dispensation of the solutions to the μ -flow sensor by the SIA system together with the stripping voltammetric procedure. The RSD of the three micro-flow sensors observed by inter-day analysis were in the range of 9.1 to 10.5 % for Cd^{2+} and 1.5 to 7.4 % for Pb^{2+} . The carbon electrode in the micro-flow sensor is quite stable; one electrode can be used for 48 hours. Thus the carbon electrode can be used as an effective sensor with good reproducibility, long stability and short analysis time for the metal ions determination.

4.2 Study of the DPASV parameters

ASV method is based on electrochemical reduction of metal ions at a working electrode to deposit the metals on the electrode surface and subsequent anodic stripping by scanning the potential to anodic direction to allow electrooxidation of the deposited metals at a characteristic potential of each metal, as recorded as a voltammogram in this step. Optimum conditions for deposition and stripping steps of DPASV of Cd^{2+} and Pb^{2+} on the carbon electrode in the μ -flow sensor coupled with the SIA system were investigated as the following.

4.2.1 Effect of the deposition potential

The effect of the deposition potential applied to the carbon electrode in the micro-flow sensor on the DPASV peak currents of Cd^{2+} and Pb^{2+} is shown in Figure 4.1.

It was found that the more negative potential used, the higher sensitivity was obtained up to -1.20 V, after that the sensitivity decreased slightly. Therefore, the deposition potential of -1.20 V was selected for the subsequent experiment.

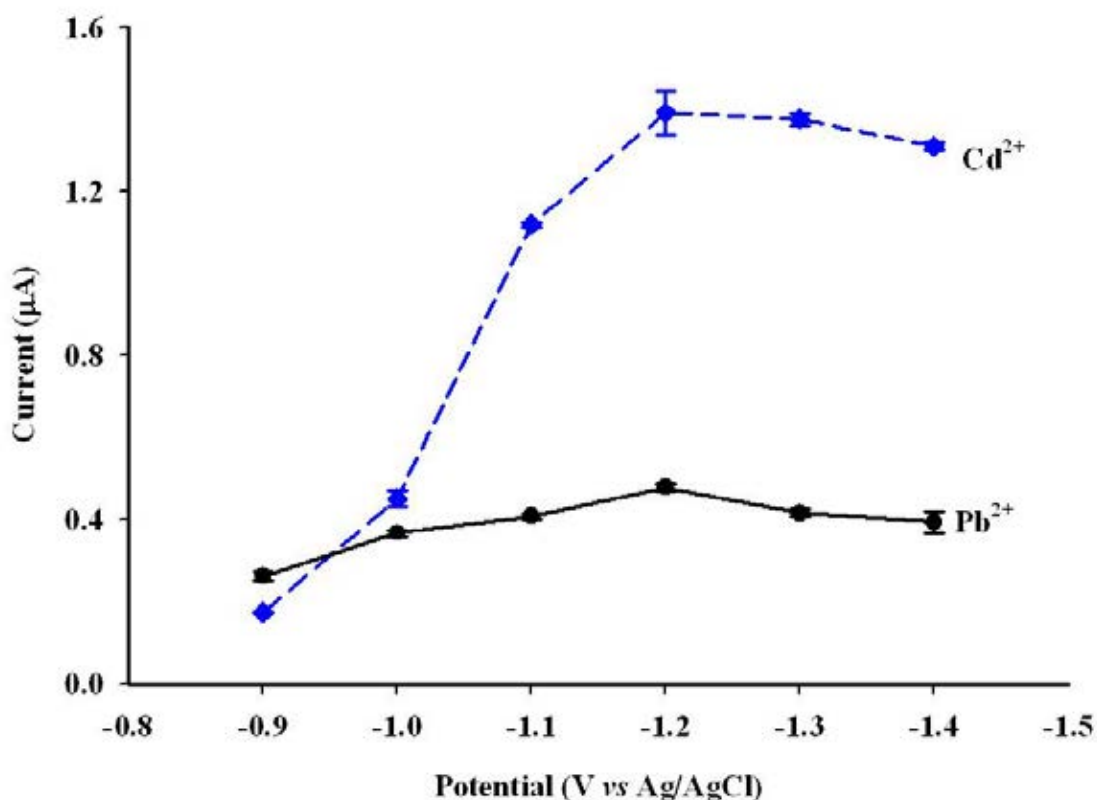


Figure 4.1 Effect of the deposition potential on the DPASV peak currents for a solution containing $50 \mu\text{g L}^{-1}$ of Cd^{2+} and Pb^{2+} in 1.0 M HCl using the carbon electrodes in the micro-flow sensor coupled with SIA operating system. Conditions: deposition time, 180 s; step potential, 0.05 V; conditioning potential, -1.00 V; scan rate, 0.05 V s^{-1} ; equilibration time, 10 s.

4.2.2 Effect of the pulse time and the pulse potential

The effect of the pulse time and the pulse potential upon the stripping response of $50 \mu\text{g L}^{-1}$ of Cd^{2+} and Pb^{2+} were examined. As shown in Figure 4.2, the signal of both metal ions decreased with the increase of the pulse time in the study range of 0.01 to 0.20 s. The optimum pulse time of 0.01 s was chosen for the following experiment.

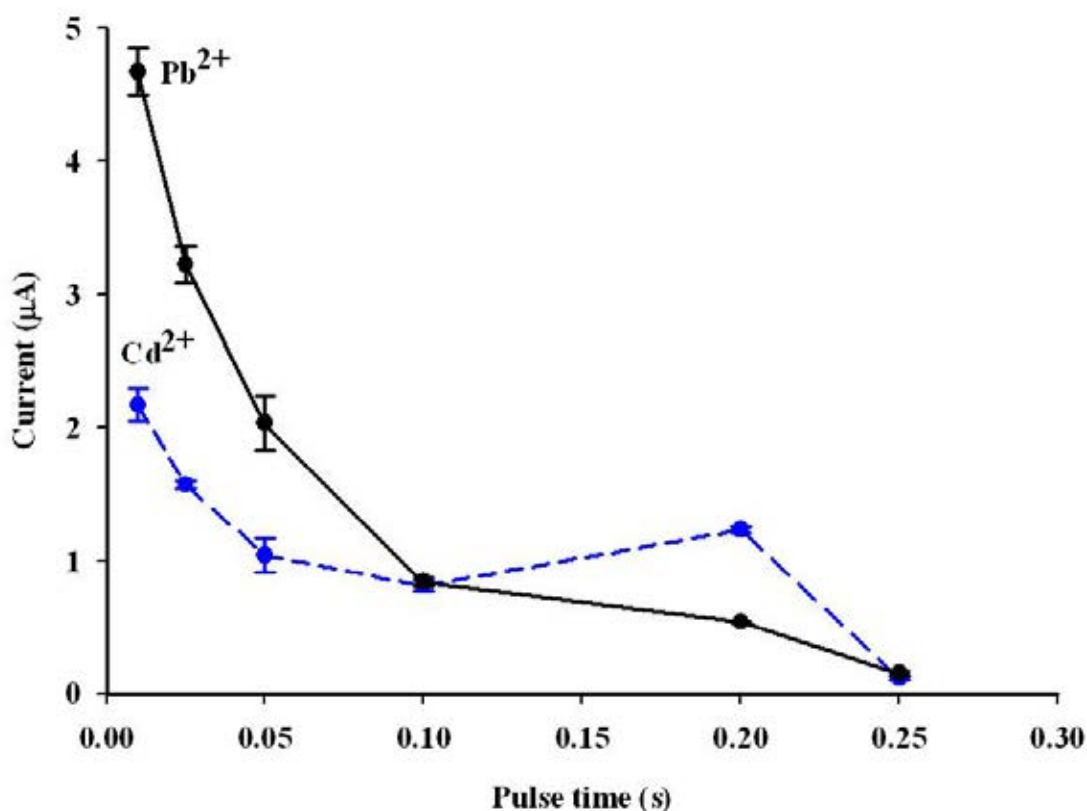


Figure 4.2 The effect of the pulse time on the DPASV peak currents for a solution containing $50 \mu\text{g L}^{-1}$ of Cd^{2+} and Pb^{2+} in 1.0 M HCl using the carbon electrode in the micro-flow sensor coupled with SIA operating system. Conditions: deposition potential, -1.2 V ; deposition time, 180 s ; step potential, 0.05 V ; conditioning potential, -1.00 V ; scan rate, 0.05 V s^{-1} ; quiet time, 10 s .

The effect of the pulse potential on the stripping peak currents of both metal ions was also investigated in the range of 5 to 100 mV . The investigative currents are plotted against the pulse potential as shown in Figure 4.3. Then, the optimized pulse potential of 50 mV was obtained for simultaneous determination of Cd^{2+} and Pb^{2+} .

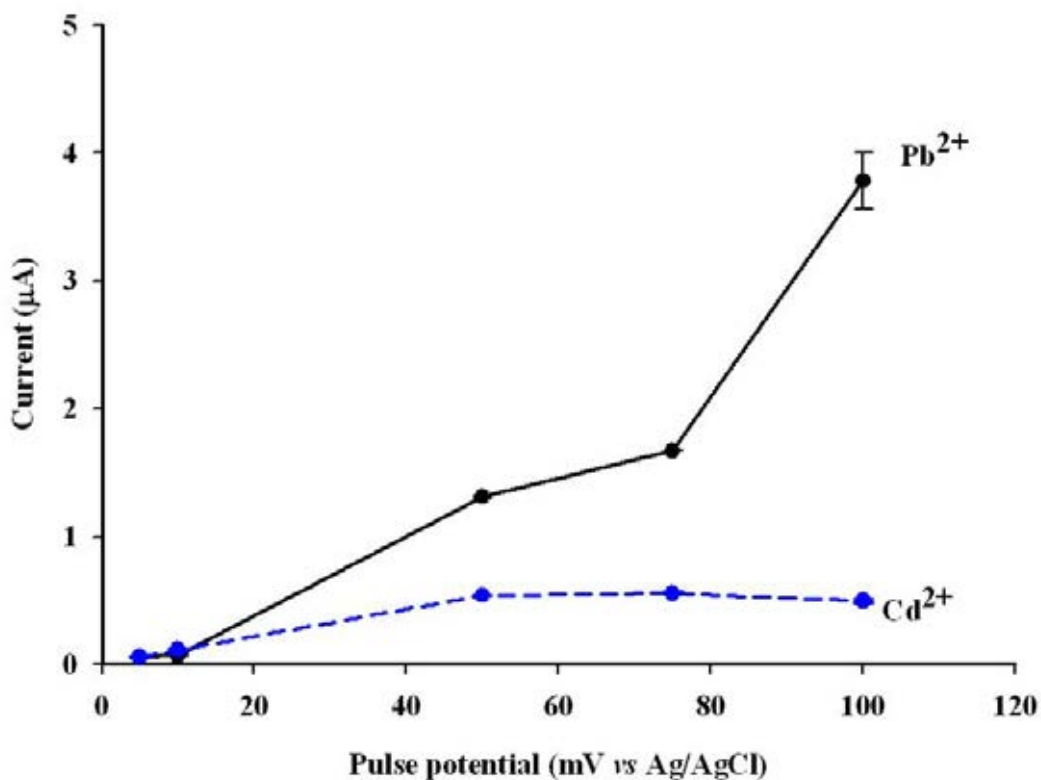


Figure 4.3 Effect of the pulse potential on the DPASV peak currents for a solution containing $50 \mu\text{g L}^{-1}$ of Cd^{2+} and Pb^{2+} in 1.0 M HCl using the carbon electrode in the micro-flow sensor coupled with SIA operating system. Conditions: deposition potential, -1.2 V; deposition time, 180 s; step potential, 0.005 V; conditioning potential, -1.00 V; scan rate, 0.005 V s^{-1} ; quiet time, 10 s.

4.3 Study of the SWASV parameters

The SWASV parameters were optimized to obtain the high sensitivity of the voltammetric determination of Cd^{2+} and Pb^{2+} ions as the following.

4.3.1 The effect of the deposition potential

The effect of the deposition potential on the SWASV peak currents of $50 \mu\text{g L}^{-1}$ of Cd^{2+} and Pb^{2+} on the carbon electrode in the micro-flow sensor was studied in the range of -0.9 to -1.5 V. The data is shown in Appendix A (Table 1-A) and the plots of the peak currents of Cd^{2+} and Pb^{2+} versus the deposition potential are shown in Figure 4.4.

At the deposition potential of -0.9 V, a peak of Cd^{2+} was not found. The current response of both metal ions increased with the increase of the negative deposition potential applied and reach the maximum at -1.5 V. However, the highest standard deviation was also obtained at this potential. Moreover, when the more negative potential was applied, the peak of Cd^{2+} and Pb^{2+} was easily destroyed. This may be caused by the hydrogen evolution, which could easily occur from the high acidic media at the more negative potential. This phenomenon destroys the metal alloy deposition process [26]. In this instance, the optimum deposition potential of -1.4 V was chosen.

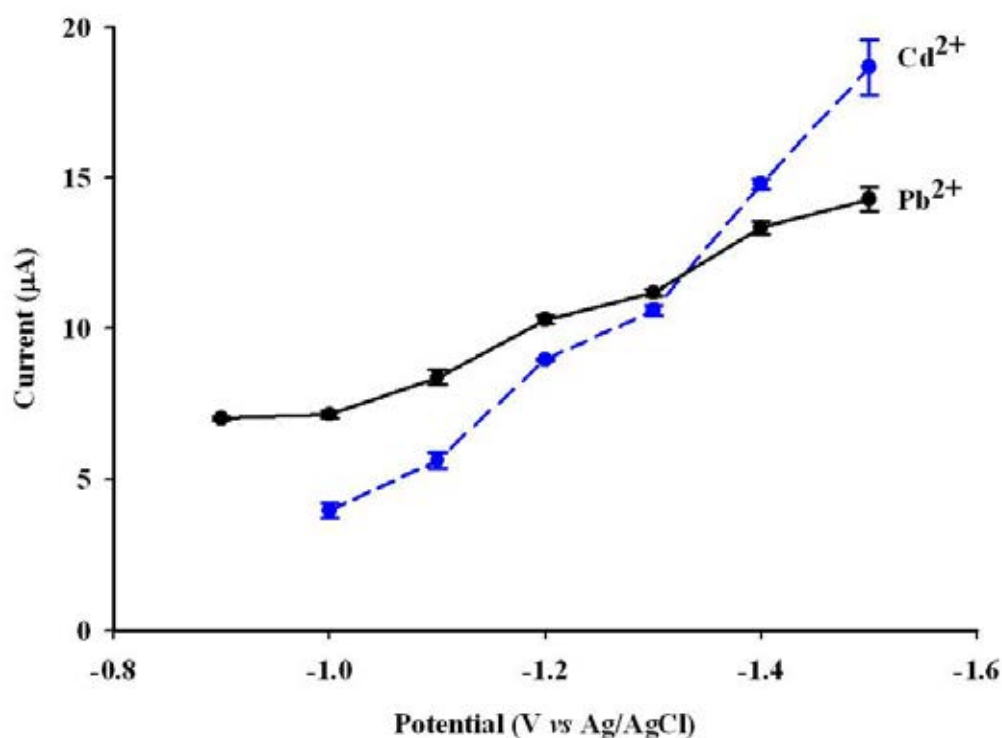


Figure 4.4 Effect of the deposition potential on the SWASV peak heights for a solution containing $50 \mu\text{g L}^{-1}$ of Cd^{2+} and Pb^{2+} in 0.1 M HCl on the carbon electrode in the micro-flow sensor coupled with the SIA operating system.

4.3.2 The effect of the square wave frequency

The results of the effect of square wave frequency are shown in Appendix A (Table 2-A). The relationship between the peak currents and the

frequency is shown in Figure 4.5. An increase in the peak currents of $50 \mu\text{g L}^{-1}$ of Cd^{2+} and Pb^{2+} from 10 up to 50 Hz was observed, after that they decreased. The maximal peak currents in Figure 4.5 indicated that 50 Hz of square wave frequency is the optimum value for the next experiment.

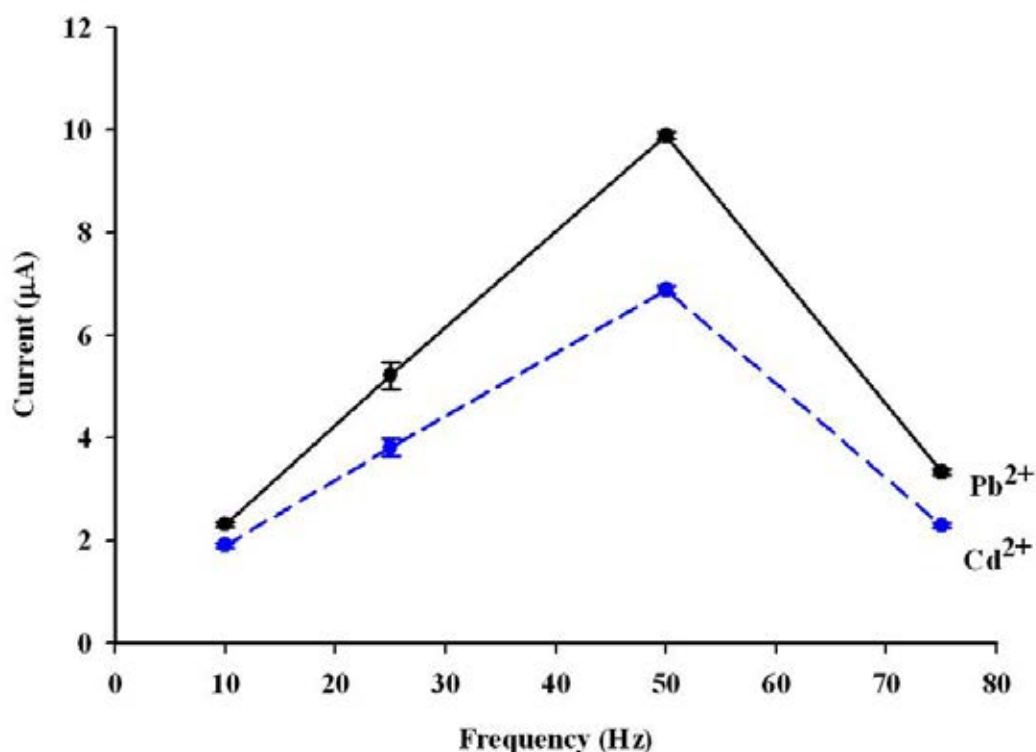


Figure 4.5 The effect of the square wave frequency on the SWASV peak currents for a solution containing $50 \mu\text{g L}^{-1}$ of Cd^{2+} and Pb^{2+} in 1.0 M HCl using the carbon electrode in the micro-flow sensor coupled with the SIA operating system.

4.3.3 Effect of the potential step

The influence of the potential step was investigated. The electrochemical data (Appendix A; Table 3-A) and the plots of the relationship between the current response and the potential step (Figure 4.6) are shown. The current increased with the increasing of the potential step in the examined range of 2.5 to 10 mV. The highest peak current was obtained at the potential step of 100 mV, however the highest standard deviation was also observed. Then, the potential step of 7.5 mV was selected for the next experiment.

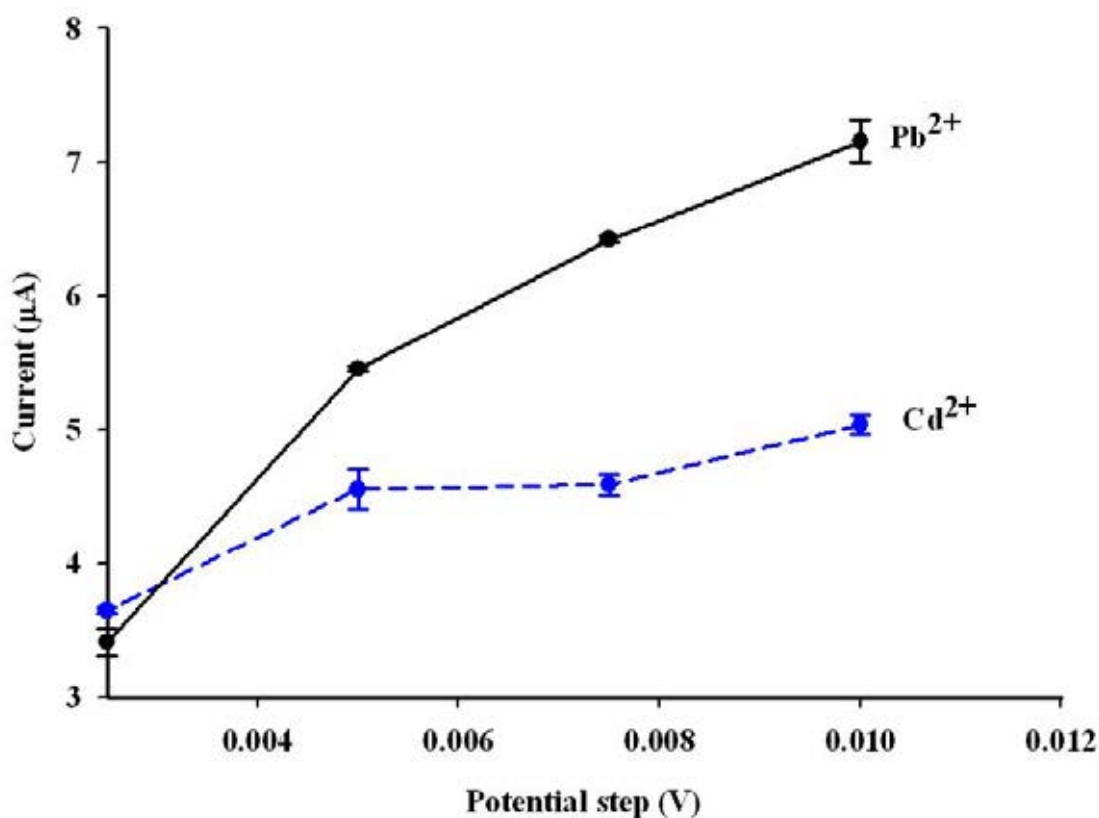


Figure 4.6 Effect of the potential step on the SWASV peak currents for a solution containing $50 \mu\text{g L}^{-1}$ of Cd^{2+} and Pb^{2+} in 1.0 M HCl using the carbon electrode in the micro-flow sensor coupled with SIA operating system.

4.3.4 Effect of the potential amplitude

The potential amplitude was studied in the range of 10 to 75 mV. From the electrochemical data as shown in Appendix A (Table 4-A), plots of the relationship between the current and the potential amplitude are shown in Figure 4.7. For Cd^{2+} , the current gradually increased with the increase of the potential amplitude, while a high standard deviation was found in the potential amplitude of 75mV. For Pb^{2+} , the current slightly increased with the increase of the potential amplitude up to 50 mV and the standard deviation was found to be high. In this instance, the optimum potential amplitude of 50 mV was chosen.

The optimum DPASV and SWASV conditions are summarized in Table 4.3.

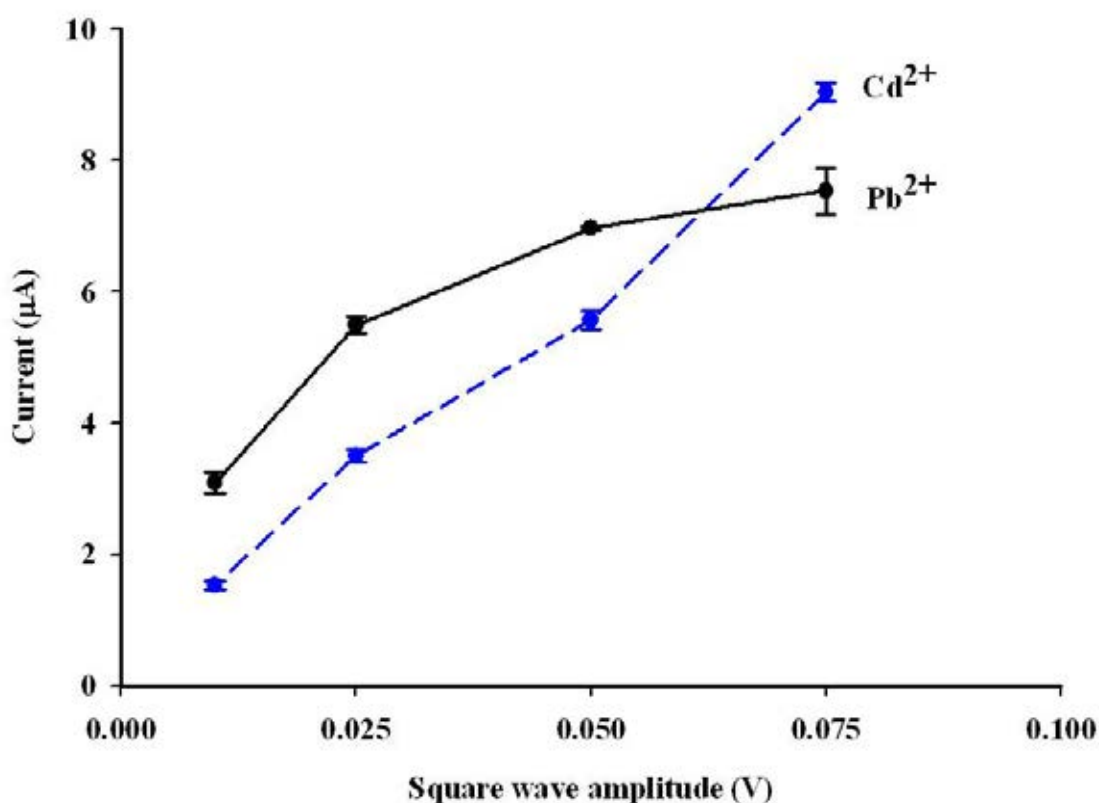


Figure 4.7 The effect of the potential amplitude on the SWASV peak currents for a solution containing $50 \mu\text{g L}^{-1}$ of Cd^{2+} and Pb^{2+} in 1.0 M HCl on the carbon electrode in the micro-flow sensor coupled with the SIA operating system.

Table 4.3 The optimized experimental parameters for the on-line DPASV and SWASV determination of Cd^{2+} and Pb^{2+} using the carbon electrode in micro-flow sensor coupled with SIA operating system.

Parameters	DPASV	SWASV
Deposition potential (V)	-1.20	-1.40
Pulse potential (V)	0.05	-
Pulse time (s)	0.01	-
Potential step (V)	-	0.0075
Potential amplitude (V)	-	0.05
Frequency (Hz)	-	50

The comparisons of the DPASV and the SWASV were carried out. As shown in Table 4.4 and Figure 4.8, the SWASV produced higher peak than the DPASV.

Table 4.4 The peak currents of $50 \mu\text{g L}^{-1}$ of Cd^{2+} and Pb^{2+} in 1.0 M HCl obtained by DPASV and SWASV at the carbon electrode in the micro-flow sensor coupled with the SIA operating system under the optimum conditions.

Current (μA)	Cd^{2+}		Pb^{2+}	
	DPASV	SWASV	DPASV	SWASV
$N = 1$	2.53	9.03	3.61	10.51
$N = 2$	2.33	8.95	3.33	10.07
$N = 3$	2.45	8.96	3.48	10.30
Average \pm SD	2.43 ± 0.10	8.98 ± 0.04	3.47 ± 0.14	10.29 ± 0.22
%RSD	4.18	0.49	3.94	2.14

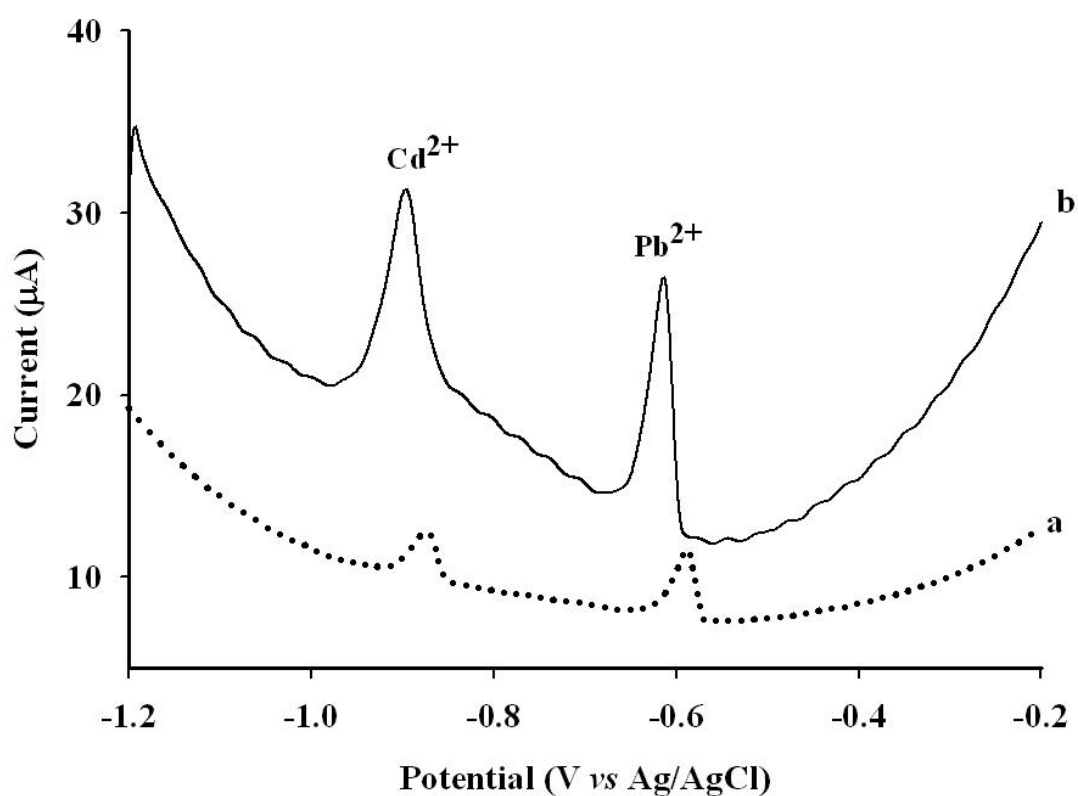


Figure 4.8 Voltammograms of a solution containing $50 \mu\text{g L}^{-1}$ of Cd^{2+} and Pb^{2+} in 1.0 M HCl by (a) DPASV and (b) SWASV on the carbon electrode in the micro-flow sensor coupled with SIA operating system under the optimum conditions.

4.4 Analytical performance

Under the optimum experimental conditions, the electrochemical performances of the on-line DPASV and SWASV of Cd^{2+} and Pb^{2+} in 1.0 M HCl on the carbon electrode in micro-flow sensor coupled with SIA operating system were studied.

The ASV determination of Cd^{2+} and Pb^{2+} was studied in the concentration range of 5.0 to 75.0 $\mu\text{g L}^{-1}$ for Cd^{2+} and 2.5 to 75 $\mu\text{g L}^{-1}$ for Pb^{2+} to obtain the linearity. The average peak currents for three consecutive analysis of the metal ions at various concentrations are shown in Table 4.5 and Table 4.6. The linear calibration plots of Cd^{2+} and Pb^{2+} as well as the corresponding linear regression equations are shown in Figure 4.9 and Figure 4.10

Table 4.5 The DPASV peak currents of Cd^{2+} and Pb^{2+} at various concentrations.

Ions	Concentration ($\mu\text{g L}^{-1}$)	Current (μA)				
		<i>N</i> = 1	<i>N</i> = 2	<i>N</i> = 3	Average \pm SD	%RSD
Cd^{2+}	10	0.33	0.30	0.32	0.32 ± 0.02	5.00
	25	1.33	1.22	1.25	1.27 ± 0.06	4.49
	50	2.53	2.33	2.44	2.43 ± 0.10	4.12
	75	4.15	3.89	4.01	4.02 ± 0.13	3.24
Pb^{2+}	5	0.27	0.26	0.26	0.26 ± 0.01	2.94
	10	0.67	0.64	0.68	0.66 ± 0.02	3.13
	25	2.26	2.19	2.25	2.23 ± 0.04	1.70
	50	3.76	3.91	3.87	3.85 ± 0.08	2.02
	75	6.39	6.43	6.40	6.41 ± 0.02	0.32

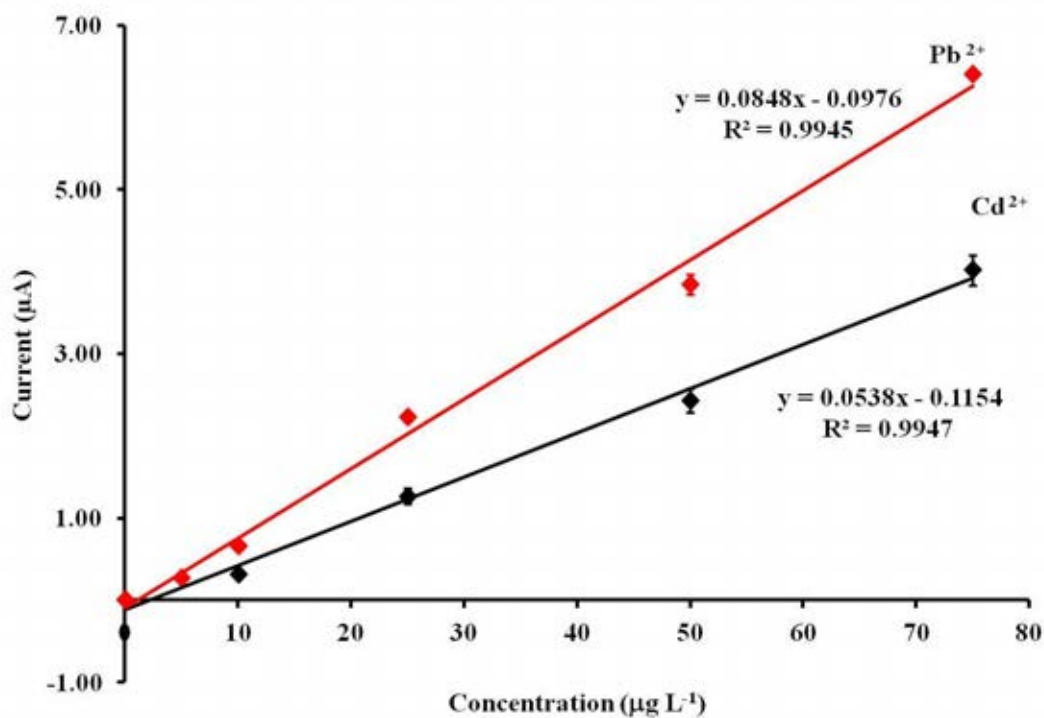


Figure 4.9 Calibration plots of Cd^{2+} and Pb^{2+} obtained from DPASV.

Table 4.6 The SWASV peak currents of Cd^{2+} and Pb^{2+} at various concentrations.

Ions	Concentration ($\mu\text{g L}^{-1}$)	Current (μA)				
		$N = 1$	$N = 2$	$N = 3$	Average \pm SD	%RSD
Cd^{2+}	5.00	0.09	0.10	0.09	0.09 ± 0.00	4.77
	10.00	2.46	2.25	2.38	2.36 ± 0.11	4.48
	25.00	6.94	7.08	6.94	6.99 ± 0.08	1.14
	50.00	12.90	12.30	12.59	12.60 ± 0.30	2.38
	75.00	18.80	19.10	18.96	18.95 ± 0.15	0.79
Pb^{2+}	2.50	0.26	0.27	0.26	0.26 ± 0.01	2.69
	5.00	0.66	0.61	0.62	0.63 ± 0.02	3.91
	10.00	2.68	2.48	2.52	2.56 ± 0.11	4.13
	25.00	9.29	8.98	8.97	9.08 ± 0.18	2.00
	50.00	21.60	20.60	21.10	21.10 ± 0.50	2.37
	75.00	33.84	32.10	33.07	33.00 ± 0.87	2.64

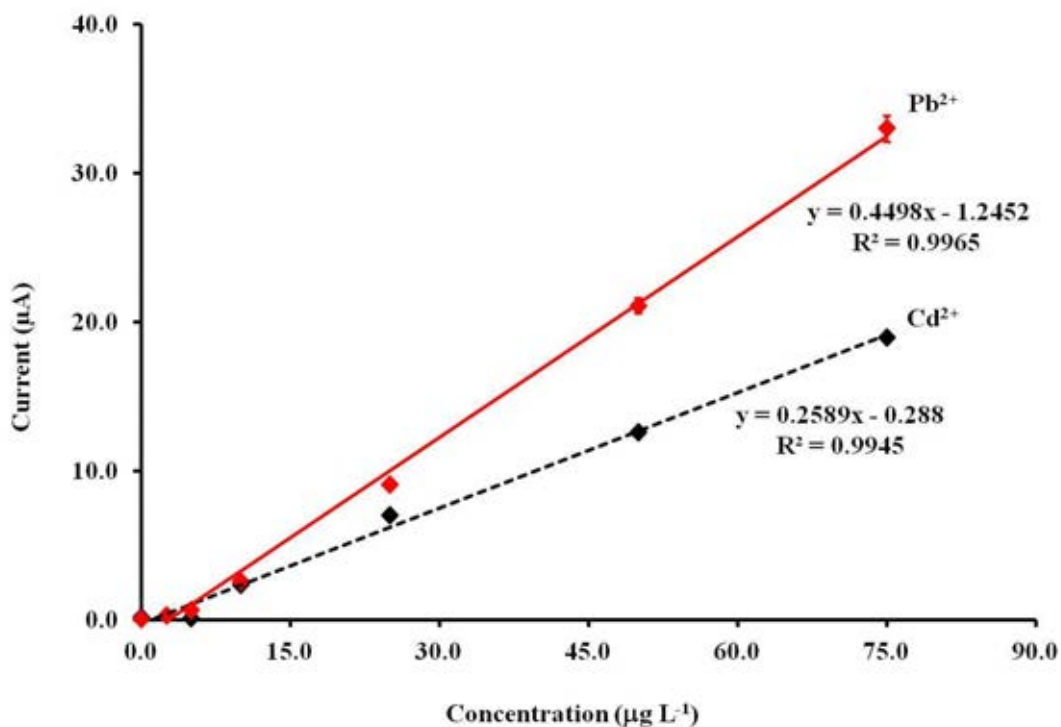


Figure 4.10 Calibration plots of Cd²⁺ and Pb²⁺ obtained from SWASV.

The limits of detection (LOD, the concentration corresponding to three times the standard deviation of the current from the blank solution) and the limit of quantification (LOQ, the concentration corresponding to ten times the standard deviation of the current from the blank solution) were examined. The LOD were 2.37 and 0.15 µg L⁻¹ for the determination of Cd²⁺ and Pb²⁺ by DPASV as well as 0.02 and 0.01 µg L⁻¹ for the determination of Cd²⁺ and Pb²⁺ by SWASV.

The relative standard deviations for the determination of 50 µg L⁻¹ Cd²⁺ and Pb²⁺ by both ASV methods were within the acceptable range, 7.6 % and 4.0 % for DPASV as well as 5.1 % and 3.2 % for SWASV.

Analytical characteristics of both voltammetric methods are summarized in Table 4.7. The obtained results proved that on-line SWASV on the carbon electrode in micro-flow sensor possesses the best analytical characteristics on three key parameters consisting of high sensitivity, good reproducibility and short analysis time.

Table 4.7 Analytical performance of the on-line DPASV and SWASV determination of Cd²⁺ and Pb²⁺ on the carbon electrode in micro-flow sensor coupled with the SIA operating system under the optimal conditions.

Ions	Method	Linear range ($\mu\text{g L}^{-1}$)	R^2	LOD ($\mu\text{g L}^{-1}$)	Average current* \pm SD (μA)	% RSD*
Cd ²⁺	DPASV	10.0 - 75.0	0.9947	2.37	2.50 \pm 0.19	7.6
	SWASV	5.0 - 75.0	0.9945	0.02	13.20 \pm 0.67	5.1
Pb ²⁺	DPASV	5.0 - 75.0	0.9945	0.15	3.41 \pm 0.14	4.0
	SWASV	2.5 - 75.0	0.9965	0.01	13.09 \pm 0.51	3.2

*At the concentration of 50 $\mu\text{g L}^{-1}$ ($N = 3$)

Part II: Highly sensitive determination of Cd^{2+} and Pb^{2+} using a low-cost electrochemical flow-through cell based on a carbon paste electrode

4.5 Design and characterization of the in-house thin-layer flow cell

4.5.1 Optimization of the channel height of the in-house flow cell

The channel height of a thin-layer cell affects the limiting current. Therefore, the dependence of the sensitivity for the determination of Cd^{2+} and Pb^{2+} by SIA-ASV at the Bi-film CPE on the channel height of the thin-layer flow cell was examined at 1.6, 2.0 and 2.5 mm. The obtained voltammograms of $50 \mu\text{g L}^{-1}$ Cd^{2+} and Pb^{2+} in 0.1 M HCl as the supporting electrolyte are presented in Figure 4.11. The average anodic stripping peak currents of each channel height were plotted against the concentrations of Cd^{2+} and Pb^{2+} . The slopes of the average current *vs.* the concentration plot of Cd^{2+} and Pb^{2+} are shown in Table 4.12. Since the highest slope leads to the highest sensitivity, the highest sensitivity was obtained at a channel height of 1.6 mm. As a result, the thin-layer flow cell of 1.6 mm channel height is the flow cell selected for further application.

Table 4.8 Slope and linear range of the current *vs.* concentration plot of Cd^{2+} and Pb^{2+} ions at the Bi-film modified CPE using thin-layer flow cells with a 1.6, 2.0 or 2.5 mm channel height

Channel height (mm)	1.6		2.0		2.5	
Metal ion	Cd^{2+}	Pb^{2+}	Cd^{2+}	Pb^{2+}	Cd^{2+}	Pb^{2+}
Slope of current <i>vs.</i> concentration plot	0.8395	0.5061	0.4424	0.4987	0.1748	0.1440
Linear range ($\mu\text{g L}^{-1}$)	0.25-100	0.25-250	0.5-75	0.5-75	10-150	10-75

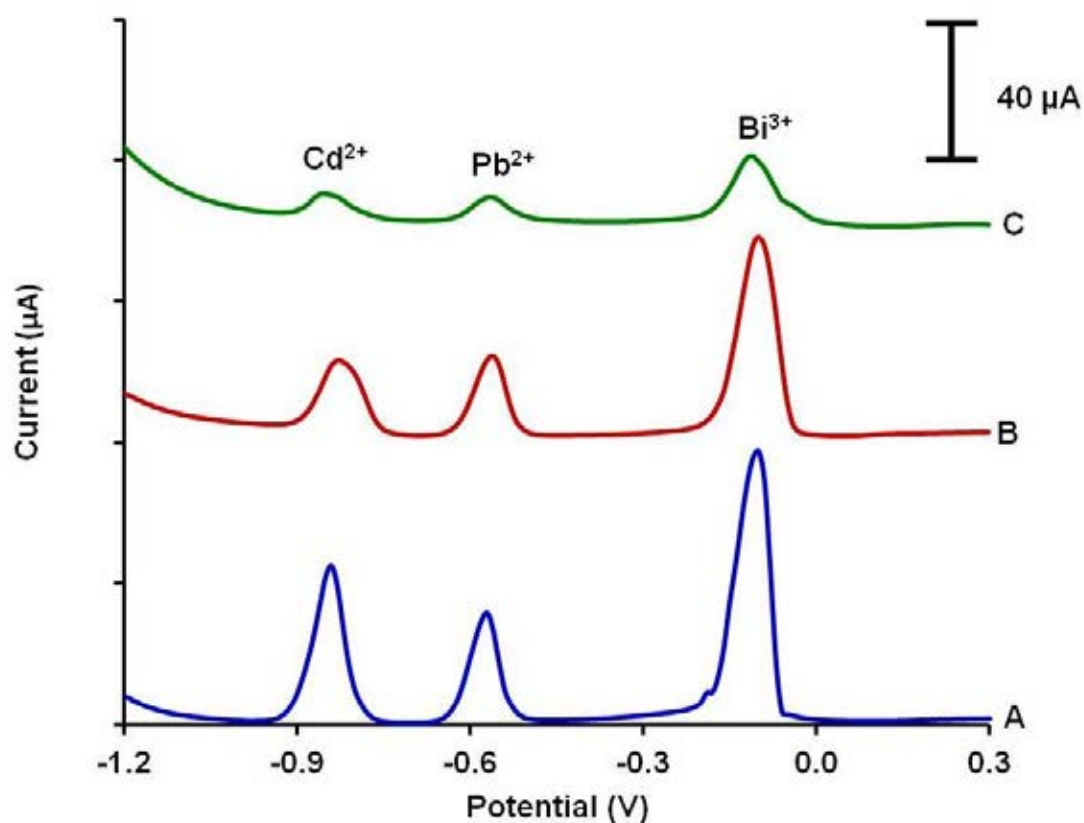


Figure 4.11 The voltammograms of $50 \mu\text{g L}^{-1}$ Cd^{2+} and Pb^{2+} using the in-house designed thin-layer flow cell with a channel height of (A) 1.6 mm, (B) 2.0 mm and (C) 2.5 mm. Voltammograms shown are representative of those seen from five independent repeats.

4.5.2 Characterization of the in-house thin layer flow cell

The thin-layer geometry of the flow cell can be characterized by investigating the relationship between the limiting current (i) and the flow rate (ν) with amperometry, as shown in Eq. (4.1).

$$i = 1.47nFC(DA/b)^{2/3}\nu^{1/3} \quad \text{-----} \blacktriangleright \quad \text{Equation 4.1}$$

where n is the number of electrons, D the diffusion coefficient, A the surface area of working electrode (cm^2), b the channel height (cm) which is the diameter of the flow channel in the in-house designed flow cell, and ν the average flow rate ($\text{cm}^3 \text{s}^{-1}$).

In order to evaluate the thin-layer geometry of the in-house designed flow cell, the amperometric study of $0.1 \text{ M Fe(CN)}_6^{3-}/\text{Fe(CN)}_6^{4-}$ in 0.1 M KCl was performed over a flow rate range from 8.3 to $33.3 \times 10^{-3} \text{ cm}^3 \text{ s}^{-1}$. As shown in Figure 4.12, the observed current signal increased linearly ($R^2 = 0.9958$) with the cube root of flow rate. That the experimental data supported Eq. (1) above then confirms that it is a thin-layer flow cell.

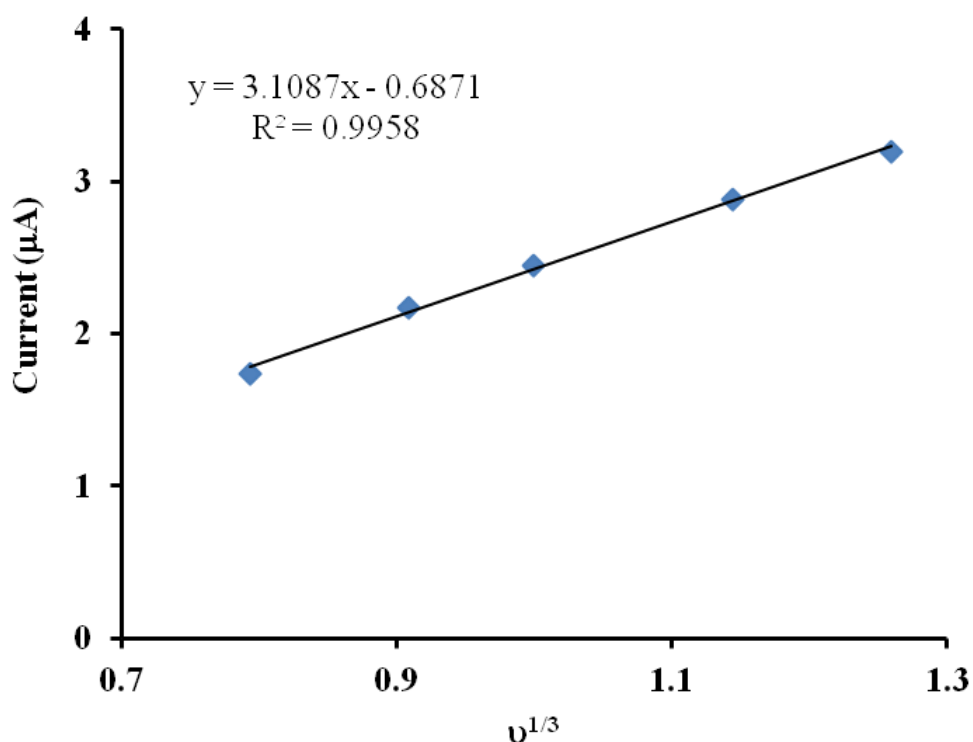


Figure 4.12 The relationship between the current of $0.1 \text{ M Fe(CN)}_6^{3-}/\text{Fe(CN)}_6^{4-}$ in 0.1 M KCl and the cube root of the flow rate.

4.6 Study of Bi-film modification method

4.6.1 *In-situ* modification from Bi^{3+} plating solution

The first method, Bi-film was generated on the CPE in the in-house flow cell by *in-situ* electrodeposition from Bi^{3+} plating solution. The average currents for the SWASV detection of $150 \mu\text{g L}^{-1} \text{ Cd}^{2+}$ and Pb^{2+} at the CPE, $100 \mu\text{g L}^{-1} \text{ Cd}^{2+}$ and Pb^{2+} at the Bi-film CPE modified from the Bi^{3+} plating solution (Bi-CPE) and the

Bi-film CPE modified from Bi_2O_3 nanopowder (BiNP-CPE) in 0.5 M HCl are shown in Table 4.13 and the voltammogram is exhibited in Figure 4.13.

4.6.2 *In-situ* modification from Bi_2O_3 nanopowder (BiNP)

The second method, Bi-film was generated on the CPE by *in-situ* electroreduction of Bi_2O_3 nanopowder previously added to CPE. The average currents and the voltammogram obtained from the SWASV detection of Pb^{2+} $100 \mu\text{g L}^{-1}$ and Cd^{2+} $150 \mu\text{g L}^{-1}$ in 0.5 M HCl using the resulted BiNP-CPE are shown in Table 4.19 and Figure 4.13, respectively.

The results show no significant differences in the current signals between *in-situ* Bi- CPE and *in-situ* BiNP-CPE. However, the BiNP-CPE exhibited a high baseline compared to that of the Bi-CPE. In addition, Bi_2O_3 nanoparticles in the CPE were able to disintegrate from the electrode surface so that irreproducible current signals were obtained. This disintegration is probably caused by the reduction of $\text{Bi}_2\text{O}_3(\text{s})$ to $\text{Bi}(\text{s})$ in the deposition step. Moreover, the stripping out of Cd, Pb and Bi from the surface of the CPE into the solution, and the use of a cleaning solution to remove residual metal ions in the flow system affected the Bi_2O_3 in CPE. This results in some uncertainty of the stripping current due to the irregularity of the Bi-film on the CPE surface for each measurement. Therefore, the modification of Bi on the CPE from Bi^{3+} plating solution was chosen.

Table 4.9 The average peak currents for $150 \mu\text{g L}^{-1}$ Cd^{2+} and Pb^{2+} detected by SWASV at the CPE, $100 \mu\text{g L}^{-1}$ Cd^{2+} and Pb^{2+} at the Bi-film CPE modified from the Bi^{3+} plating solution (Bi-CPE) and the Bi-film CPE modified from Bi_2O_3 nanopowder (BiNP-CPE).

Kind of electrode	Average current \pm SD (μA)	
	Cd^{2+}	Pb^{2+}
CPE	12.10 ± 1.05	8.57 ± 0.77
Bi-CPE	64.10 ± 0.83	52.29 ± 0.19
BiNP-CPE	64.18 ± 2.68	63.21 ± 1.83

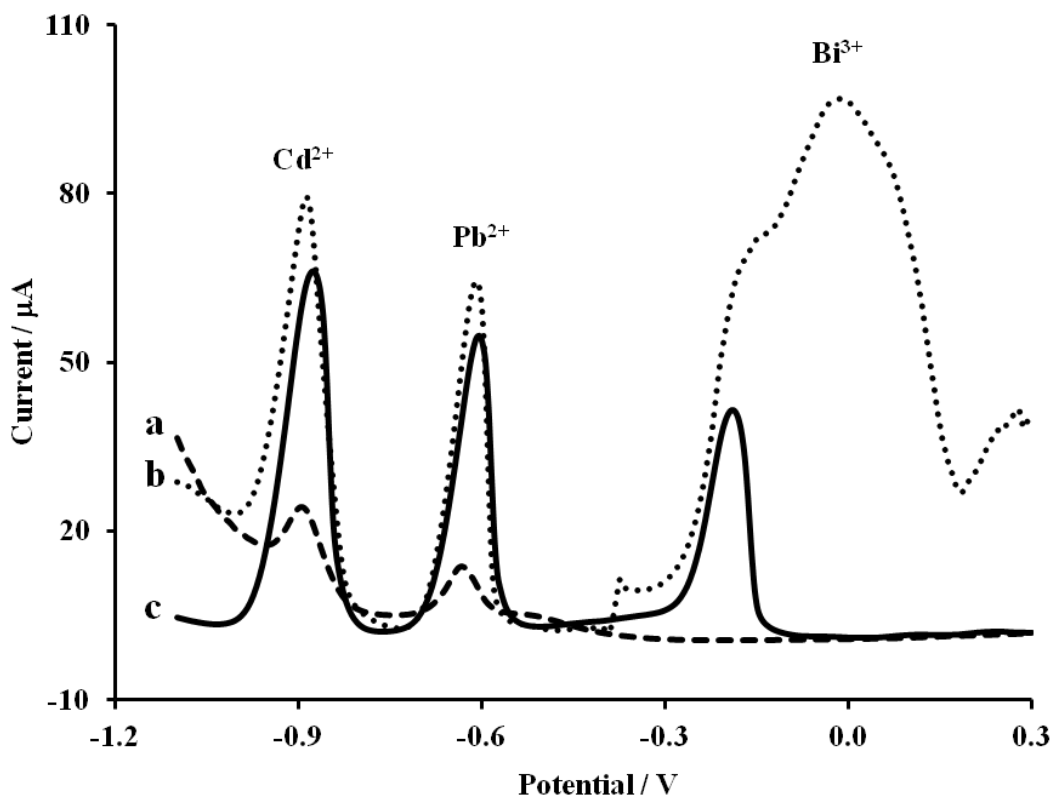


Figure 4.13 The voltammograms of $150 \mu\text{g L}^{-1}$ Cd^{2+} and Pb^{2+} at the CPE (a: dash line), $100 \mu\text{g L}^{-1}$ Cd^{2+} and Pb^{2+} at Bi_2O_3 nanopowder-modified CPE (b: dot line), and the Bi^{3+} plating solution-modified CPEs (c: solid line). Voltammograms shown are representative of those seen from three independent repeats.

4.7 Characterization of Bi-film electrode

4.7.1 Study of the redox behavior

The *in situ* Bi-film modified CPE was characterized by cyclic voltammetry of a $0.5 \text{ mM Fe}(\text{CN})_6^{3-}/\text{Fe}(\text{CN})_6^{4-}$ solution in 0.1 M KCl at a potential range of -0.25 to 0.80 V and a 0.025 V s^{-1} scan rate. The cyclic voltammogram of $0.5 \text{ mM Fe}(\text{CN})_6^{3-}/\text{Fe}(\text{CN})_6^{4-}$ is shown in Figure 4.14. The results exhibited two redox current peaks at $+0.21$ and $+0.27 \text{ V vs. Ag/AgCl (3 M KCl)}$. The separation of the cathodic and anodic peak potentials (ΔE_p) was 0.065 V , with $i_{pc}/i_{pa} = 1.04$, indicating that the electrochemical behavior of the Bi-film CPE for $\text{Fe}(\text{CN})_6^{3-}/\text{Fe}(\text{CN})_6^{4-}$ was a reversible reaction.

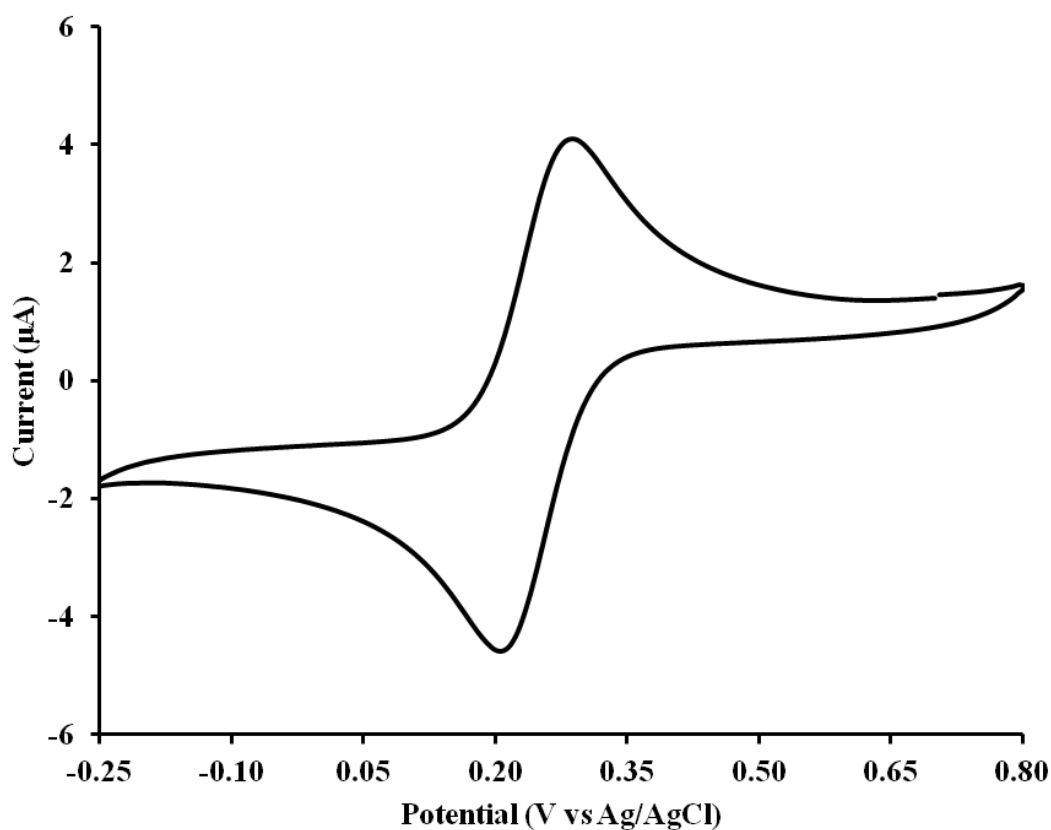


Figure 4.14 Cyclic voltammogram of 0.5 mM $\text{Fe}(\text{CN})_6^{3-}/\text{Fe}(\text{CN})_6^{4-}$ solution in 0.1 M KCl at a potential range of -0.25 to 0.80 V and a 0.025 V s^{-1} scan rate. Cyclic voltammogram shown is representative of those seen from three independent repeats.

4.7.2 Study of the mass transfer process

The rate of the electron transfer was also investigated by cyclic voltammetry of 0.5 mM $\text{Fe}(\text{CN})_6^{3-}/\text{Fe}(\text{CN})_6^{4-}$ solution in 0.1 M KCl. From Randles-Sevcik equation as shown in equation (4.2), the peak current is directly proportional with the root of the scan rate.

$$I_p = 2.69 \times 10^5 n^{3/2} A D^{1/2} C_0^{1/2} \nu^{1/2} \quad \text{-----} \blacktriangleright \quad \text{Equation 4.2}$$

The plot of the relationship between the current and the root of the scan rate is shown in Figure 4.15. The result indicating that the diffusion controlled process occurred on the electrode surface. Therefore, it was suitable to use in the voltammetric technique.

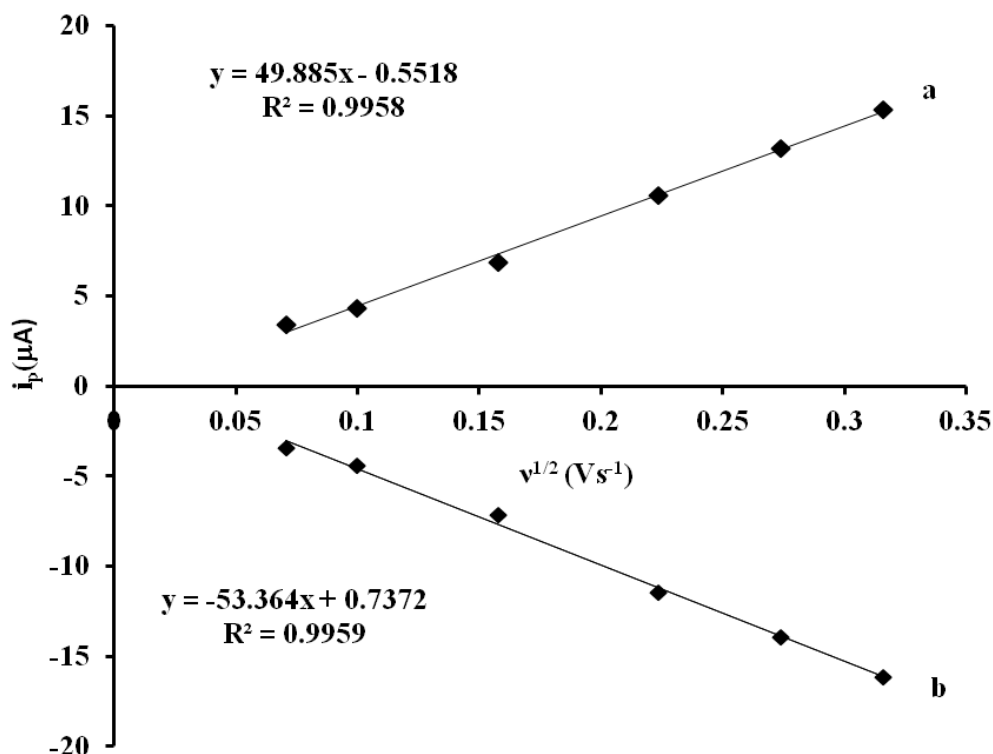


Figure 4.15 The linear relationship of the cathodic current; i_{pc} (a) and the anodic current; i_{ac} (b) versus scan rate ($v^{1/2}$) of 0.5 mM $Fe(CN)_6^{3-}/Fe(CN)_6^{4-}$ solution in 0.1 M KCl. The data is shown as the mean \pm SD, and is derived from three independent repeats.

4.8 Study of the electrode stability

For reliable Cd^{2+} and Pb^{2+} ion detection on the Bi-film modified CPE using the in-house thin-layer flow cell, the stability of the electrode is one of the most important factors. To ascertain the operational stability, the electrodes were tested with $5 \mu g L^{-1}$ Cd^{2+} and Pb^{2+} solution in 0.1 M HCl. The obtained current signals of the electrode as shown in Figure 4.16 were found at 8.59 ± 0.19 and $10.04 \pm 0.29 \mu A$ ($N = 50$) for Cd^{2+} and Pb^{2+} ions, respectively. Moreover, the electrode could be used continuously for at least 12 h without any difference in the potential and current signal. Therefore, the electrode appears to have a good stability and ensuring reproducible quantification even at low metal concentration [146].

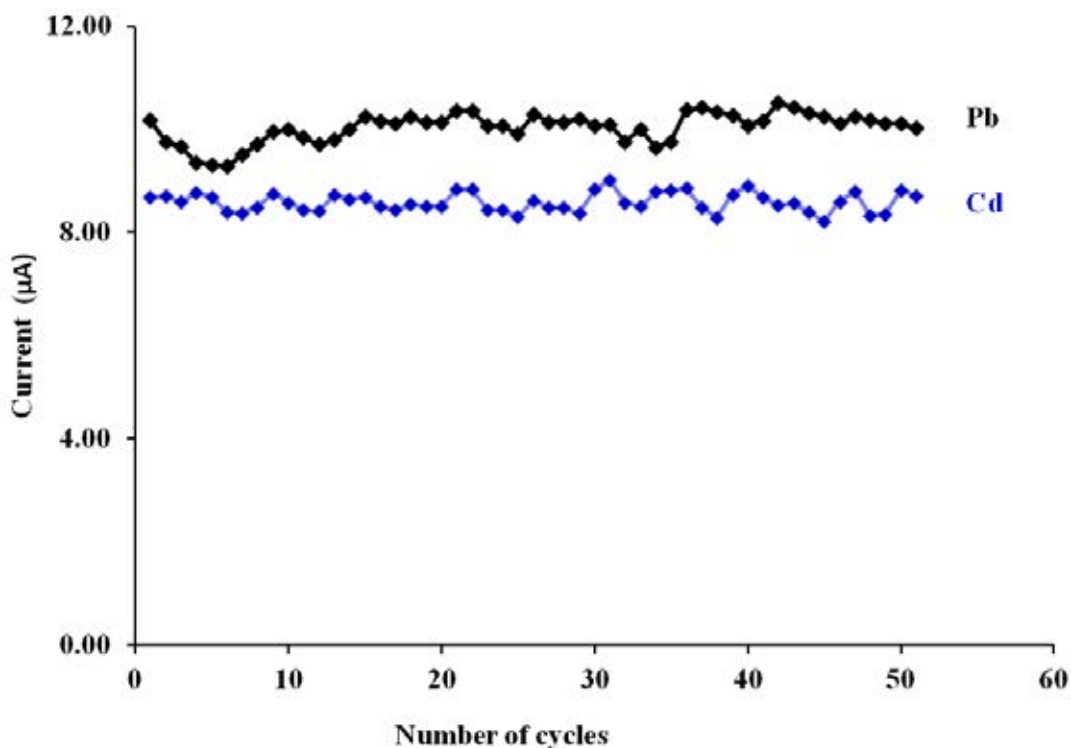


Figure 4.16 The plot of the measurement number and the anodic current of $5 \mu\text{g L}^{-1}$ Cd^{2+} and Pb^{2+} solution in 0.1 M HCl.

4.9 Optimization of the condition for Cd^{2+} and Pb^{2+} analysis

4.9.1 Effect of Bi^{3+} concentration

In the in-house thin-layer flow cell, the effect of Bi^{3+} concentration was evaluated in the range of 0.01 to 10.0 mg L^{-1} . The results in the Figure 4.17 showed that the peak currents of Cd^{2+} and Pb^{2+} significantly increased as the Bi^{3+} concentration increased, reaching a maximum current at a Bi^{3+} concentration of 5 mg L^{-1} . At higher Bi^{3+} concentrations above 5 mg L^{-1} , a decreasing peak current and peak broadening were observed which is likely to be the mass transfer limitation of metal ions diffusing out of the film during the stripping step [147] and the effect of hydrogen evolution. Indeed, the optimum Bi^{3+} concentration has been evaluated for the complete formation of multi-component alloys [148], the prevention of a high hydrogen evolution rate at negative potentials and the saturation effect of Bi-film on the surface of CPE [79, 149, 81]. As reported by Svancara *et al.* [79], the Bi^{3+}

concentration must be 10 times higher than the target analyte concentration to avoid a saturation effect. Thus, a concentration of 5 mg L^{-1} was used as the optimal Bi^{3+} concentration in the preparation of the CPE for this in-house designed thin-layer flow cell.

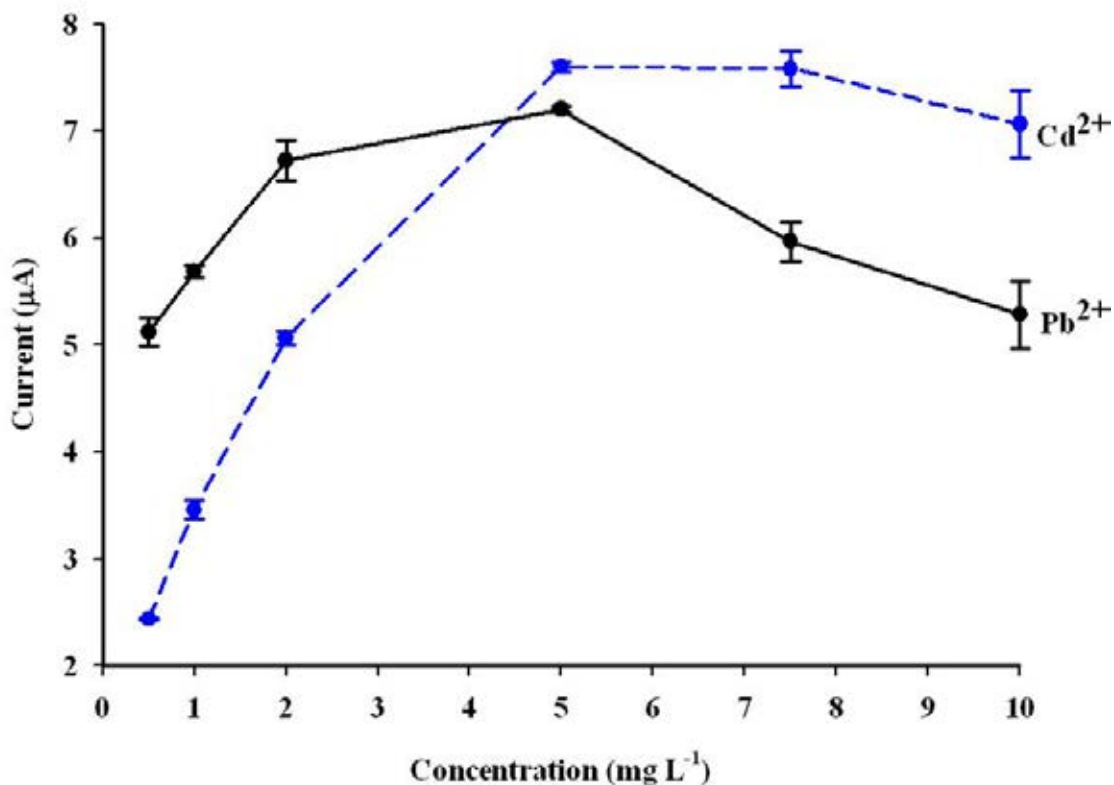


Figure 4.17 Effect of Bi^{3+} concentration on the ASV peak currents of $10 \mu\text{g L}^{-1}$ Cd^{2+} and Pb^{2+} in 0.1 M HCl at a deposition potential of -1.2 V for 140 s . The data are shown as the mean \pm SD, and are derived from three independent repeats.

4.9.2 Optimization of the condition for Cd^{2+} and Pb^{2+} determination using the in-house flow cell and commercial flow cell

4.9.2.1 Effect of HCl concentration

Previously, the best results were reported to be obtained when using HCl as the supporting electrolyte [145]. Thus, in this work the HCl is used as the supporting electrolyte. The HCl concentration was verified from 0.1 to 2.0 M for

in-house thin layer flow cell and commercial flow cell. The relationship between the average current and HCl concentrations for in-house flow cell is shown in Figure 4.18. The corresponding peak was well defined and the maximum peak current was obtained at 0.1 M HCl for the in-house thin-layer flow cell and 0.5 M HCl for the commercial flow cell. From the results, electrochemical oxidation of Cd^{2+} and Pb^{2+} rapidly occurs in the in-house flow-through cell even at the lower concentration of supporting electrolyte (0.1 M HCl). This indicated that the in-house electrochemical flow-through cell provided a better flow profile or homogeneous mixing of the solution in the flow channel than the commercial flow cell.

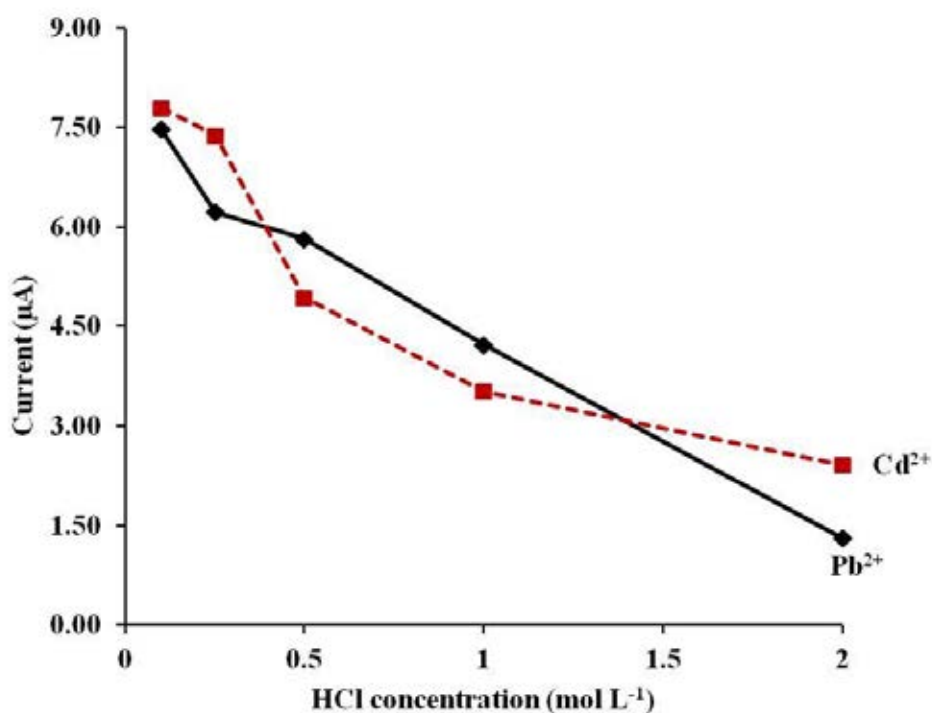


Figure 4.18 Dependence of the average current on the HCl concentration for in-house designed thin-layer flow cell. Conditions: $10 \mu\text{g L}^{-1} \text{Cd}^{2+}$ and $50 \mu\text{g L}^{-1} \text{Pb}^{2+}$ solution in HCl, $500 \text{mg L}^{-1} \text{Bi}^{3+}$, deposition time of 140 s and -1.2 V deposition potential. The data is shown as the mean \pm SD, and is derived from three independent repeats.

4.9.3 Study of the SWASV parameters for Cd^{2+} and Pb^{2+} determination using the in-house thin layer flow cell and the commercial flow cell

4.9.3.1 Effect of the deposition potential

The influence of the deposition potential on the analytical signal was studied in the range of -0.8 to -1.4 V using the deposition time of 140 s. The current responses were recorded with $10 \mu\text{g L}^{-1}$ of Cd^{2+} and Pb^{2+} in 0.1 M HCl for the in-house thin-layer flow cell and 0.5 M HCl for the commercial flow cell. As shown in Figure 4.19 and Figure 4.20, the current signals gradually increased with an increase in the deposition potential until the highest current signals were obtained at -1.2 V and afterwards the signal declined. Therefore, a deposition potential of -1.2 V was selected for all subsequent experiments of both flow cells.

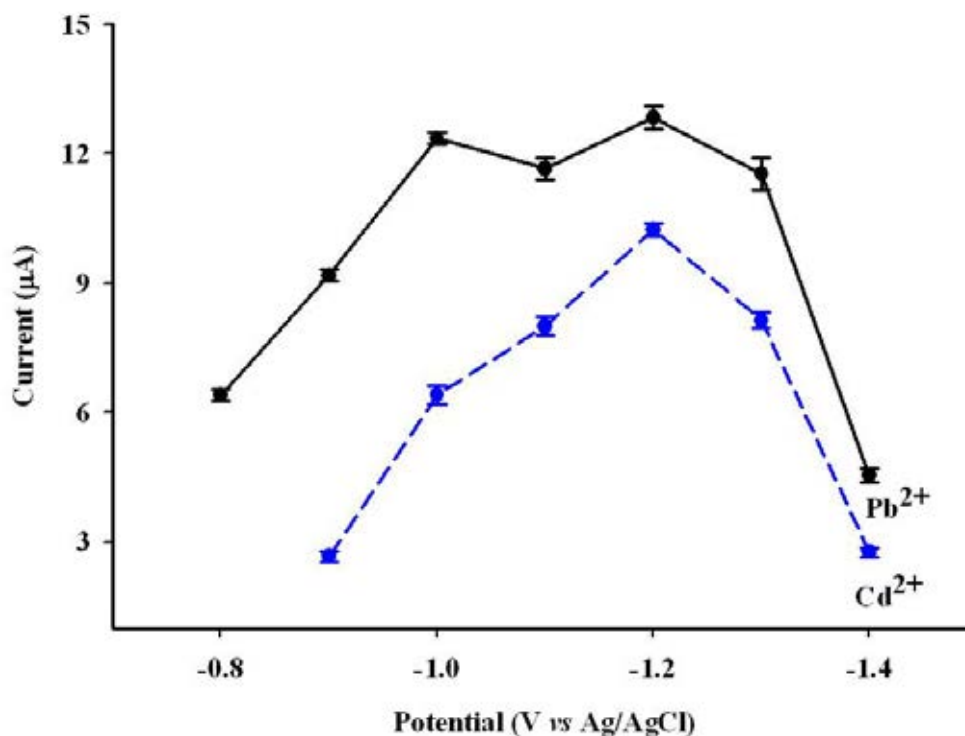


Figure 4.19 Effect of the deposition potential on the SWASV peak currents of $10 \mu\text{g L}^{-1}$ Cd^{2+} and Pb^{2+} in 0.1 M HCl using the in-house flow cell at a deposition potential of -1.2 V for 140 s; The data is shown as the mean \pm SD, and is derived from three independent repeats.

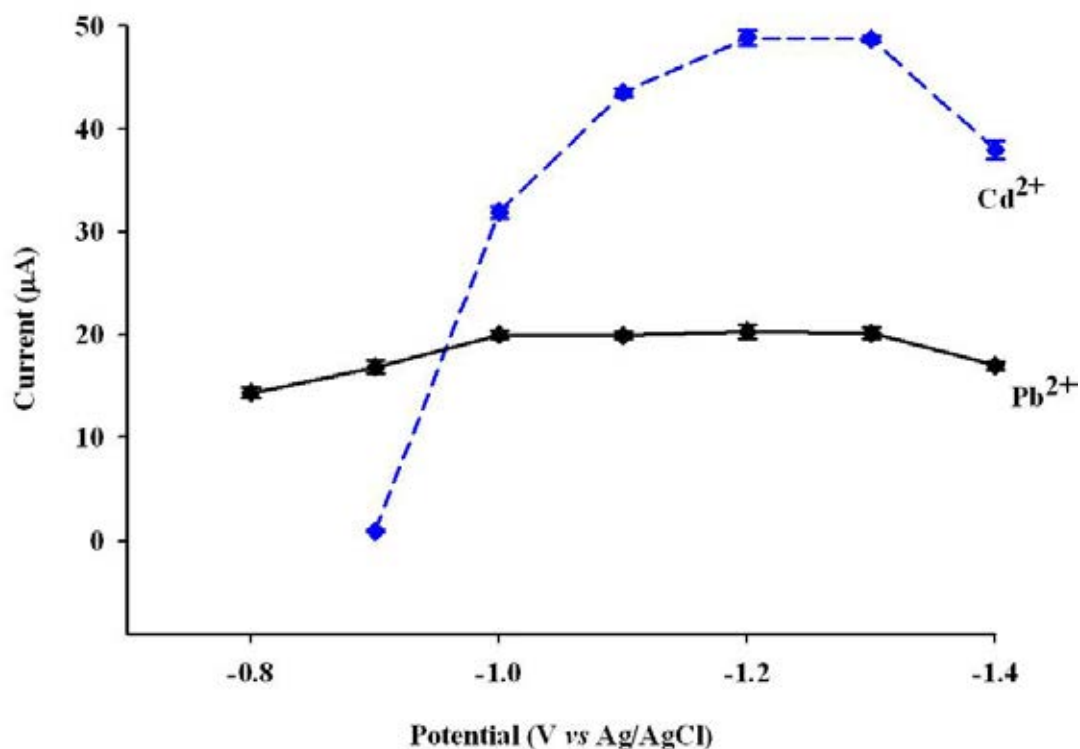


Figure 4.20 The effect of the deposition potential on the ASV peak currents of $100 \mu\text{g L}^{-1} \text{Cd}^{2+}$ and $50 \mu\text{g L}^{-1} \text{Pb}^{2+}$ in 0.5 M HCl using the commercial flow cell at a deposition potential of -1.2 V for 140 s ; The data is shown as the mean \pm SD, and is derived from three independent repeats.

4.9.3.2 Effect of the square wave frequency

The square wave frequency is a critically important parameter that influences the current response. The frequency was studied in the range of 10 to 100 Hz, as shown in Figure 4.21. The current peak heights in the in-house thin-layer flow cell increased with the increasing applied frequency up to the square wave frequency of 50 Hz, and then declined above this. Thus, an applied square wave frequency of 50 Hz gave the best peak heights for the in-house thin-layer flow cell. On the other hand, the current peak height in the commercial flow cell gradually increased from 10 to 100 Hz, as shown in Figure 4.22. Then, the optimum square wave frequency of 75 Hz was chosen for the next experiment in the commercial flow cell because we should not select the optimum value at the limiting value of the instrument.

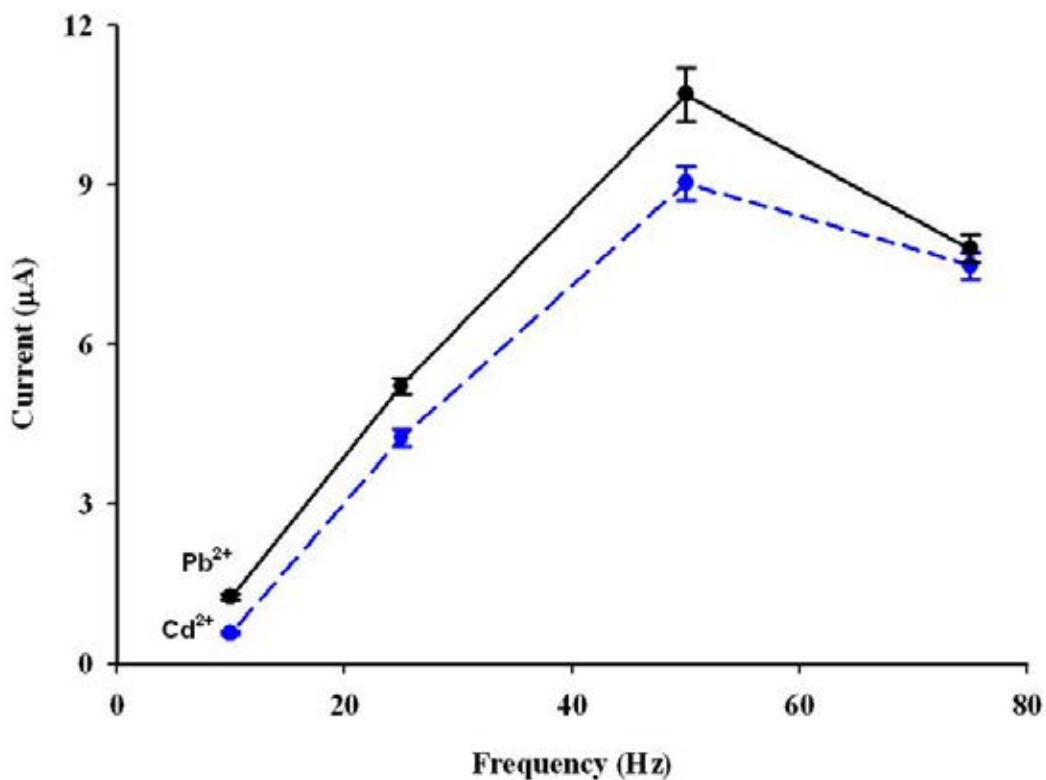


Figure 4.21 The effect of the square wave frequency on the ASV peak currents of $10 \mu\text{g L}^{-1}$ Cd^{2+} and Pb^{2+} in 0.1 M HCl using the in-house flow cell at a deposition potential of -1.2 V for 140 s ; The data is shown as the mean \pm SD, and is derived from three independent repeats.

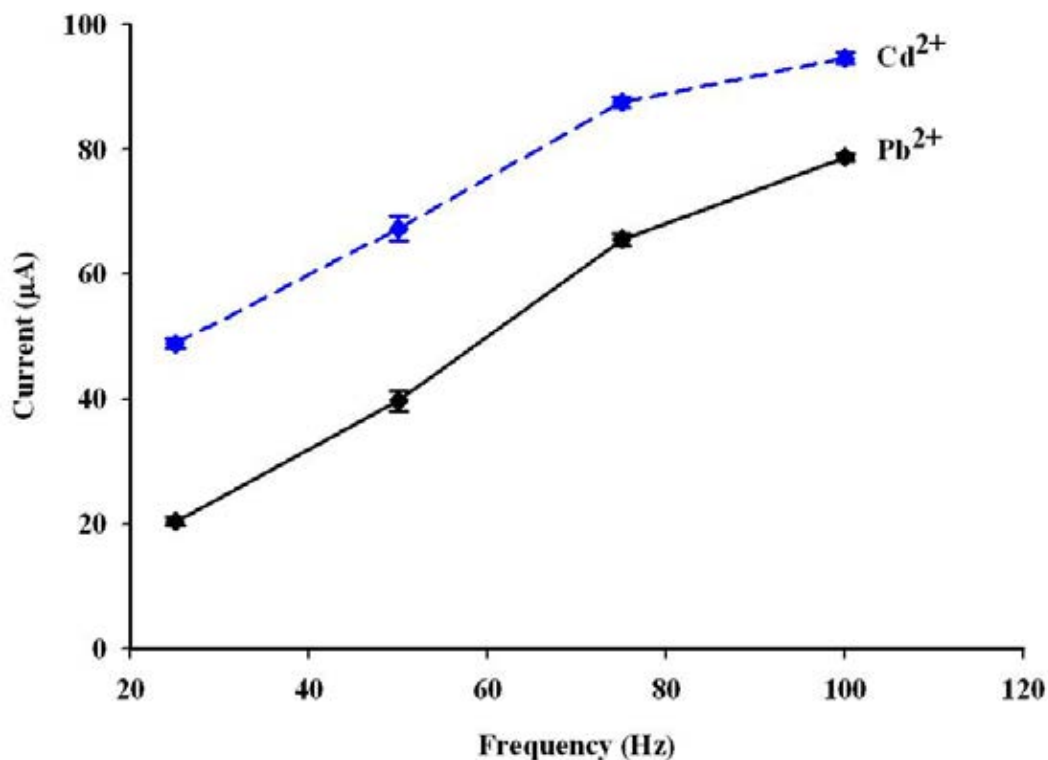


Figure 4.22 The effect of the square wave frequency on the ASV peak currents of $100 \mu\text{g L}^{-1} \text{Cd}^{2+}$ and $50 \mu\text{g L}^{-1} \text{Pb}^{2+}$ in 0.5 M HCl using the commercial flow cell at a deposition potential of -1.2 V for 140 s ; The data is shown as the mean \pm SD, and is derived from three independent repeats.

4.9.3.3 The effect of the step potential and the potential amplitude

The independence of the current on the step potential was investigated in the range of 0.0025 to 0.025 V . The results (Figure 4.23 and Figure 4.24) showed that the peak current increased as the step potential increased for both flow cells. However, a broadening of the metal peak with a low resolution was found when the step potential was higher than 0.01 V . Therefore, a step potential of 0.01 V was chosen for the in-house designed thin-layer flow cell and 0.0075 V was selected for the commercial flow cell.

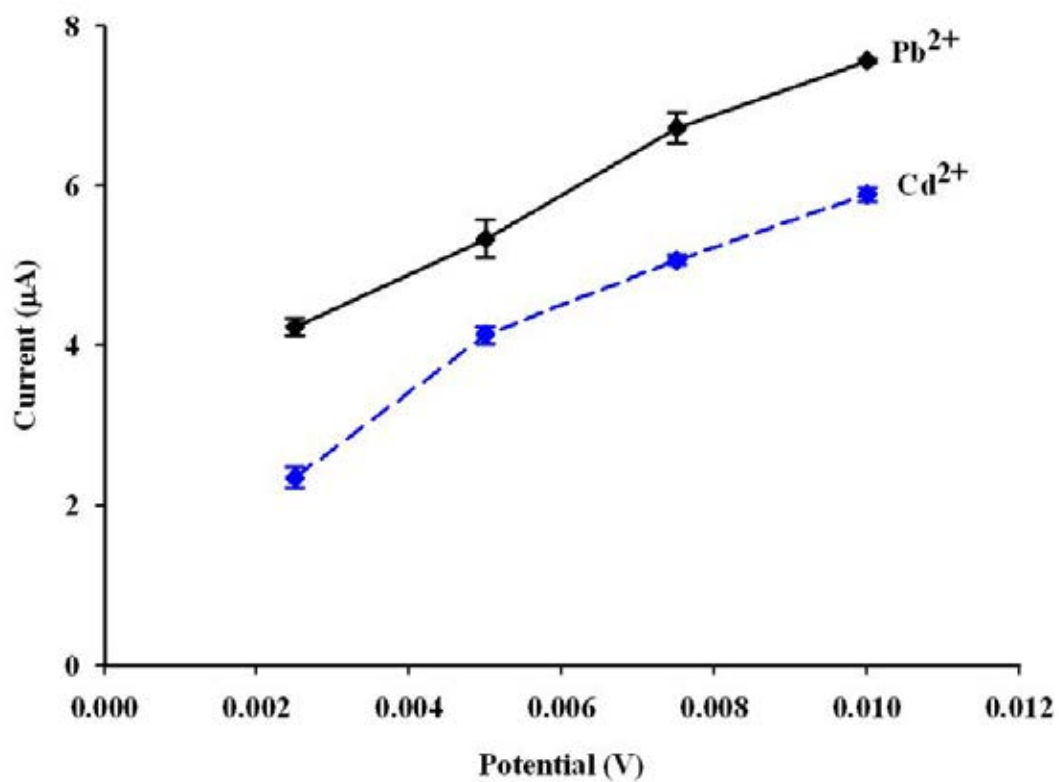


Figure 4.23 The effect of the step potential on the ASV peak currents of $10 \mu\text{g L}^{-1}$ Cd^{2+} and Pb^{2+} in 0.1 M HCl using the in-house flow cell at a deposition potential of -1.2 V for 140 s ; The data is shown as the mean \pm SD, and is derived from three independent repeats.

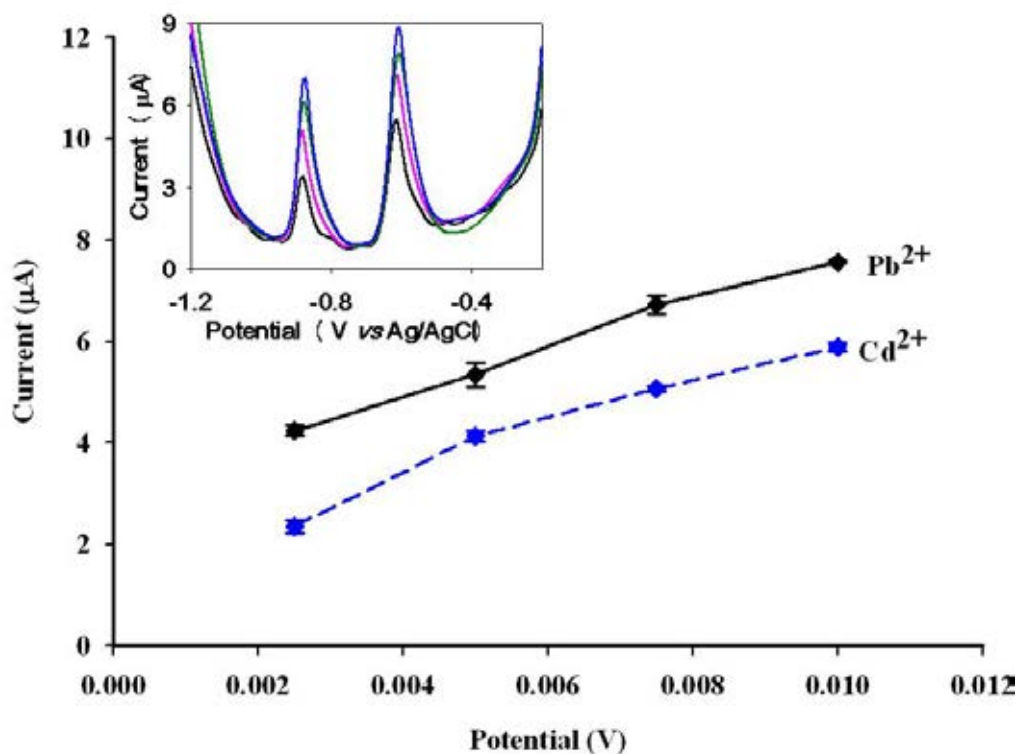


Figure 4.24 The effect of the step potential on the ASV peak currents of $100 \mu\text{g L}^{-1}$ Cd^{2+} and $50 \mu\text{g L}^{-1}$ Pb^{2+} in 0.5 M HCl using the commercial flow cell at a deposition potential of -1.2 V for 140 s ; the in-set is the voltammograms of $100 \mu\text{g L}^{-1}$ Cd^{2+} and $50 \mu\text{g L}^{-1}$ Pb^{2+} in 0.5 M HCl at various step potential; The data is shown as the mean \pm SD, and is derived from three independent repeats.

Lastly, the influence of the square wave pulse height or potential amplitude on the analyte peak currents, within the range of 0.005 to 0.075 V , was evaluated and the results are shown in Figure 4.25 for the in-house thin-layer flow cell and Figure 4.26 for the commercial flow cell. For the in-house thin-layer flow cell, the peak current rapidly increased upon increasing the potential amplitude up to 0.025 V , then slightly increased and reached the maximum value at 0.05 V before declining at 0.075 V . Therefore, 0.05 V was chosen as the optimal potential amplitude. For the commercial flow cell, the increase of the current from 0.005 to 0.075 V was obtained. Then, the applied potential amplitude for the commercial flow cell is 0.075 V . The optimum value of both flow cells were obtained and summarized in Table 4.14.

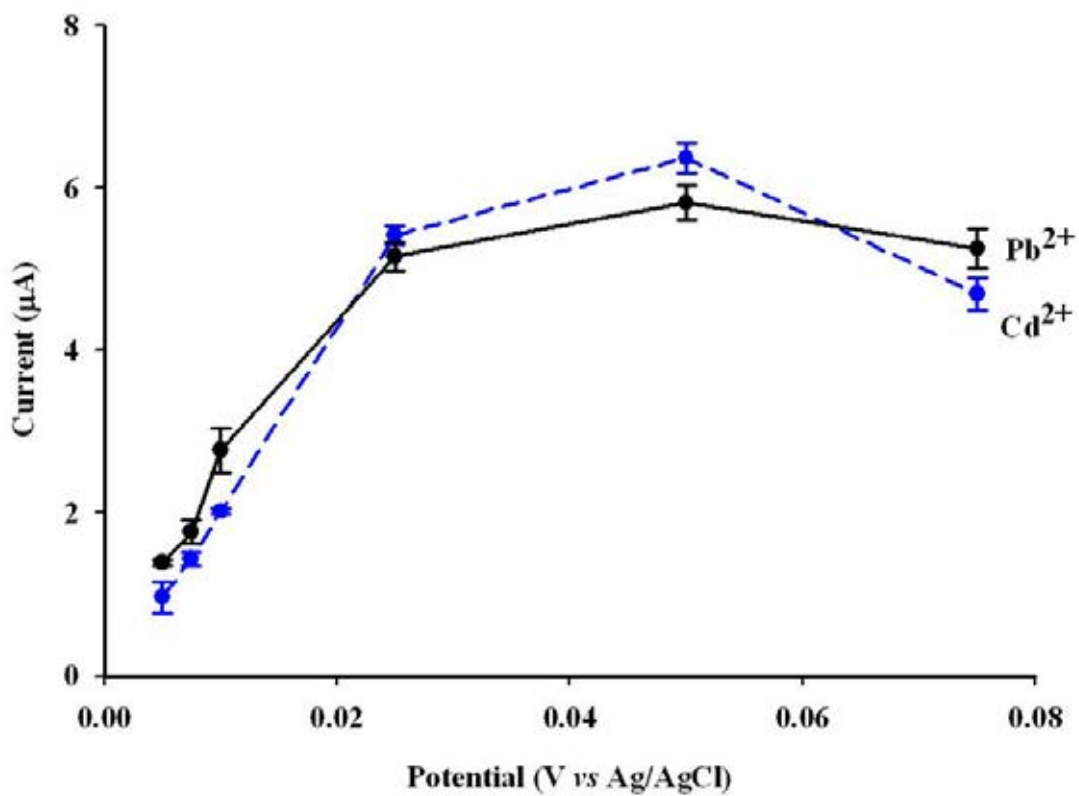


Figure 4.25 The effect of the potential amplitude on the ASV peak currents of $10 \mu\text{g L}^{-1}$ Cd^{2+} and Pb^{2+} in 0.1 M HCl using the in-house flow cell at a deposition potential of -1.2 V for 140 s; The data is shown as the mean \pm SD, and is derived from three independent repeats.

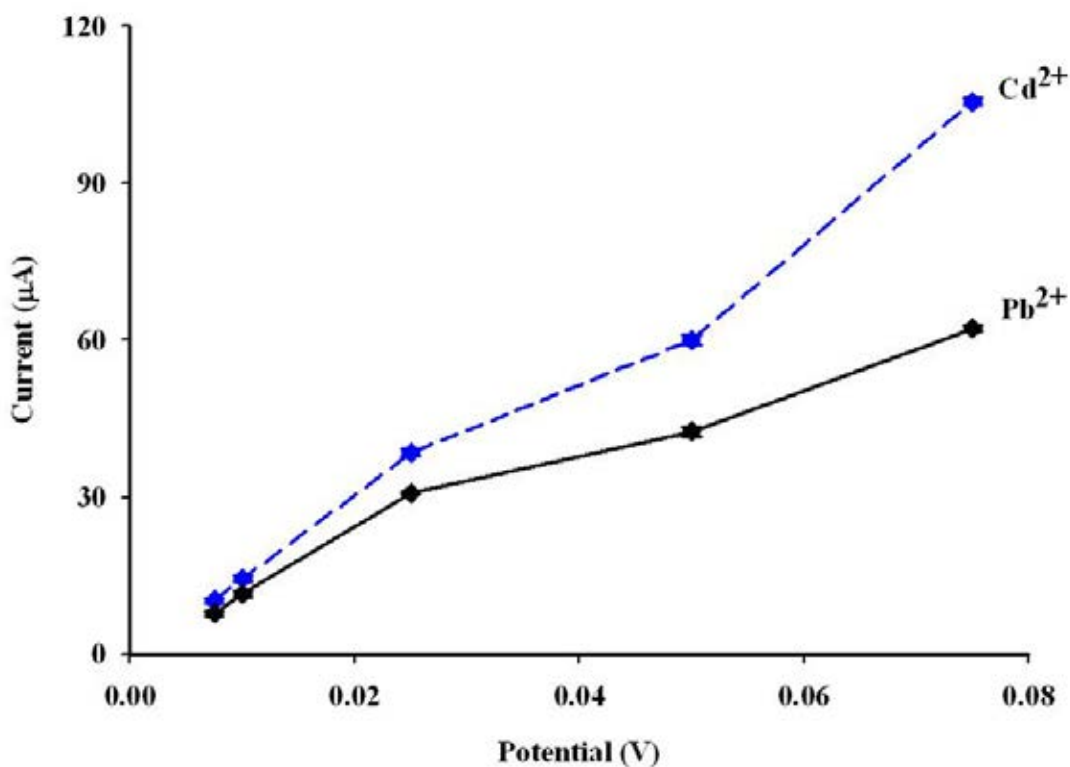


Figure 4.26 The effect of the potential amplitude on the ASV peak currents of $100 \mu\text{g L}^{-1} \text{Cd}^{2+}$ and $50 \mu\text{g L}^{-1} \text{Pb}^{2+}$ in 0.5 M HCl using the commercial flow cell at a deposition potential of -1.2 V for 140 s , The data is shown as the mean \pm SD, and is derived from three independent repeats.

The optimum conditions for both flow cells are summarized in Table 4.10.

Table 4.10 Summary of the optimum conditions in the in-house and commercial flow cells

Parameters	In-house flow cell	Commercial flow cell
HCl concentration (M)	0.1	0.5
Bismuth concentration (mg L^{-1})	5.0	2.0
Deposition potential (V)	-1.20	-1.20
Frequency (Hz)	50	75
Potential step (V)	0.01	0.0075
Potential amplitude (V)	0.05	0.075

4.10 Calibration data

A series of stripping voltammetric measurements of Cd^{2+} and Pb^{2+} in the concentration range of either 0.5 to 75 $\mu\text{g L}^{-1}$ in the commercial flow cell or 0.25 to 500 $\mu\text{g L}^{-1}$ in the in-house designed flow cell were performed under the optimum conditions of each flow cell. The voltammograms for an increasing concentration of Cd^{2+} and Pb^{2+} recorded at the Bi-film modified CPE using the in-house designed flow cell are shown in Figure 4.27. The current response at the Bi-film CPE in the in-house designed thin-layer and the commercial flow cells were plotted against the Cd^{2+} and Pb^{2+} concentrations as shown in Figure 4.28 – 4.31.

In the commercial flow cell, the detection limit and the quantification limit were 1.1 and 3.7 $\mu\text{g L}^{-1}$ for Cd^{2+} and 0.8 and 2.9 $\mu\text{g L}^{-1}$ for Pb^{2+} detection, respectively. Whereas, the in-house designed flow cell revealed LOD values at 13.8- to 11.4-fold lower, 0.08 and 0.07 $\mu\text{g L}^{-1}$ for Cd^{2+} and Pb^{2+} , respectively. The LOQ values were 0.30 and 0.26 $\mu\text{g L}^{-1}$ for Cd^{2+} and Pb^{2+} , respectively.

Analytical characteristics of SWASV at Bi-CPE in both flow cells are summarized in Table 4.11.

Table 4.11 Summary of the analytical performance for the detection of Cd^{2+} and Pb^{2+} ions by the commercial and the in-house designed flow cell

Parameter	Commercial flow cell		In-house designed flow cell	
	Cd^{2+}	Pb^{2+}	Cd^{2+}	Pb^{2+}
Equation	$y = 1.250x + 1.187$	$y = 1.386x + 1.141$	$y = 0.839x + 0.852$	$y = 0.506x + 1.277$
R^2	0.9952	0.9950	0.9966	0.9978
Linear range ($\mu\text{g L}^{-1}$)	2.5 – 50.0	0.5 – 50.0	0.5 – 100	0.25 – 250
LOD ($\mu\text{g L}^{-1}$)	1.1	0.8	0.08	0.07
LOQ ($\mu\text{g L}^{-1}$)	3.7	2.9	0.30	0.26

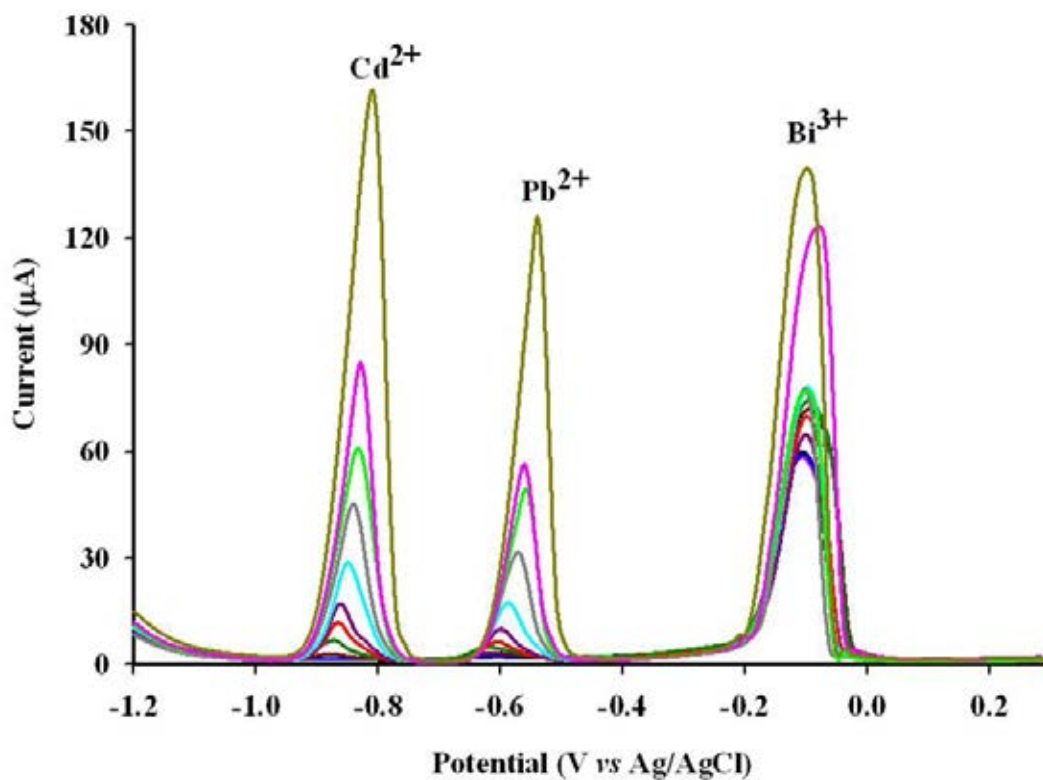


Figure 4.27 The square wave anodic stripping voltammogram for an increasing concentration level of 0.5 - 100 $\mu\text{g L}^{-1}$ Cd^{2+} and 0.25 - 250 $\mu\text{g L}^{-1}$ Pb^{2+} together with background response recorded at *in-situ* Bi-film modified CPE using the in-house designed flow cell. Voltammograms shown are representative of those seen from three independent repeats.

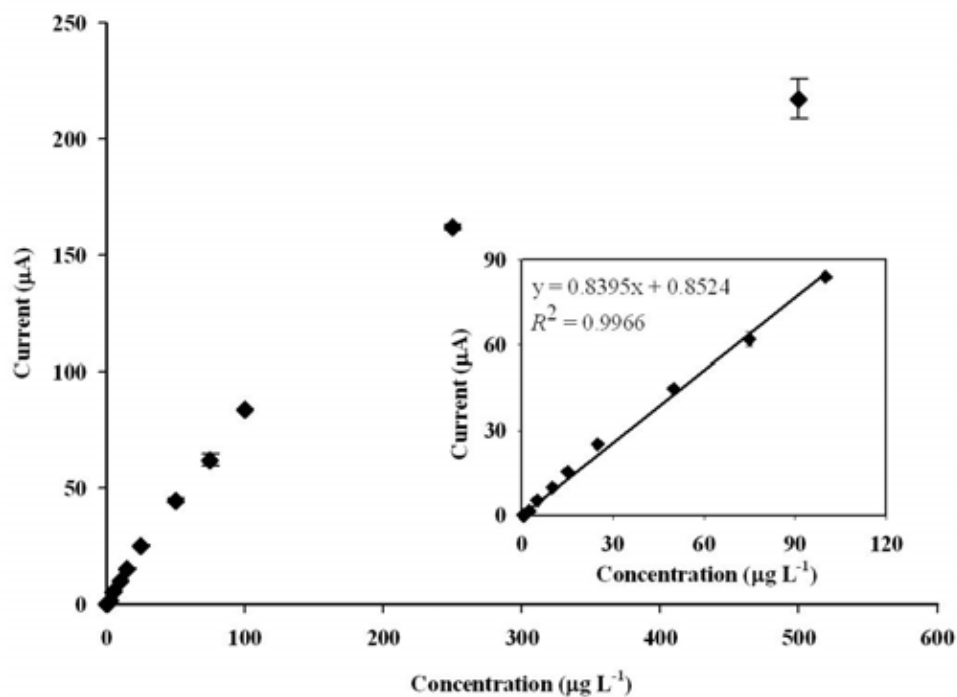


Figure 4.28 Calibration curve of Cd²⁺ by SWASV using *in-situ* Bi-film modified CPE in the in-house designed flow cell.

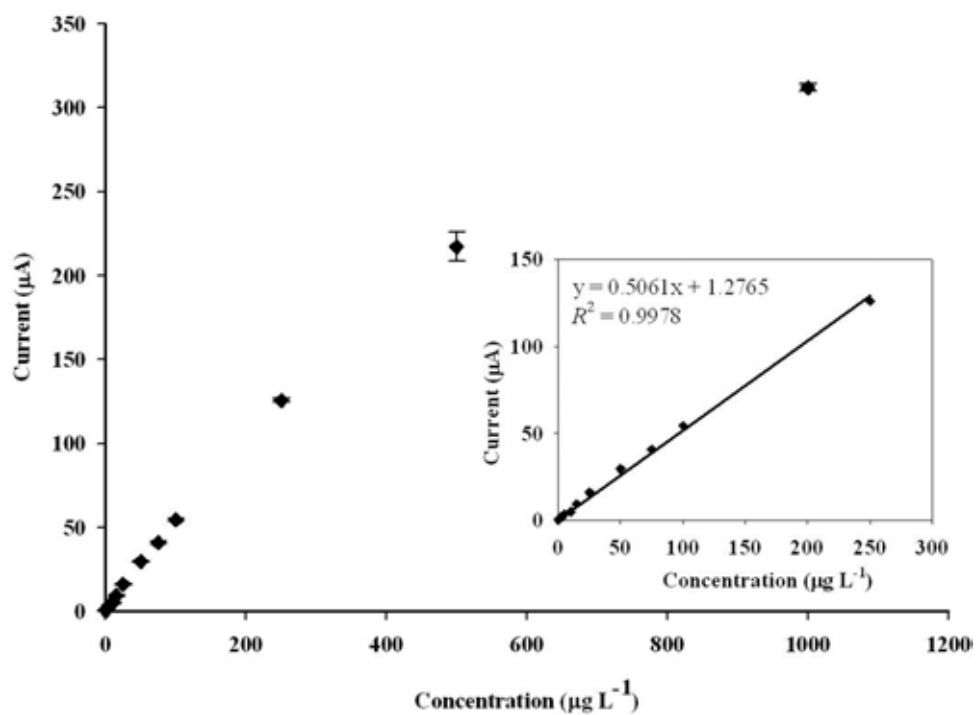


Figure 4.29 Calibration curve of Pb²⁺ by SWASV using *in-situ* Bi-film modified CPE in the in-house designed flow cell.

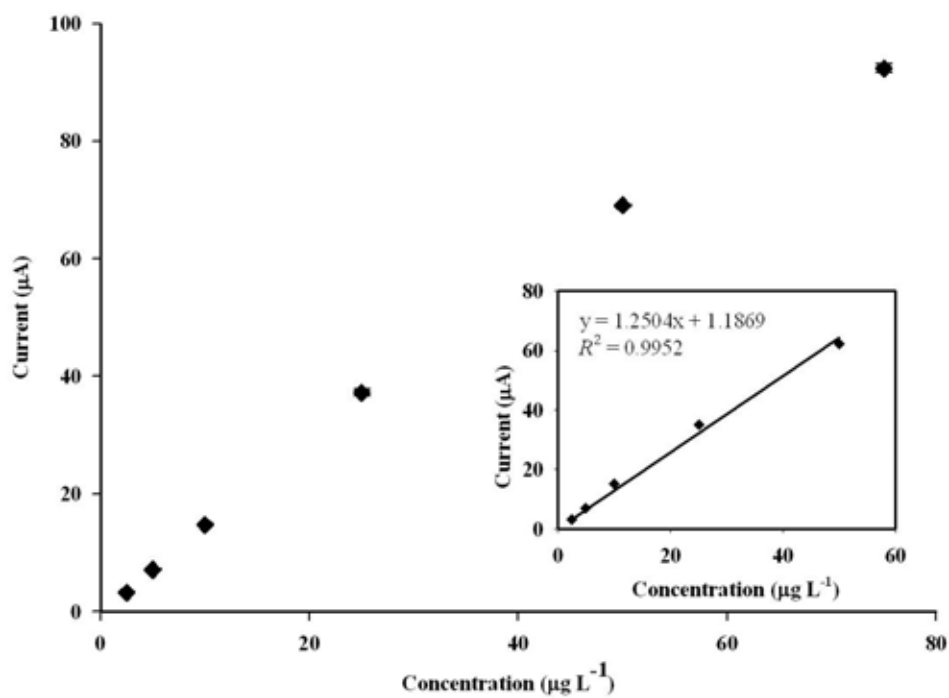


Figure 4.30 Calibration curve of Cd^{2+} by SWASV using *in-situ* Bi-film modified CPE in a commercial flow cell.

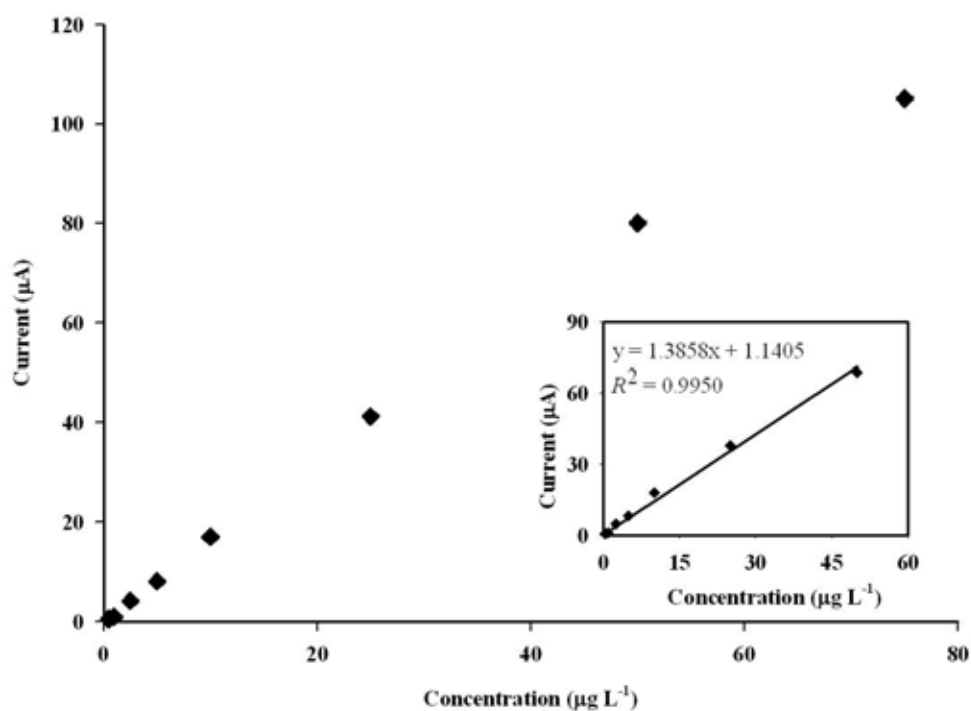


Figure. 4.31 Calibration curve of Pb^{2+} by SWASV using *in-situ* Bi-film modified CPE in a commercial flow cell.

4.11 Applications

Both the commercial and the in-house designed electrochemical flow-through cells, based on the Bi-film modified CPE, were applied to test three types of water samples, including a high organic matter containing pond water, drinking water and tap water. The determination were done with the samples after spiking with 5 or 25 $\mu\text{g L}^{-1}$ of Cd^{2+} and Pb^{2+} . The data obtained is summarized in Table 4.12.

The determination of Cd^{2+} and Pb^{2+} levels in the spiked drinking and tap water samples, using both the in-house designed and a commercial thin-layer flow cell, showed good recoveries, but in general, the in-house designed flow cell showed higher recoveries than the commercial one. The Bi-film CPE coupled with the electrochemical flow-through cell was also applied to untreated pond water that contained an abundant level of organic matter; the results confirmed that the in-house designed flow cell and electrode had been successfully developed for the determination of trace heavy metals.

Table 4.12 Determination of the Cd²⁺ and Pb²⁺ ion levels in water samples (*N* = 3)

Water sample	Added ($\mu\text{g L}^{-1}$)	Commercial flow-through cell			
		Found ($\mu\text{g L}^{-1}$)		Recovery (%)	
		Cd ²⁺	Pb ²⁺	Cd ²⁺	Pb ²⁺
Drinking water	0	< QL	< QL	< QL	< QL
	5	4.63 ± 0.03	4.55 ± 0.05	92.6 ± 0.6	91.0 ± 0.9
	25	25.6 ± 0.1	25.6 ± 0.4	102.6 ± 0.5	102.5 ± 1.5
Tap water	0	< QL	< QL	< QL	< QL
	5	4.20 ± 0.12	4.77 ± 0.20	84.0 ± 2.3	95.3 ± 4.05
	25	25.7 ± 0.4	26.6 ± 0.1	103.0 ± 1.6	106.3 ± 0.36
Pond water	0	< QL	< QL	< QL	< QL
	5	3.76 ± 0.23	3.85 ± 0.17	75.1 ± 4.5	77.0 ± 3.5
	25	18.7 ± 0.4	20.3 ± 0.6	75.0 ± 1.5	81.4 ± 2.4
Water sample	Added ($\mu\text{g L}^{-1}$)	In-house designed flow-through cell			
		Found ($\mu\text{g L}^{-1}$)		Recovery (%)	
		Cd ²⁺	Pb ²⁺	Cd ²⁺	Pb ²⁺
Drinking water	0	< QL	< QL	< QL	< QL
	5	4.65 ± 0.11	5.42 ± 0.04	93.0 ± 2.3	108.5 ± 0.7
	25	22.4 ± 0.04	24.5 ± 0.10	89.7 ± 0.2	98.0 ± 0.4
Tap water	0	< QL	< QL	< QL	< QL
	5	4.33 ± 0.03	4.11 ± 0.06	86.6 ± 0.7	82.2 ± 1.2
	25	25.8 ± 0.04	24.6 ± 0.09	103.3 ± 0.2	98.4 ± 0.4
Pond water	0	< QL	< QL	< QL	< QL
	5	5.03 ± 0.17	4.69 ± 0.22	100.5 ± 3.4	93.8 ± 4.4
	25	26.5 ± 0.68	25.4 ± 1.76	106.2 ± 2.7	101.6 ± 7.0

Part III: Graphene-modified carbon paste electrode for Cd^{2+} and Pb^{2+} monitoring with flow based system

4.12 Structural characterization of graphene and graphite powder

The Fourier transform infrared (FT-IR) spectra of the as-used graphite and graphene samples are shown in Figure 4.32. The spectra of graphite and graphene showed similar band positions, except that the transmission band of graphite exhibited much stronger bands for the O-H ($3,400\text{ cm}^{-1}$), the C=O ($1,736$ and $1,641\text{ cm}^{-1}$) and the C-O groups ($1,473$ to $1,379\text{ cm}^{-1}$) compared to graphene [14,40–43]. Thus, the oxygen-containing groups were observed at much higher density on the graphite than on the graphene. Therefore, a lower background current might be obtained from the graphene, while the oxide groups on the graphite electrode surface would most likely decrease the sensitivity of the analyte peak during electrochemical detection.

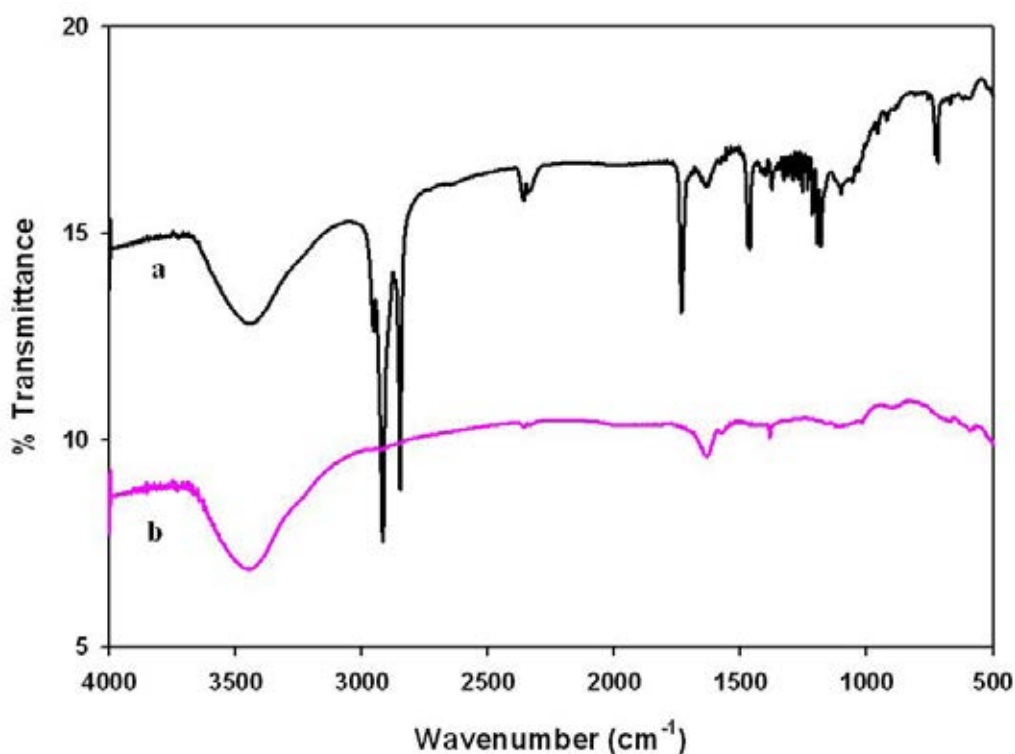


Figure 4.32 FT-IR spectra of the as-used (a) graphite and (b) graphene samples.

4.13 Electrochemical behavior of Graphene-Carbon Paste Electrode (GCPE)

Presently, graphene can be considered as an ideal material for electrochemical analysis because they showed fast electron-transfer kinetics for the redox substance [112]. In order to test the redox properties of the graphene-carbon paste electrode (GCPE), the electrochemical redox response of 0.5 mM $\text{K}_3\text{Fe}(\text{CN})_6/\text{K}_4\text{Fe}(\text{CN})_6$ in 0.1 M HCl is used. Figure 4.33 shows the cyclic voltammetric curves of 0.5 mM $\text{K}_3\text{Fe}(\text{CN})_6/\text{K}_4\text{Fe}(\text{CN})_6$ solution at GCPE compared to that of CPE. From the voltammograms, the electron transfer is diffused on the electrode surface, while they have well defined reversible peak on the GCPE surface. The oxidation peaks on the CPE and GCPE surface were observed at approximately 0.4 and 0.3 V *vs.* Ag/AgCl, respectively. While, the reduction peaks on the CPE and GCPE surface were observed at approximately 0 and 0.2 V *vs.* Ag/AgCl, respectively. Incidentally, it can be easily understood that the GCPE was able to better show the electrochemical redox behavior than the bare CPE. From this phenomenon, graphene was chosen for modifying the electrode surface in this part.

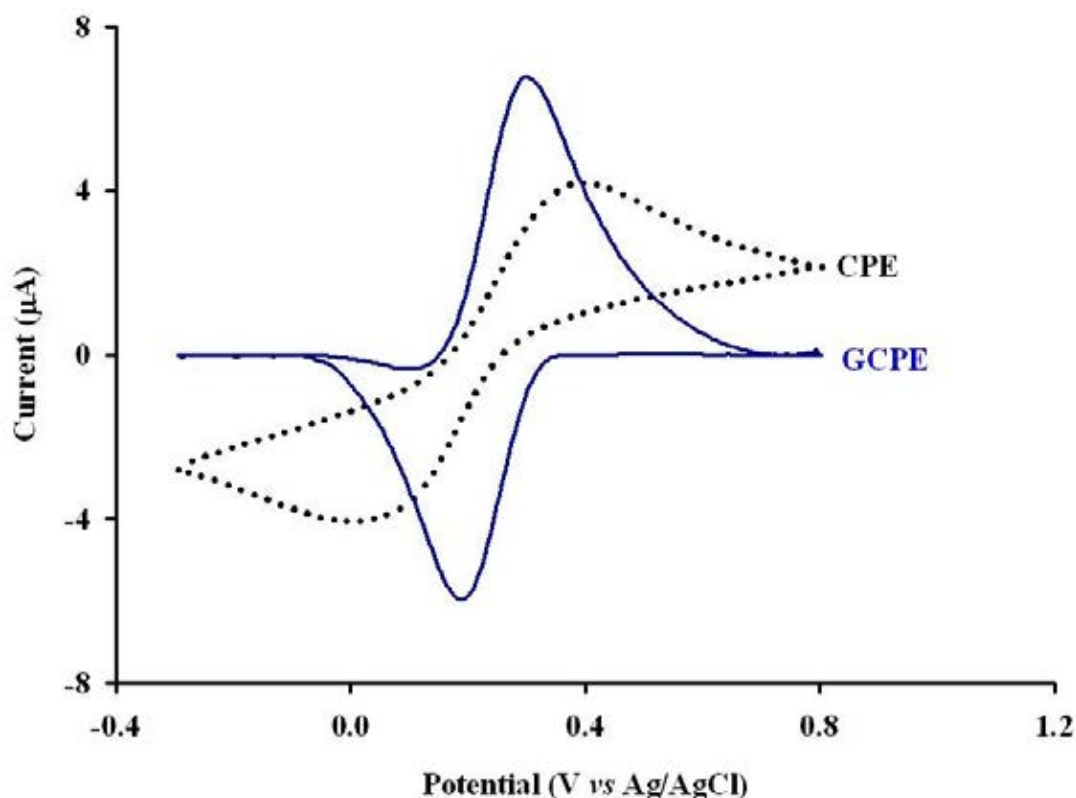


Figure 4.33 Cyclic voltammograms of 0.5 mM $\text{K}_3\text{Fe}(\text{CN})_6/\text{K}_4\text{Fe}(\text{CN})_6$ in 0.1 M HCl on bare CPE and GCPE (The weight ratio of the carbon powder toward graphene powder is 1 : 5). The scan rate is 50 mV s^{-1} . The voltammograms shown are representative of those seen from three independent repeats.

4.14 Effect of the parameters on the GCPE measurement

4.14.1 Effect of mass ratio of graphene/carbon paste

The amount of graphene mixed with the carbon paste has an effect on the electrical conductivity [136,144]. The weight fraction of graphene in the GCPE was evaluated by varying weight of graphene from 0.5 to 5.0 mg in a constant weight of graphite nanopowder. The electrochemical response of $10 \mu\text{g L}^{-1} \text{Cd}^{2+}$ and Pb^{2+} was used to characterize the electrical conductivity of different amounts of graphene in GCPE. Figure 4.34 shows the peak current of Cd^{2+} and Pb^{2+} on bare CPE and GCPE with different amount of graphene. From the experiment, it was found that Cd^{2+} and Pb^{2+} exhibited a poor current response on the bare CPE. The GCPE showed a slight

improvement in the electrochemical response of Cd^{2+} and Pb^{2+} of Cd^{2+} and Pb^{2+} with an increase in the amount of graphene until the highest current responses were obtained at 5.0 mg of graphene and subsequently the signals decreased. In order to receive the best electrochemical responses, 5.0 mg was chosen as the proper amount of graphene.

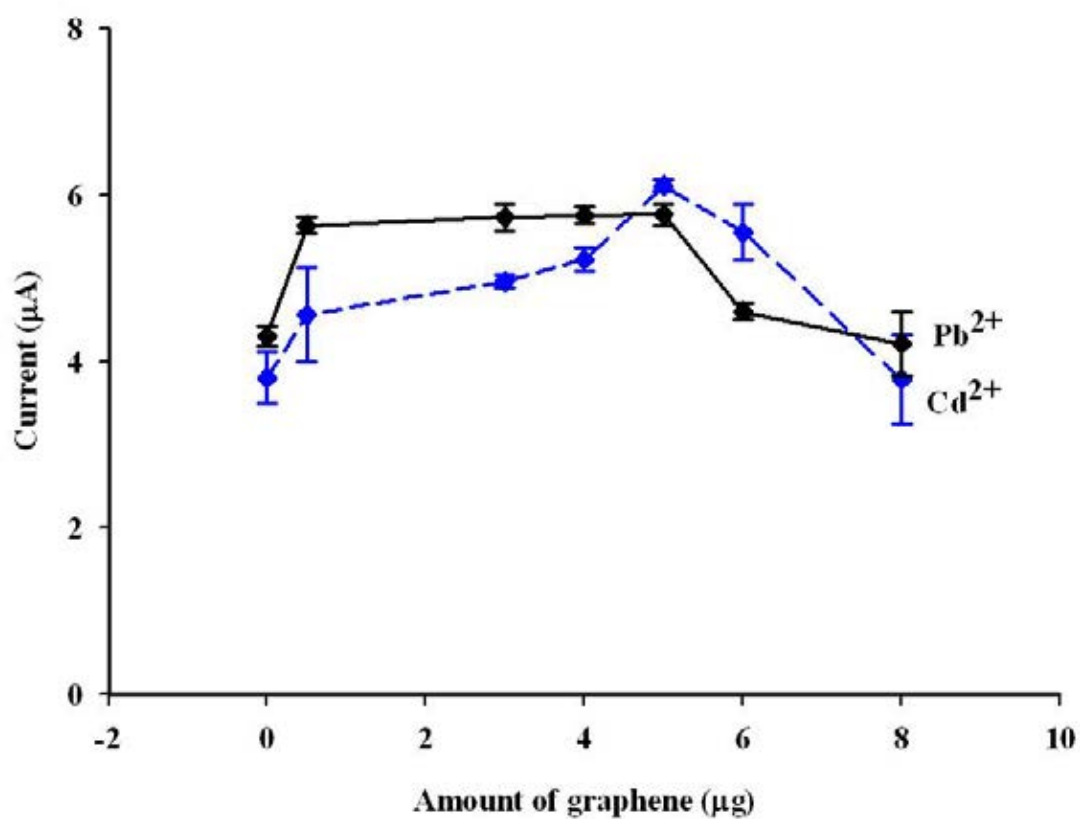


Figure 4.34 The relationship between current responses towards the amount of graphene in the GCPE registered with SWASV of $10 \mu\text{g L}^{-1}$ Pb^{2+} and Cd^{2+} in 0.1 M HCl. The data is shown as the mean \pm SD, and is derived from four independent repeats.

4.14.2 The optimal Bi^{3+} concentration used to modify the GCPE

The coating of electrodes with a Bi film is a well-known method that is used to prevent the electrode surface from degradation by chlorine gas in the supporting electrolyte (HCl) during oxidation, which results in a more reproducible

peak current [150]. Therefore, a Bi film was selected to modify the GCPEs in this work. The Bi film thickness on the GCPE was first optimized because the diffusion process of the analyte onto the electrode surface is reported to be influenced by the film thickness. To obtain a satisfactory mechanical film stability and current signal, the influence of the Bi^{3+} ion concentration in the plating solution was evaluated from 1.0 to 5.0 mg L^{-1} for a fixed plating time, and the resulting Bi-GCPEs were evaluated using a deposition potential of -1.25 V, a SW frequency of 50 Hz and a step potential of 0.01 V (Figure 4.35). The mean anodic peak current for the 10 $\mu\text{g L}^{-1}$ Cd^{2+} solution increased as the Bi^{3+} concentration in the plating solution increased up to 4.0 mg L^{-1} and then decreased at 5.0 mg L^{-1} , whereas the mean anodic peak current for the 10 $\mu\text{g L}^{-1}$ Pb^{2+} solution continuously increased and was maximal at 5.0 mg L^{-1} (the highest tested concentration). The high concentration of the Bi^{3+} solution may cause different forms of Cd-Bi and Pb-Bi intermetallic compounds that result in the partial or full dissociation of metal complex compounds during the stripping step. This phenomenon is likely to be the mass transfer limitation of Cd^{2+} diffusing out of the film during the stripping step, whereas Pb^{2+} continued to diffuse out. Therefore, an optimum concentration of 4.0 mg L^{-1} for the Bi^{3+} plating solution was chosen for all further work as a compromise between the best sensitivity for both Cd^{2+} and Pb^{2+} detection and the minimum measurement error.

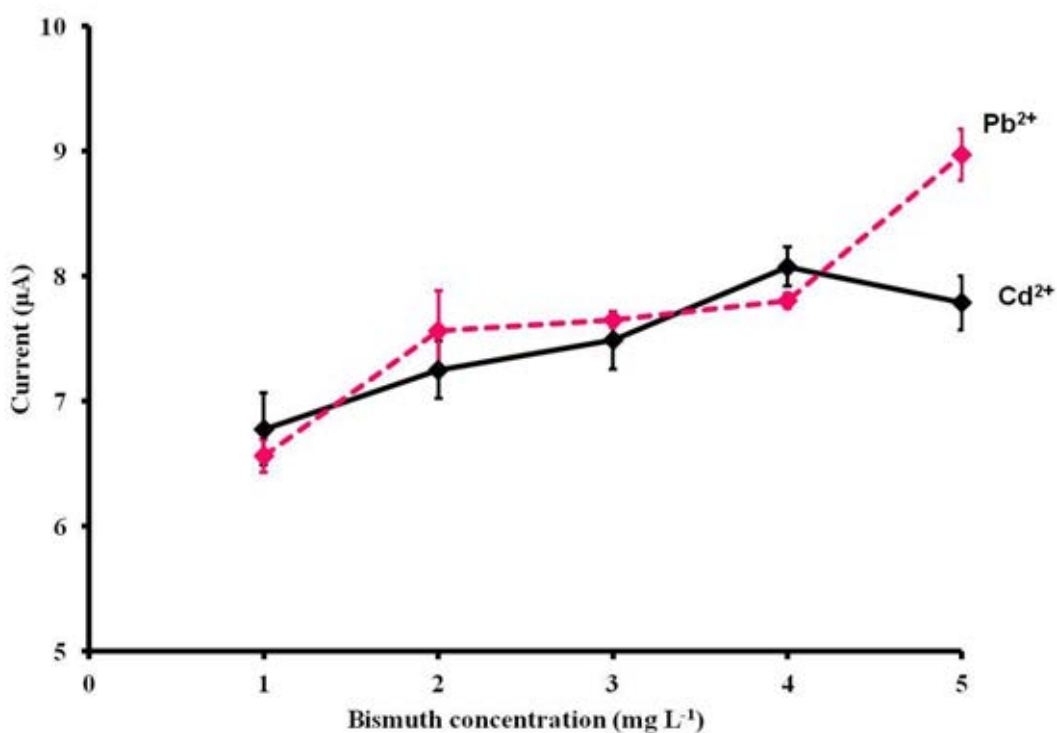


Figure 4.35 The effect of the Bi³⁺ concentration in the plating solution on the current obtained for a 10 µg L⁻¹ of Cd²⁺ and Pb²⁺. The data is shown as the mean ± SD, and is derived from four independent repeats.

4.14.3 Effect of HCl concentration

The effect of HCl concentration was verified in the range of 0.01 to 1.0 M. Results obtained from the SWASV analysis of 10 mg L⁻¹ Cd²⁺ and Pb²⁺ are shown in Table 4.13 and Figure 3.46. The acid concentration of 0.05 M was allowed to be used in the next experiment because it provided the highest peak current.

Table 4.13 Optimization of HCl concentration ($N = 3$)

HCl concentration (M)	Cd^{2+}		Pb^{2+}	
	Mean peak height \pm SD (μA)	%RSD	Mean peak height \pm SD (μA)	%RSD
0.01	6.98 ± 0.12	1.67	6.87 ± 0.16	2.39
0.05	10.42 ± 0.20	1.93	10.50 ± 0.19	1.86
0.10	8.41 ± 0.11	1.34	11.71 ± 0.08	0.67
0.50	6.37 ± 0.12	1.92	9.07 ± 0.36	4.01
1.00	4.10 ± 0.16	3.83	4.32 ± 0.22	5.03

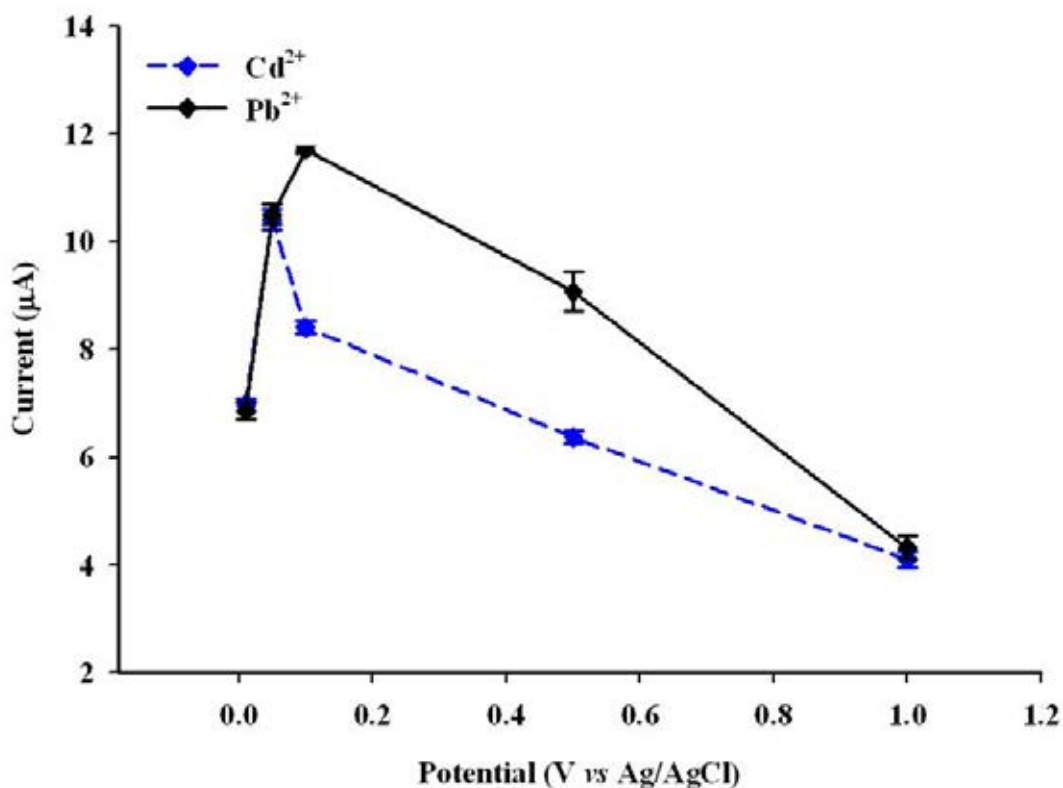


Figure 4.36 The relationship between the peak current and the HCl concentration of a $10 \mu\text{g L}^{-1}$ Cd^{2+} and Pb^{2+} ; The data is shown as the mean \pm SD, and is derived from four independent repeats.

4.14.4 Optimization of Bi-GCPE electrochemical parameters

The current signal obtained in SWASV is dependent on the instrument and method parameters, including the deposition potential, the SW frequency and the step potential so these three parameters were optimized next using the optimized Bi-GCPE and 0.05 M HCl as the electrolyte. Firstly, the influence of deposition potential or accumulation potential was evaluated in the range of -1.3 to -0.9 V, with a SW frequency of 50 Hz and a step potential of 0.01 V. For both Cd^{2+} and Pb^{2+} detection, maximal anodic peak currents were observed at a depositional potential of -1.2 V vs. Ag/AgCl as shown in Figure 4.37. Higher or lower deposition potentials gave lower currents and poor standard deviations (worse reproducibility). Thus, a deposition potential of -1.2 V vs. Ag/AgCl was selected.

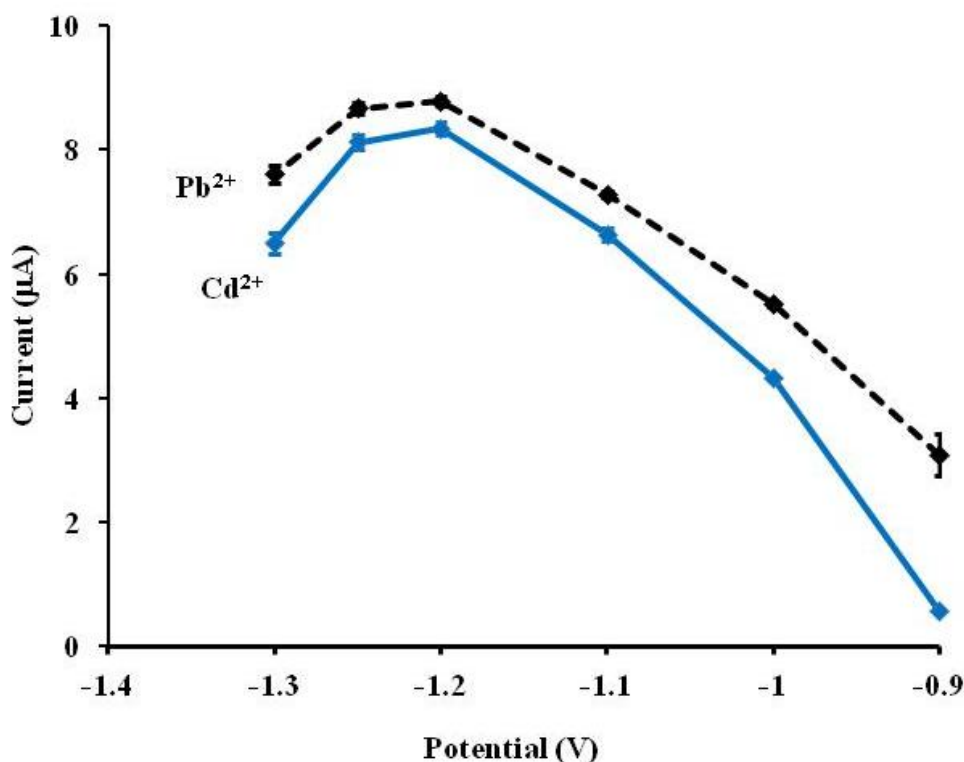


Figure 4.37 The influence of the deposition potential on the current obtained for a $10 \mu\text{g L}^{-1}$ of Cd^{2+} and Pb^{2+} . The data is shown as the mean \pm SD, and is derived from four independent repeats.

The SW frequency is related to the scan rate of the method [46, 48], and was evaluated in the range of 30 to 90 Hz using a deposition potential of -1.2 V vs. Ag/AgCl and a step potential of 0.01 V (Figure 4.38). The anodic peak current for both Pb^{2+} and Cd^{2+} increased as the SW frequency increased up to 80 Hz, and then decreased with a larger standard error at 90 Hz. Thus, the SW frequency of 80 Hz was selected.

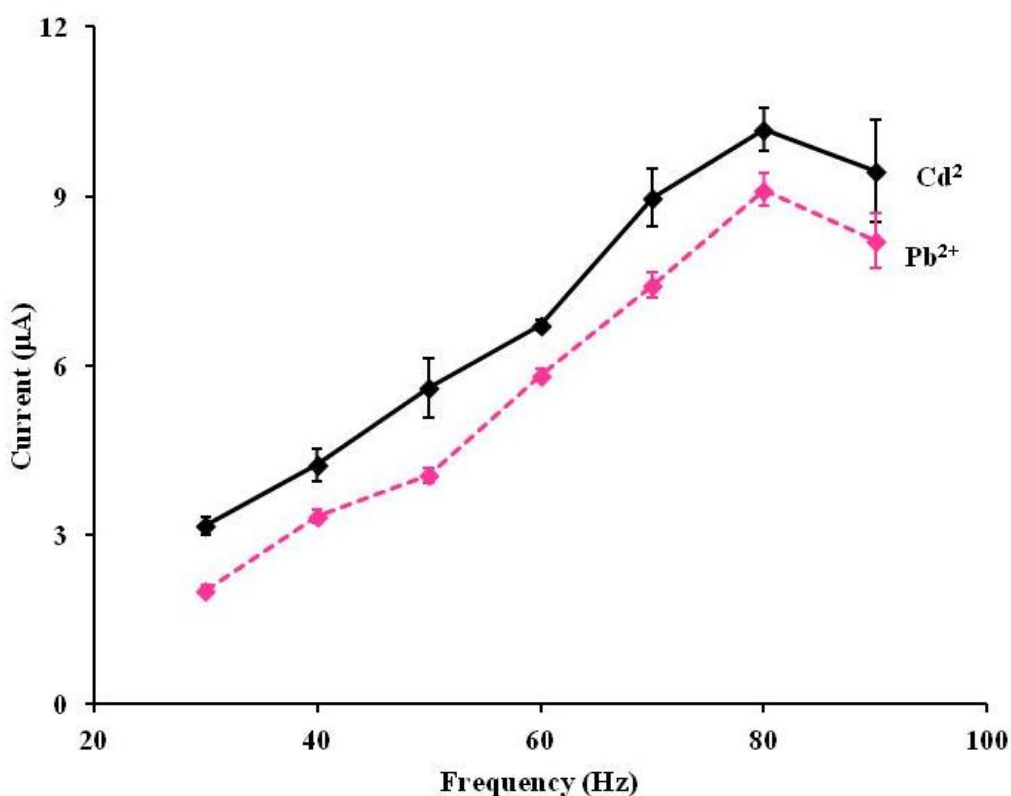


Figure 4.38 The influence of the square wave frequency on the current obtained for a $10 \mu\text{g L}^{-1}$ of Cd^{2+} and Pb^{2+} . The data is shown as the mean \pm SD, and is derived from four independent repeats.

Finally, the effect of varying the step potential was investigated in the range 5.0 to 20 mV, with a depositional potential of -1.2 V vs. Ag/AgCl and a SW frequency of 80 Hz. The analytical signal was increased as the step potential and increased up to 15 mV for both Cd^{2+} and Pb^{2+} detection and then decreased at higher step potential values (Figure 4.39). Thus, a step potential of 15 mV was selected for use in subsequent experiments.

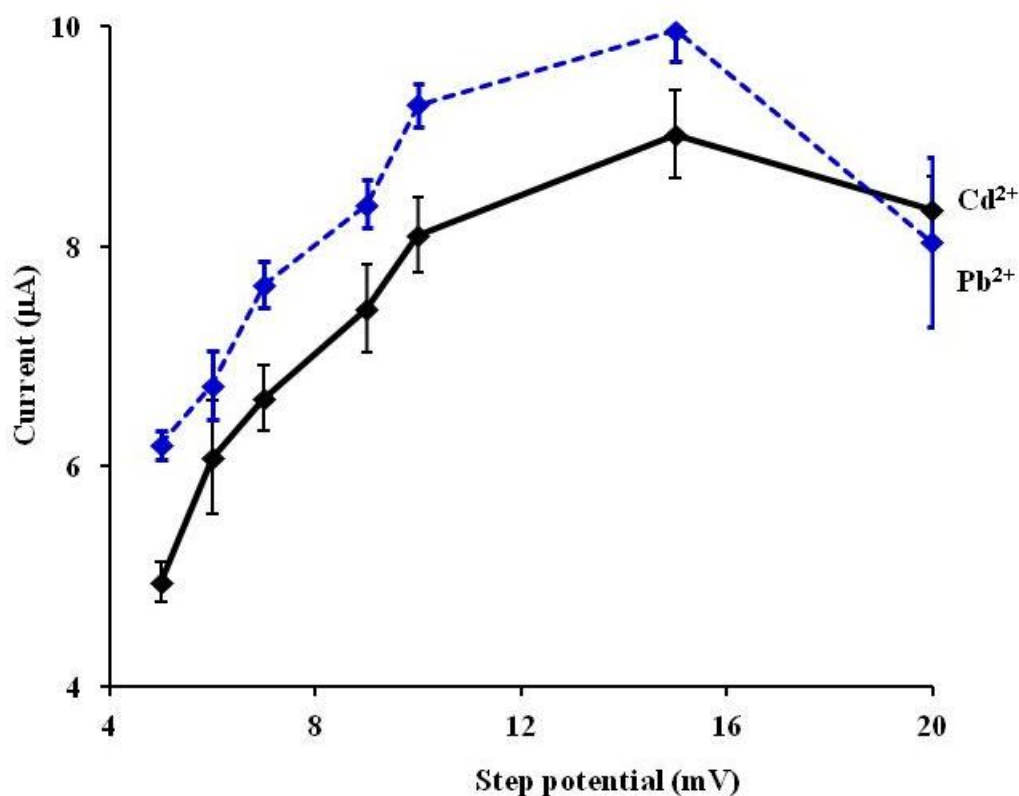


Figure 4.39 The influence of the step potential on the current obtained for a $10 \mu\text{g L}^{-1}$ of Cd^{2+} and Pb^{2+} . The data is shown as the mean \pm SD, and is derived from four independent repeats.

The optimum conditions for the determination Cd^{2+} and Pb^{2+} by Bi-GCPE in SIA-SWASV are summarized in Table 4.14

Table 4.14 Summary of the optimum conditions for determination of Cd^{2+} and Pb^{2+} by Bi-GCPE

Parameters	Examined range	Optimum value
HCl concentration (M)	0.01 to 1.0	0.05
Bismuth concentration (mg L^{-1})	1.0 to 5.0	4.0
Deposition potential (V)	-1.3 to -0.9	-1.20
Frequency (Hz)	30 to 90	80
Potential step (V)	0.005 to 0.02	0.015

Under the optimum condition, the comparison between the voltammograms obtained from CPE, GCPE, Bi-CPE and Bi-GCPE are shown in Figure 4.40. The anodic peak current of both metal ions exhibited a well-defined peak, with the highest peak current being observed with the Bi-GCPE followed by that from the Bi-CPE and then weaker and very weak peaks from the GCPE and CPE, respectively. These data illustrate the importance of the Bi film and also suggest that the high conductivity, surface area and the electron transfer rate between the analytes and the electrode surface of graphene could enhance the sensitivity. Thus, for the determination of Cd^{2+} and Pb^{2+} by an automated flow system, the Bi-GCPE appears to be more sensitive than the other kinds of carbon electrodes previously applied in flow systems.

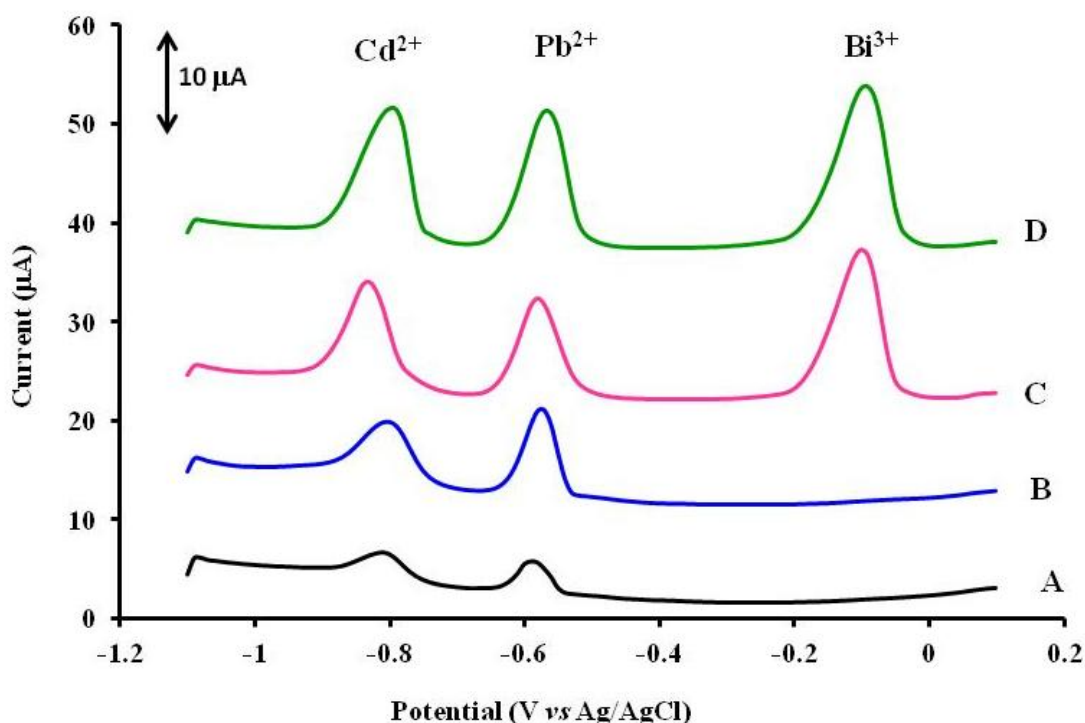


Figure 4.40 Square wave anodic stripping voltammograms obtained from (A) CPE, (B) GCPE, (C) Bi-CPE, and (D) Bi-GCPE with a $10 \mu\text{g L}^{-1}$ of Cd^{2+} and Pb^{2+} . Voltammograms shown are representative of those seen from four independent repeats.

4.15 Calibration data

4.15.1 Linearity

Under the optimized Bi-GCPE and electrochemical analytical condition, the calibration data of the Cd²⁺ and Pb²⁺ anodic peak current obtained at different metal ion concentrations (0.1 to 100 µg L⁻¹ for both metal ions) was performed (Figure 4.41). From the results, the stripping peak currents were found to be proportional to the concentration of Cd²⁺ and Pb²⁺ within the range of 0.1 to 50.0 µg L⁻¹, with good linear regression correlation coefficients (r^2) of greater than 0.995. The precision of the procedure, expressed by the relative standard deviation for four measurements of each metal ions, was also calculated. The results of this study are summarized in Table 4.18, suggesting that the Bi-GCPE give the satisfied sensitivity for applying to the real sample without complicating the sample preparation method.

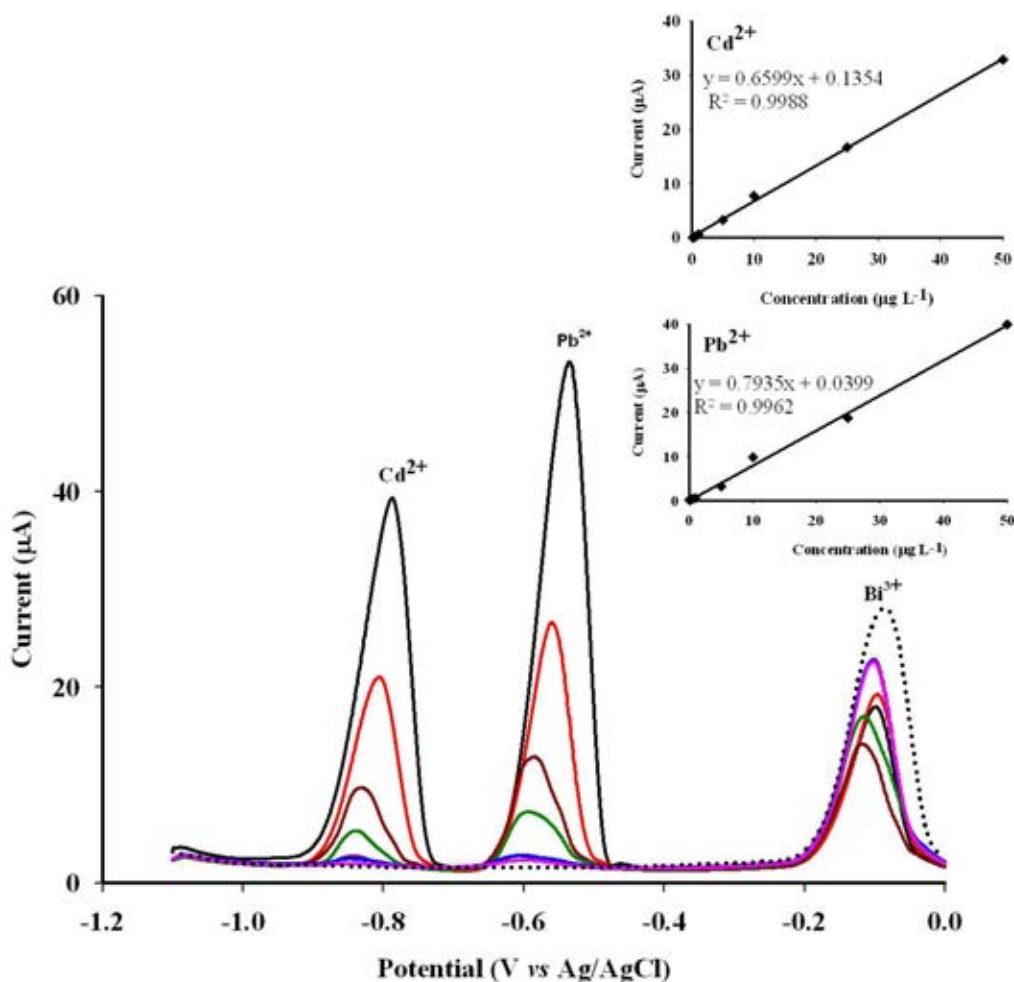


Figure 4.41 Voltammograms of Cd²⁺ and Pb²⁺ in a linear concentration range of 0.1 – 50 μg L⁻¹ measured under the optimum conditions and (In-set) the plot of the relationship between the anodic current peak height and the heavy metal ion concentration. Voltammograms shown are representative of those seen from four independent repeats.

4.15.2 Limit of detection (LOD) and limit of quantification (LOQ)

The detection limits (LOD), evaluated as the concentration that gives a response equivalent to three times the standard deviation (SD) of the blank ($N = 10$), the quantification limits (LOQ), evaluated as the concentration that gives a response equivalent to ten times the SD of the blank. In this study, the lowest detectable concentration (LOD) of 0.07 μg L⁻¹ Cd²⁺ and 0.04 μg L⁻¹ Pb²⁺ were obtained, and the

upper limit concentration at the linear range of $50 \mu\text{g L}^{-1}$ Cd^{2+} and Pb^{2+} were also reported with 140 s accumulation time.

The calibration data of the developed method for the determination of Cd^{2+} and Pb^{2+} are summarized in Table 4.15. We conclude that the Bi-GCPE under these optimized automated flow conditions gives a satisfactorily high sensitivity, an acceptable level of precision and a rapid analysis.

Table 4.15 The summary of the calibration data of Cd^{2+} and Pb^{2+} determination by SWASV at Bi-GCPE

Ions	Linearity ($\mu\text{g L}^{-1}$)	r^2	LOD ($\mu\text{g L}^{-1}$)	LOQ ($\mu\text{g L}^{-1}$)
Cd^{2+}	0.1 – 50.0	0.9988	0.07	0.23
Pb^{2+}	0.1 – 50.0	0.9962	0.04	0.15

4.16 Applications

In order to test the sensitivity of the Bi-GCPE with this method, the proposed method was applied for determination Cd^{2+} and Pb^{2+} in the non-complicated matrix sample: tap water and complicated matrix sample: undulated surf clams and sea bass fish.

4.16.1 Non-complicated matrix sample: Tap water sample

The concentration of Cd^{2+} and Pb^{2+} in the tap water sample was evaluated by the calibration method without pretreatment and filtration. No signal of Cd^{2+} and Pb^{2+} was obtained in the unspiked tap water sample. The average concentrations of Cd^{2+} and Pb^{2+} in spiked tap water samples were found to be slightly lower than the spiked amount and the recoveries were found within the acceptable values, 79-86 % and 87-92% recovery, when spiked at 7.0 and 20.0 $\mu\text{g L}^{-1}$, respectively (Table 4.19). The standard deviations were relatively small suggesting a reasonable level of reproducibility.

4.16.2 Complicated matrix sample: Undulate surf clams and sea bass fish

After the sample preparation, the ability to detect and quantify trace levels of Cd^{2+} and Pb^{2+} ions in undulated surf clam and sea bass fish tissues under optimized conditions were evaluated by the standard addition method, which is used for samples when matrix effects could influence the analytical method. The accuracy of the SWASV procedure with the Bi-GCPE was evaluated by the recovery assay using Cd^{2+} and Pb^{2+} additions (spiking levels) of 1.0 and 5.0 $\mu\text{g L}^{-1}$ into the undulated surf clams and sea bass fish tissue before starting the extraction process. The voltammetric curves obtained are presented in Figure 4.42, and the results obtained in these heavy metal determinations are summarized in Table 4.16. The shape and width of the peak was similar to that obtained for the standard solution. However, when the samples had a low concentration of Cd^{2+} or Pb^{2+} , a significant level of interference from the matrix was obtained, and the current peak of Cd^{2+} was destroyed. This problem was overcome by changing the initial scan in the stripping step to improve the resolution of Cd^{2+} , as previously reported [158], to start the initial scan in the stripping step at -1.10 V vs. Ag/AgCl. The current from the matrix diffusion was then eliminated from the voltammogram and the recovery percentages for both metals when spiked at either 1 or 5 $\mu\text{g L}^{-1}$ were very satisfactory (Table 4.16).

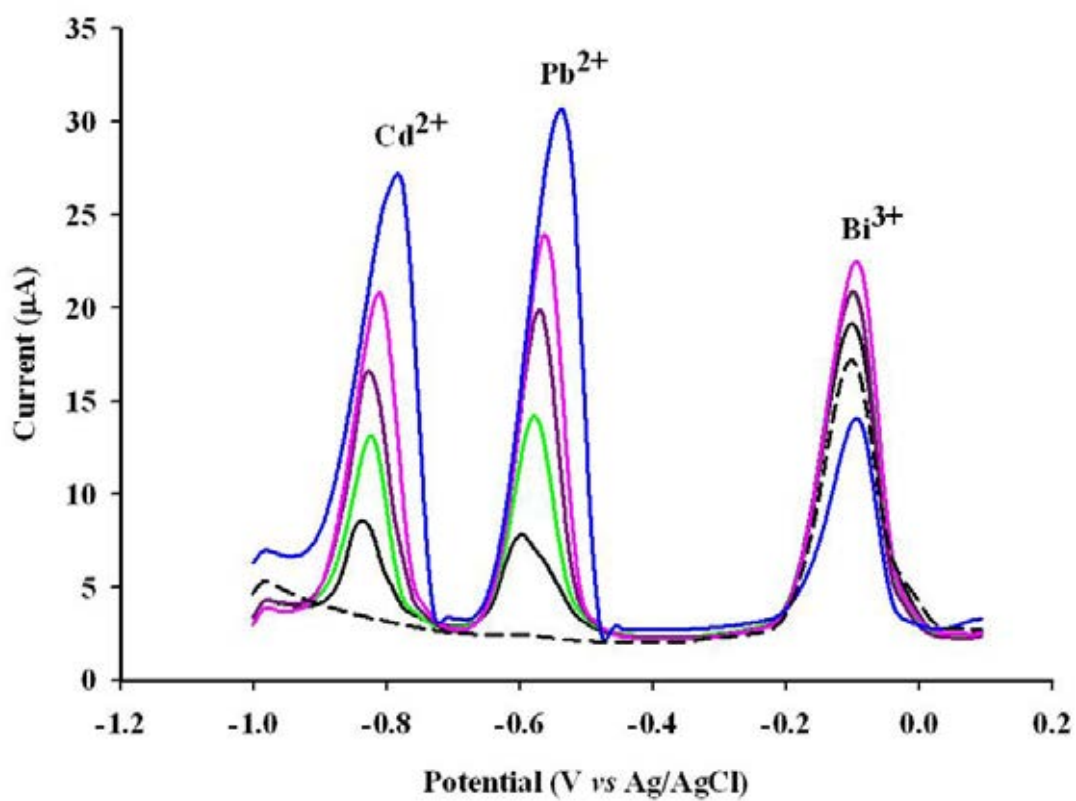


Figure 4.42 An overlay square wave anodic stripping voltammogram for consecutive additions of $5 \mu\text{g L}^{-1}$ Cd^{2+} and Pb^{2+} in 0.05 M HCl, deposition potential at -1.2 V vs. Ag/AgCl for 140 s.

Table 4.16 Determination of (spiked) Cd^{2+} and Pb^{2+} levels in a non-complicated (tap water) or complicated (sea bass fish and undulated surf clam tissues) matrix with the Bi-GCPE under SWASV ($N = 4$).

Non-complicated matrix sample	Spiked level ($\mu\text{g L}^{-1}$)	Found \pm SD ($\mu\text{g L}^{-1}$)		Recovery \pm SD (%)	
		Cd^{2+}	Pb^{2+}	Cd^{2+}	Pb^{2+}
	0	ND	ND	ND	ND
Tap water	7	6.13 ± 0.06	6.11 ± 0.03	87.6 ± 0.82	88.1 ± 0.44
	20	18.4 ± 0.20	19.3 ± 0.30	91.8 ± 1.0	96.3 ± 1.4
Complicated matrix sample	Spiked level ($\mu\text{g kg}^{-1}$)	Found \pm SD ($\mu\text{g kg}^{-1}$)		Recovery \pm SD (%)	
		Cd^{2+}	Pb^{2+}	Cd^{2+}	Pb^{2+}
	0	ND	ND	ND	ND
Sea bass fish	25	25.25 ± 0.05	27.50 ± 0.05	101.0 ± 5.5	110.0 ± 5.0
	125	76.25 ± 0.01	81.5 ± 0.06	61.0 ± 0.2	65.2 ± 1.1
Undulated surf clams tissue	0	ND	ND	ND	ND
	25	28.13 ± 0.02	28.75 ± 0.01	112.5 ± 1.6	115.0 ± 1.2
	125	147.8 ± 0.11	135.3 ± 0.30	118.2 ± 2.3	108.2 ± 6.0

ND = not detectable

4.17 Control of the analytical performance of the proposed method

An analytical performance of the proposed SWASV method using Bi-GCPE in a flow based system was compared with the ICP-OES method used as a standard method. The concentration of Cd^{2+} and Pb^{2+} in complicated matrix samples (undulated surf clams and sea bass fish) spiked with 25, 125 and 250 $\mu\text{g Kg}^{-1}$ of both metal ions were determined by the proposed method and the ICP-OES method. At the spiked concentration of 25 and 125 $\mu\text{g Kg}^{-1}$, the ICP-OES could not detect the Cd^{2+} and Pb^{2+} , only SWASV results were obtained (shown in Table 4.19) suggesting the higher sensitivity of the proposed method. The experiment results of 250 $\mu\text{g Kg}^{-1}$ Cd^{2+} and Pb^{2+} are shown in Table 4.17, suggested that there was a satisfactory agreement between the two methods with Student's pair t -test ($P > 0.05$, $N = 3$ and $t_{\text{calculated}} <$

$t_{critical}$). Therefore, the proposed SWASV method using Bi-GCPE can be used for the simultaneous determination of Cd^{2+} and Pb^{2+} in a complicated matrix sample.

Table 4.17 Results for the determination of Cd^{2+} and Pb^{2+} in a complicated matrix sample (undulated surf clams and sea bass fish); (spiked level = $250 \mu\text{g kg}^{-1}$, $N = 3$, $P = 0.95$, $t_{critical} = 4.30$)

Sample	Spike level ($\mu\text{g kg}^{-1}$)	SWASV		ICP-OES		$t_{calculated}$	
		Cd^{2+} ($\mu\text{g kg}^{-1}$)	Pb^{2+} ($\mu\text{g kg}^{-1}$)	Cd^{2+} ($\mu\text{g kg}^{-1}$)	Pb^{2+} ($\mu\text{g kg}^{-1}$)	Cd^{2+}	Pb^{2+}
Clams	0	ND	ND	ND	ND	-	-
	250	228.3 ± 0.49	246.5 ± 0.27	267.0 ± 1.63	252.8 ± 0.93	3.93	2.07
Sea bass fish	0	ND	ND	ND	ND	-	-
	250	227.5 ± 0.25	295.3 ± 0.46	251.25 ± 0.25	280.5 ± 0.87	1.88	0.40

ND = not detectable

CHAPTER V

CONCLUSIONS AND FURTHER WORKS

This thesis examines the electrochemical analysis of heavy metals (Cd^{2+} and Pb^{2+}) using an automated flow system. The conclusion in this research has been separated into three parts as follows:

Part I: Electrochemical characterization of Carbon Electrode in μ -Flow Sensor by an On-Line Automated Flow System

The electrochemical characteristics of the carbon electrode in the micro-flow sensor were studied using on-line determination of Cd^{2+} and Pb^{2+} based on an anodic stripping voltammetric method. The sensor showed a linear response in the concentration range of $5.0 - 75.0 \mu\text{g L}^{-1}$ for Cd^{2+} and $2.5 - 75.0 \mu\text{g L}^{-1}$ for Pb^{2+} . The carbon electrode showed excellent response and the LOD values obtained for the determination of model metals were found to be in very low ppb levels. This electrode provided good reproducibility and was stable for at least 4 days (160 samples). This part of the research proved the advantages of the determination of heavy metal ions by on-line ASV using a micro-flow sensor consisted of both a preconcentration membrane and a three electrode system in one piece which is appropriate for field analysis.

Part II: Highly sensitive determination of Cd^{2+} and Pb^{2+} using a low-cost electrochemical flow-through cell based on a carbon paste electrode

The problem which arose from part I of the research were the inspirations for the research in part II. In this part, the low-cost thin-layer electrochemical flow-through cell was designed and fabricated in house to use as a voltammetric detector in conjunction with a SIA system. The CPE was used as a working electrode in the in-house designed flow cell because of its low-cost, extreme simplicity of the electrode preparation, excellent binding affinity with various materials and easy renewal. The

determination of trace heavy metal ions by flow-based SWASV using a Bi-CPE in the in-house designed flow cell offered a better sensitivity and wider linear detection range than the commercially available flow cell. Moreover, the cost of our flow cell is much lower than that of the commercial flow cell because our flow cell is made of Plexiglas. This material is much less expensive and much easier to handle, cut and fabricate when compared to the material used for fabrication of the commercially available BAS flow cell (polyether ether ketone, PEEK). In addition, our flow cell is a one-piece flow cell which is very easy to assemble because it does not require the use of a gasket, clamp and screws for holding and tightening two removable blocks together. These reasons result in the dramatic price reduction of our thin-layer flow cell. As such, it is suitable for use in conjunction with the CPE as a metal sensor in field analysis in future research.

Part III: Graphene-modified carbon paste electrode for Cd²⁺ and Pb²⁺ monitoring with a flow based system

A highly enhanced sensing electrode, a Bi-GCPE composite film was successfully established for the automated simultaneous determination of trace levels of the heavy metal Cd²⁺ and Pb²⁺ ions by SWASV in a SIA system. This report is the first demonstration of the application of a Bi-GCPE to SIA for the SWASV measurement of trace levels of Cd²⁺ and Pb²⁺ in real-world samples. This method can be used for the determination of trace levels of Cd²⁺ and Pb²⁺ in high matrix samples, which was exemplified by sea bass fish and undulated surf clam tissues. It offers the significant advantage of an excellent electrical conductivity and increased surface area from the graphene that was mixed with graphite nanopowder. This use of the graphene composite film electrode in a flow system, combined with a Bi film, enabled the LODs of only 0.07 and 0.04 µg L⁻¹ for Cd²⁺ and Pb²⁺, respectively, which are lower than those previously obtained by CNT-based electrodes at 0.80 and 0.20 µg L⁻¹ for Cd²⁺ and Pb²⁺, respectively [131].

Further work

The micro-flow sensor used in part I of this research is very interesting for field analysis because it is a small size sensor consisting of both a sample preconcentration part and a three electrode system for electrochemical detection in one piece. Whereas, the high sensitivity of the in-house designed flow cell used with the CPE electrode was successfully achieved. From the advantages mentioned above, the in-house designed flow cell consisting of a three electrode system and a preconcentration part in one piece should be designed for highly sensitive determination of heavy metal ions by ASV coupled with an automated flow-based system.

Improving the sensitivity of the graphene modified working electrode is another interesting aspect. The high purity graphene can be fabricated by the electrochemical reduction of graphene oxide. Graphene obtained from the electrochemical method exhibits high electrical conducting properties which lead to the higher sensitivity of the working electrode.

The automated flow-based analytical system comprising of a syringe pump, a selection valve, a holding coil and a computer controller is convenient and easy to operate. The automated flow-based system can be applied for monitoring the electrochemical species from the reaction and can be applied with immunosensors.

REFERENCES

- [1] Wang, J., **Fundamental Concepts: In Analytical Electrochemistry**. New York: John Wiley & Sons, 2006.
- [2] Wang, J., **Controlled-Potential Techniques: In Analytical Electrochemistry**. New York: John Wiley & Sons, 2006.
- [3] Wang, J., **Stripping Analysis**. VCH Publishers, 1985.
- [4] Kelly, R. S. Analytical Electrochemistry: The Basic Concepts [online]. Available from: http://www.asdlib.org/onlineArticles/ecourseware/Kelly_Potentiometry/PDF-14-EChemCells.pdf (2012, March 14),
- [5] G.Henze, F. G. T. a., **Introduction to Voltammetric analysis**. Australia: 1st ed.; Csiro Publishing: Collingwood VIC, 1933.
- [6] Wang, J., **Practical Considerations: In Analytical Electrochemistry**, John Wiley & Sons, 2006.
- [7] Kelly, R. S., Analytical Electrochemistry: The Basic Concepts. 2012.
- [8] Biotechnology, D. o. C. E. a. Mass Transport. [online]. Available from : <http://www.ceb.cam.ac.uk/pages/mass-transport.html> (2012, March 12),
- [9] K. Tóth, K. S., W. Kutner, Z. Fehér and E. Lindner, Electrochemical detection in liquid flow analytical techniques: Characterization and classification (IUPAC Technical Report). Pure Appl. Chem. 76(6) (2004): 1119 -1138.
- [10] Faulkner, A. J. B. a. L. R., **Electrochemical methods: fundamentals and applications**. 2nd ed.; John Wiley & Sons, : New York, 2001.
- [11] A, E., Sequential-injection analysis (SIA): A useful tool for on-line sample-handling and pre-treatment. TrAC Trends Anal. Chem. 24(5) (2005): 416-425.
- [12] Pérez-Olmos, R.; Soto, J. C.; Zárate, N.; Araújo, A. N.; Lima, J. L. F. C.; Saraiva, M. L. M. F. S., Application of sequential injection analysis (SIA) to food analysis. Food Chem. 90(3) (2005): 471-490.
- [13] Pérez-Olmos, R.; Soto, J. C.; Zárate, N.; Araújo, A. N.; Montenegro, M. C. B. S. M., Sequential injection analysis using electrochemical detection: A review. Anal. Chim. Acta 554(1-2) (2005): 1-16.

- [14] Mesquita, R. B. R.; Rangel, A. O. S. S., A review on sequential injection methods for water analysis. Anal. Chim. Acta, 648(1) (2009): 7-22.
- [15] Barnett, N. W.; Lenehan, C. E.; Lewis, S. W., Sequential injection analysis: an alternative approach to process analytical chemistry. TrAC Trends Anal. Chem. 18(5) (1999): 346-353.
- [16] Cerdà, V.; Cerdà, A.; Cladera, A.; Oms, M. T.; Mas, F.; Gómez, E.; Bauzá, F.; Miró, M.; Forteza, R.; Estela, J. M., Monitoring of environmental parameters by sequential injection analysis. TrAC Trends Anal. Chem., 20(8) (2001): 407-418.
- [17] Koblová, P.; Sklenářová, H.; Chocholouš, P.; Polášek, M.; Solich, P., Simple automated generation of gradient elution conditions in sequential injection chromatography using monolithic column. Talanta, 84(5) (2011): 1273-1277.
- [18] Šmirjdáková, S., Ondrašovičová O., Kašková., Laktičová, K, The Effect of Cadmium and Lead Pollution on Human and Animal Health. Folia Veterinaria, 49(3) (2005): 31-32.
- [19] Farida Agha; Agha Sadaruddin; Khatoon, N., Effect of environmental lead pollution on blood lead levels in traffic police constables in Islamabad, Pakistan. J. Pak. Med. Assoc., 55(10) (2005): 410-413.
- [20] Yurtsever, M.; Şengil, İ. A., Biosorption of Pb(II) ions by modified quebracho tannin resin. J. Hazard. Mater. 163(1) (2009): 58-64.
- [21] Yang, G.; Fen, W.; Lei, C.; Xiao, W.; Sun, H., Study on solid phase extraction and graphite furnace atomic absorption spectrometry for the determination of nickel, silver, cobalt, copper, cadmium and lead with MCI GEL CHP 20Y as sorbent. J. Hazard. Mater. 162(1) (2009): 44-49.
- [22] Wang, J.; Hansen, E. H., Coupling on-line preconcentration by ion-exchange with ETAAS: A novel flow injection approach based on the use of a renewable microcolumn as demonstrated for the determination of nickel in environmental and biological samples. Anal. Chim. Acta 424(2) (2000): 223-232.
- [23] Duran, C.; Senturk, H. B.; Elci, L.; Soylak, M.; Tufekci, M., Simultaneous preconcentration of Co(II), Ni(II), Cu(II), and Cd(II) from environmental

- samples on Amberlite XAD-2000 column and determination by FAAS. J..Hazard.Mater. 162(1) (2009): 292-299.
- [24] Chen, D.; Hu, B.; Huang, C., Chitosan modified ordered mesoporous silica as micro-column packing materials for on-line flow injection-inductively coupled plasma optical emission spectrometry determination of trace heavy metals in environmental water samples. Talanta 78(2) (2009): 491-497.
- [25] Economou, A.; Voulgaropoulos, A., On-line stripping voltammetry of trace metals at a flow-through bismuth-film electrode by means of a hybrid flow-injection/sequential-injection system. Talanta 71(2) (2007): 758-765.
- [26] Wang, Y.; Liu, Z.; Hu, X.; Cao, J.; Wang, F.; Xu, Q.; Yang, C., On-line coupling of sequential injection lab-on-valve to differential pulse anodic stripping voltammetry for determination of Pb in water samples. Talanta 77(3) (2009): 1203-1207.
- [27] Auroux, P.-A.; Iossifidis, D.; Reyes, D. R.; Manz, A., Micro Total Analysis Systems. 2. Analytical Standard Operations and Applications. Anal. Chem. 74(12) (2002): 2637-2652.
- [28] Christian, G. D., Flow analysis and its role and importance in the analytical sciences. Anal. Chim. Acta, 499(1-2) (2003): 5-8.
- [29] Brennstainer, A.; Zondlo, J. W.; Stiller, A. H.; Stansberry, P. G.; Tian, D. C.; Xu, Y., Environmental pollution control devices based on novel forms of carbon: Heavy metals. Energy Fuels 11(2) (1997): 348-353.
- [30] Martinotti, W.; Queirazza, G.; Guarinoni, A.; Mori, G., In-flow speciation of copper, zinc, lead and cadmium in fresh waters by square wave anodic stripping voltammetry Part II. Optimization of measurement step. Anal. Chim. Acta 305(1-3) (1995): 183-191.
- [31] Tur'yan, Y. I., Microcells for voltammetry and stripping voltammetry. Talanta 44 (1) (1997): 1-13.
- [32] Jaenicke, S.; Sabarathinam, R. M.; Fleet, B.; Gunasingham, H., Determination of lead in blood by hydrodynamic voltammetry in a flow injection system with wall-jet detector. Talanta 45(4) (1998): 703-711.

- [33] Richter, P.; Toral, M. I.; Abbott, B., Anodic Stripping Voltammetric Determination of Mercury in Water by Using a New Electrochemical Flow Through Cell. Electroanalysis 14(18) (2002): 1288-1293.
- [34] Paixão, T. R. L. C.; Matos, R. C.; Bertotti, M., Design and characterisation of a thin-layered dual-band electrochemical cell. Electrochim. Acta 48(6) (2003) : 691-698.
- [35] Lindquist, J., Carbon paste electrode with a wide anodic potential range. Anal.Chem. 45(6) (1973): 1006-1008.
- [36] Somerset, V.; Iwuoha, E.; Hernandez, L., Stripping Voltammetric Measurement of Trace Metal Ions at Screen-printed Carbon and Carbon Paste Electrodes. Procedia Chem. 1(1) (2009): 1279-1282.
- [37] Wang, J.; Anik Kirgыз, I.; Mo, J.-W.; Lu, J.; Nasser Kawde, A.; Muck, A., Glassy carbon paste electrodes. Electrochem. Commun. 3(4) (2001): 203-208.
- [38] Flechsig, G.-U.; Kienbaum, M.; Gründler, P., Ex situ atomic force microscopy of bismuth film deposition at carbon paste electrodes. Electrochem. Commun. 7 (11) (2005): 1091-1097.
- [39] Hocevar, S. B.; Ogorevc, B., Preparation and characterization of carbon paste micro-electrode based on carbon nano-particles. Talanta 7 (3) (2007): 405-411.
- [40] METELKA, K. V. I. Š. R., Carbon paste electrodes in electroanalytical chemistry. J. Serb. Chem. Soc. 74 (10) (2009): 1021-1033.
- [41] Svancara, I.; Vytras, K.; Kalcher, K.; Walcarius, A.; Wang, J., Carbon Paste Electrodes in Facts, Numbers, and Notes: A Review on the Occasion of the 50-Years Jubilee of Carbon Paste in Electrochemistry and Electroanalysis. Electroanalysis 21(1) (2009): 7-28.
- [42] Tomáš Mikysek, M. S., Ivan Švancara, and Jiří Ludvík, Relation Between the Composition and Properties of Carbon Nanotubes Paste Electrodes (CNTPEs). Sensing in Electroanalysis 5 (2010): 69-75.
- [43] Bennouna, A.; Kheribech, A.; Scharff, J. P.; Chassagneux, F.; Durand, B.; Vittori, O., Evaluation of preconcentration response of a carbon paste

- electrode with conducting binder. Application to lead. Electrochim. Acta 42(17) (1997) : 2659-2665.
- [44] Liu, H.; He, P.; Li, Z.; Sun, C.; Shi, L.; Liu, Y.; Zhu, G.; Li, J., An ionic liquid-type carbon paste electrode and its polyoxometalate-modified properties. Electrochem. Commun. 7(12) (2005): 1357-1363.
- [45] Fanjul-Bolado, P.; Hernández-Santos, D.; Lamas-Ardisana, P. J.; Martn-Perña, A.; Costa-Garça, A., Electrochemical characterization of screen-printed and conventional carbon paste electrodes. Electrochim. Acta 53(10) (2008): 3635-3642.
- [46] Shahrokhian, S.; Karimi, M.; Khajehsharifi, H., Carbon-paste electrode modified with cobalt-5-nitroisalophen as a sensitive voltammetric sensor for detection of captopril. Sens. Actuators, B 109(2) (2005): 278-284.
- [47] Ramos, L. A. n.; Cavalheiro, E. T. G.; Chierice, G. O., Evaluation of the electrochemical behavior and analytical potentialities of a carbon paste electrode modified with a ruthenium (III) piperidinedithiocarbamate complex. Il Farmaco 60(2) (2005): 149-155.
- [48] Popescu, I. C.; Zetterberg, G.; Gorton, L., Influence of graphite powder, additives and enzyme immobilization procedures on a mediatorless HRP-modified carbon paste electrode for amperometric flow-injection detection of H₂O₂. Biosens. Bioelectron. 10(5) (1995): 443-461.
- [49] Albareda-Sirvent, M.; Merkoçi, A.; Alegret, S., Configurations used in the design of screen-printed enzymatic biosensors. A review. Sens. Actuators, B 69(1-2) (2000): 153-163.
- [50] Yabuki, S.; Mizutani, F., Modifications to a carbon paste glucose-sensing enzyme electrode and a reduction in the electrochemical interference from L-ascorbate. Biosens. Bioelectron. 10(3-4) (1995): 353-358.
- [51] Zhang, Y.; Zheng, J., Sensitive voltammetric determination of rutin at an ionic liquid modified carbon paste electrode. Talanta 77(1) (2008): 325-330.
- [52] Brondani, D.; Dupont, J.; Spinelli, A.; Vieira, I. C., Development of biosensor based on ionic liquid and corn peroxidase immobilized on chemically crosslinked chitin. Sens. Actuators, B 138 (1) (2009): 236-243.

- [53] Wang, C. Y.; Hu, X. Y.; Jin, G. D.; Leng, Z. Z., Differential pulse adsorption voltammetry for determination of procaine hydrochloride at a pumice modified carbon paste electrode in pharmaceutical preparations and urine. J. Pharm. and Biomed. Anal. 30 (1) (2002): 131-139.
- [54] Liu, Z.-M.; Yang, H.-F.; Li, Y.-F.; Liu, Y.-L.; Shen, G.-L.; Yu, R.-Q., Core-shell magnetic nanoparticles applied for immobilization of antibody on carbon paste electrode and amperometric immunosensing. Sens.Actuators, B 113(2) (2006) : 956-962.
- [55] Shu, H.-C.; Wu, N.-p., A chemically modified carbon paste electrode with d-lactate dehydrogenase and alanine aminotranferase enzyme sequences for d-lactic acid analysis. Talanta 54(2) (2001): 361-368.
- [56] Paredes, P. A.; Parellada, J.; Fernández, V. M.; Katakis, I.; Domínguez, E., Amperometric mediated carbon paste biosensor based on D-fructose dehydrogenase for the determination of fructose in food analysis. Biosens. Bioelectron. 12(12) (1997): 1233-1243.
- [57] Alvarez-Romero, G. A.; Rojas-Hernández, A.; Morales-Prez, A.; Ramirez-Silva, M. T., Determination of [beta]-D-glucose using flow injection analysis and composite-type amperometric tubular biosensors. Biosens.Bioelectron. 19(9) (2004): 1057-1065.
- [58] Volikakis, G. J.; Efstathiou, C. E., Determination of rutin and other flavonoids by flow-injection/adsorptive stripping voltammetry using nujol-graphite and diphenylether-graphite paste electrodes. Talanta 51(4) (2000): 775-785.
- [59] Dominguez, E.; Lan, H. L.; Okamoto, Y.; Hale, P. D.; Skotheim, T. A.; Gorton, L.; Hahnagerdal, B., Reagentless chemically modified carbon paste electrode based on a phenothiazine polymer derivative and yeast alcohol dehydrogenase for the analysis of ethanol. Biosens.Bioelectron. 8(3-4) (1993): 229-237.
- [60] Stefan, R.-I.; Bokretzion, R. G.; van Staden, J. F.; Aboul-Enein, H. Y., Immunosensor for the determination of azidothymidine: Its utilization as detector in a sequential injection analysis system. Talanta 59(5) (2003): 883-887.

- [61] Dong, S.; Zhang, S.; Cheng, X.; He, P.; Wang, Q.; Fang, Y., Simultaneous determination of sugars and ascorbic acid by capillary zone electrophoresis with amperometric detection at a carbon paste electrode modified with polyethylene glycol and Cu₂O. J.Chromatogr. A 1161(1-2) (2007): 327-333.
- [62] Stefan, R.-I.; Bokretzion, R. G.; van Staden, J. F.; Aboul-Enein, H. Y., Simultaneous determination of - and -methotrexate using a sequential injection analysis/amperometric biosensors system. Biosen. .Bioelectron. 19(3) (2003): 261-267.
- [63] Stefan, R.-I.; van Staden, J. F.; Aboul-Enein, H. Y., Simultaneous detection of S and R captopril using sequential injection analysis. Talanta 51(5) (2000): 969-975.
- [64] Stefan, R.-I.; van Staden, J. F.; Mulaudzi, L. V.; Aboul-Enein, H. Y., On-line simultaneous determination of S- and R-perindopril using amperometric biosensors as detectors in flow systems. Anal. Chim. Acta 467(1-2) (2002): 189-195.
- [65] Stefan, R.-I.; van Staden, J. F.; Aboul-Enein, H. Y., On-line assay of S-captopril using an amperometric biosensor/sequential injection system. Anal. Chim.Acta 411(1-2) (2000): 51-56.
- [66] Bolger, F. B.; McHugh, S. B.; Bennett, R.; Li, J.; Ishiwari, K.; Francois, J.; Conway, M. W.; Gilmour, G.; Bannerman, D. M.; Fillenz, M.; Tricklebank, M.; Lowry, J. P., Characterisation of carbon paste electrodes for real-time amperometric monitoring of brain tissue oxygen. J. Neurosci. Methods 195(2) (2010): 135-142.
- [67] Walcarius, A.; Barbaise, T.; Bessiere, J., Factors affecting the analytical applications of zeolite-modified electrodes preconcentration of electroactive species. Anal. Chim. Acta 340(1-3) (1997): 61-76.
- [68] Khani, H.; Rofouei, M. K.; Arab, P.; Gupta, V. K.; Vafaei, Z., Multi-walled carbon nanotubes-ionic liquid-carbon paste electrode as a super selectivity sensor: Application to potentiometric monitoring of mercury ion(II). J. Hazard. Mater. 183(1-3) (2010): 402-409.

- [69] Ensafi, A. A.; Ghaderi, A. R., On-line solid phase selective separation and preconcentration of Cd(II) by solid-phase extraction using carbon active modified with methyl thymol blue. *J.Hazard. Mater.* 148(1-2) (2007): 319-325.
- [70] Abbasi, S.; Khodarahmiyan, K.; Abbasi, F., Simultaneous determination of ultra trace amounts of lead and cadmium in food samples by adsorptive stripping voltammetry. *Food Chem.* In Press (2011): Corrected Proof.
- [71] Safavi, A.; Pakniat, M.; Maleki, N., Design and construction of a flow system for determination of Cu(II) ions in water by means of a chemically modified carbon paste electrode. *Anal. Chim.Acta* 335(3) (1996): 275-282.
- [72] Yantasee, W.; Timchalk, C.; Fryxell, G. E.; Dockendorff, B. P.; Lin, Y., Automated portable analyzer for lead(II) based on sequential flow injection and nanostructured electrochemical sensors. *Talanta* 68(2) (2005): 256-261.
- [73] Wang, J.; Lu, J., Bismuth film electrodes for adsorptive stripping voltammetry of trace nickel. *Electrochem. Commun.* 2(6) (2000): 390-393.
- [74] Serrano, N.; Díaz-Cruz, J.; Ariño, C.; Esteban, M., Stripping analysis of heavy metals in tap water using the bismuth film electrode. *Anal.Bioanal.Chem.* 396 (3) (2010): 1365-1369.
- [75] Wang, J.; Lu, J.; Hocevar, S. B.; Farias, P. A. M.; Ogorevc, B., Bismuth-Coated Carbon Electrodes for Anodic Stripping Voltammetry. *Anal. Chem.* 72(14) (2000): 3218-3222.
- [76] Hutton, E. A.; Hocevar, S. B.; Ogorevc, B.; Smyth, M. R., Bismuth film electrode for simultaneous adsorptive stripping analysis of trace cobalt and nickel using constant current chronopotentiometric and voltammetric protocol. *Electrochem. Commun.* 5(9) (2003): 765-769.
- [77] Wang, J., Stripping Analysis at Bismuth Electrodes: A Review. *Electroanalysis* 17 (15-16) (2005): 1341-1346.
- [78] Economou, A., Bismuth-film electrodes: recent developments and potentialities for electroanalysis. *TrAC Trends Anal.Chem.*, 24(4) (2005): 334-340.
- [79] Švancara, I.; Baldrianová, L.; Tesařová, E.; Hočevár, S. B.; Elsuccary, S. A. A.; Economou, A.; Sotiropoulos, S.; Ogorevc, B.; Vytřas, K., Recent Advances

- in Anodic Stripping Voltammetry with Bismuth-Modified Carbon Paste Electrodes. Electroanalysis 18(2) (2006): 177-185.
- [80] Baldrianova, L.; Svancara, I.; Sotiropoulos, S., Anodic stripping voltammetry at a new type of disposable bismuth-plated carbon paste mini-electrodes. Anal.Chim. Acta 599(2) (2007): 249-255.
- [81] de Carvalho, L. M.; do Nascimento, P. C.; Koschinsky, A.; Bau, M.; Stefanello, R. F.; Spengler, C.; Bohrer, D.; Jost, C., Simultaneous Determination of Cadmium, Lead, Copper, and Thallium in Highly Saline Samples by Anodic Stripping Voltammetry (ASV) Using Mercury-Film and Bismuth-Film Electrodes. Electroanalysis 19(16) (2007): 1719-1726.
- [82] Nunes, L. M. S.; Faria, R. C., The Influence of the Electrodeposition Conditions on the Electroanalytical Performance of the Bismuth Film Electrode for Lead Determination. Electroanalysis 20(20) (2008): 2259-2263.
- [83] Granado Rico, M. Á.; Olivares-Marín, M.; Gil, E. P., A Novel Cell Design for the Improved Stripping Voltammetric Detection of Zn(II), Cd(II), and Pb(II) on Commercial Screen-Printed Strips by Bismuth Codeposition in Stirred Solutions. Electroanalysis 20(24) (2008): 2608-2613.
- [84] Lu, D.; Belle, J. L.; Ninivin, C. L.; Mabic, S.; Dimitrakopoulos, T., In situ electrochemical detection of trace metal vapors at bismuth doped carbon screen printed electrodes. J. Electroanal. Chem. 642(2) (2010): 157-159.
- [85] Frena, M.; Campestrini, I.; de Braga, O. C.; Spinelli, A., In situ bismuth-film electrode for square-wave anodic stripping voltammetric determination of tin in biodiesel. Electrochim. Acta 56(12) (2011): 4678-4684.
- [86] Fischer, E.; van den Berg, C. M. G., Anodic stripping voltammetry of lead and cadmium using a mercury film electrode and thiocyanate. Anal. Chim. Acta 385(1-3) (1999): 273-280.
- [87] Tesarova, E.; Baldrianova, L.; Hocevar, S. B.; Svancara, I.; Vytras, K.; Ogorevc, B., Anodic stripping voltammetric measurement of trace heavy metals at antimony film carbon paste electrode. Electrochim. Acta 54(5) (2009): 1506-1510.

- [88] Farghaly, O. A.; Ghandour, M. A., Square-wave stripping voltammetry for direct determination of eight heavy metals in soil and indoor-airborne particulate matter. Environ. Res. 97(3) (2005): 229-235.
- [89] Li, Y.; Liu, X.; Zeng, X.; Liu, Y.; Liu, X.; Wei, W.; Luo, S., Simultaneous determination of ultra-trace lead and cadmium at a hydroxyapatite-modified carbon ionic liquid electrode by square-wave stripping voltammetry. Sens.Actuators, B 139(2) (2009): 604-610.
- [90] Güell, R.; Aragay, G.; Fontás, C.; Anticó, E.;Merkoçi, A., Sensitive and stable monitoring of lead and cadmium in seawater using screen-printed electrode and electrochemical stripping analysis. Anal. Chim. Acta 627(2) (2008): 219-224.
- [91] Fan, L.; Chen, J.; Zhu, S.; Wang, M.; Xu, G., Determination of Cd²⁺ and Pb²⁺ on glassy carbon electrode modified by electrochemical reduction of aromatic diazonium salts. Electrochem. Commun. 11(9) (2009): 1823-1825.
- [92] Ivaska, A.; Kubiak, W. W., Application of sequential injection analysis to anodic stripping voltammetry. Talanta 44(4) (1997): 713-723.
- [93] Legeai, S.; Bois, S.; Vittori, O., A copper bismuth film electrode for adsorptive cathodic stripping analysis of trace nickel using square wave voltammetry. J.Electroanal.Chem. 591(1) (2006): 93-98.
- [94] Hu, C.; Wu, K.; Dai, X.; Hu, S., Simultaneous determination of lead(II) and cadmium(II) at a diacetyldioxime modified carbon paste electrode by differential pulse stripping voltammetry. Talanta 60(1) (2003): 17-24.
- [95] Chuang, H.; Arnold, M. A., Radioluminescent Light Source for Optical Oxygen Sensors. Anal. Chem. 69(10) (1997): 1899-1903.
- [96] Krieg Jr, E. F.; Butler, M. A., Blood lead, serum homocysteine, and neurobehavioral test performance in the third National Health and Nutrition Examination Survey. Neurotoxicology 30(2) (2009): 281-289.
- [97] Ensafi, A. A.; Shiraz, A. Z., On-line separation and preconcentration of lead(II) by solid-phase extraction using activated carbon loaded with xylene orange and its determination by flame atomic absorption spectrometry. J. Hazard. Mater. 150(3) (2008): 554-559.

- [98] Acar, O., Evaluation of V, Ir, Ru, V-Ir, V-Ru, and W-V as permanent chemical modifiers for the determination of cadmium, lead, and zinc in botanic and biological slurries by electrothermal atomic absorption spectrometry. Anal. Chim. Acta 545(2) (2005): 244-251.
- [99] Zheng, H.; Yan, Z.; Dong, H.; Ye, B., Simultaneous determination of lead and cadmium at a glassy carbon electrode modified with Langmuir-Blodgett film of p-tert-butylthiacalix[4]arene. Sens.Actuators, B 120(2) (2007): 603-609.
- [100] Marcano, D. C.; Kosynkin, D. V.; Berlin, J. M.; Sinitskii, A.; Sun, Z.; Slesarev, A.; Alemany, L. B.; Lu, W.; Tour, J. M., Improved Synthesis of Graphene Oxide. ACS Nano 4(8) (2010): 4806-4814.
- [101] Abu-Shawish, H. M.; Ghalwa, N. A.; Zaggout, F. R.; Saadeh, S. M.; Al-Dalou, A. R.; Assi, A. A. A., Improved determination of tramadol hydrochloride in biological fluids and pharmaceutical preparations utilizing a modified carbon paste electrode. Biochem.Eng. J. 48(2) (2010): 237-245.
- [102] Gudarzi, M. M.; Sharif, F., Characteristics of polymers that stabilize colloids for the production of graphene from graphene oxide. J.Colloid Interface Sci. 349 (1) (2010): 63-69.
- [103] Liang, M.; Luo, B.; Zhi, L., Application of graphene and graphene-based materials in clean energy-related devices. Int. J. Energy Res. 33(13) (2009): 1161-1170.
- [104] Merkoçi, A.; Pumera, M.; Llopis, X.; Pérez, B.; del Valle, M.; Alegret, S., New materials for electrochemical sensing VI: Carbon nanotubes. *TrAC Trends in Anal. Chem.* 24(9) (2005): 826-838.
- [105] Boyle, E. A.; Bergquist, B. A.; Kayser, R. A.; Mahowald, N., Iron, manganese, and lead at Hawaii Ocean Time-series station ALOHA: Temporal variability and an intermediate water hydrothermal plume. Geochim. Cosmochim. Acta 69(4) (2005): 933-952.
- [106] Chen, Y.; Lin, Z.; Chen, J.; Sun, J.; Zhang, L.; Chen, G., New capillary electrophoresis-electrochemiluminescence detection system equipped with an electrically heated Ru(bpy)(3)(2+)/multi-wall-carbon-nanotube paste electrode. J.Chromatogr. A 1172 (1) (2007): 84-91.

- [107] Babula, P.; Huska, D.; Hanustiak, P.; Baloun, J.; Krizkova, S.; Adam, V.; Hubalek, J.; Havel, L.; Zemlicka, M.; Horna, A.; Beklova, M.; Kizek, R., Flow injection analysis coupled with carbon electrodes as the tool for analysis of naphthoquinones with respect to their content and functions in biological samples. Sensors 6(11) (2006): 1466-1482.
- [108] Yoo, J. J.; Balakrishnan, K.; Huang, J.; Meunier, V.; Sumpter, B. G.; Srivastava, A.; Conway, M.; Mohana Reddy, A. L.; Yu, J.; Vajtai, R.; Ajayan, P. M., Ultrathin Planar Graphene Supercapacitors. Nano Lett. 11(4) (2011): 1423-1427.
- [109] Choi, B. G.; Im, J.; Kim, H. S.; Park, H., Flow-injection amperometric glucose biosensors based on graphene/Nafion hybrid electrodes. Electrochim. Acta 56 (27) (2011): 9721-9726.
- [110] Pumera, M.; Ambrosi, A.; Bonanni, A.; Chng, E. L. K.; Poh, H. L., Graphene for electrochemical sensing and biosensing. TrAC Trends Anal. Chem. 29(9) (2010): 954-965.
- [111] Li, W.; Tan, C.; Lowe, M. A.; Abrunwa, H. c. D.; Ralph, D. C., Electrochemistry of Individual Monolayer Graphene Sheets. ACS Nano 5(3) (2011): 2264-2270.
- [112] Shang, N. G.; Papakonstantinou, P.; McMullan, M.; Chu, M.; Stamboulis, A.; Potenza, A.; Dhesi, S. S.; Marchetto, H., Catalyst-Free Efficient Growth, Orientation and Biosensing Properties of Multilayer Graphene Nanoflake Films with Sharp Edge Planes. Adv. Funct. Mater. 18(21) (2008): 3506-3514.
- [113] Willemse, C. M.; Tlhomelang, K.; Jahed, N.; Baker, P. G.; Iwuoha, E. I., Metallo-Graphene Nanocomposite Electrocatalytic Platform for the Determination of Toxic Metal Ions. Sensors 11(4) (2011): 3970-3987.
- [114] Gong, J.; Zhou, T.; Song, D.; Zhang, L., Monodispersed Au nanoparticles decorated graphene as an enhanced sensing platform for ultrasensitive stripping voltammetric detection of mercury(II). Sens. Actuators, B 150(2) (2010): 491-497.

- [115] Anderson, J. L.; Bowden, E. F.; Pickup, P. G., Dynamic Electrochemistry: Methodology and Application. Anal. Chem. 68(12) (1996): 379-444.
- [116] Guo, J.; Chai, Y.; Yuan, R.; Song, Z.; Zou, Z., Lead (II) carbon paste electrode based on derivatized multi-walled carbon nanotubes: Application to lead content determination in environmental samples. Sens. Actuators, B In Press, Corrected Proof.
- [117] Bas, B.; Jakubowska, M.; Jez, M.; Ciepela, F., Novel renovated silver ring electrode for anodic stripping analysis of Pb(II) and Cd(II) traces in water samples without removal of oxygen and surfactants. J. Electroanal. Chem. 638(1) (2010): 3-8.
- [118] Absalan, G.; Asadi, M.; Kamran, S.; Torabi, S.; Sheikhan, L., Design of a cyanide ion optode based on immobilization of a new Co(III) Schiff base complex on triacetylcellulose membrane using room temperature ionic liquids as modifiers. Sens. Actuators, B 147(1) (2010): 31-36.
- [119] Hsieh, C.-T.; Wei, J.-M.; Lin, J.-S.; Chen, W.-Y., Pulse electrodeposition of Pt nanocatalysts on graphene-based electrodes for proton exchange membrane fuel cells. Catal. Commun. 16(1) (2011): 220-224.
- [120] Chen, B.; Liu, H.; Li, X.; Lu, C.; Ding, Y.; Lu, B., Fabrication of a graphene field effect transistor array on microchannels for ethanol sensing. Appl. Surf. Sci. 258(6) (2012): 1971-1975.
- [121] Huang, K.-J.; Niu, D.-J.; Sun, J.-Y.; Han, C.-H.; Wu, Z.-W.; Li, Y.-L.; Xiong, X.-Q., Novel electrochemical sensor based on functionalized graphene for simultaneous determination of adenine and guanine in DNA. Colloids Surf., B 82(2) (2011): 543-549.
- [122] Wei Yu; Huaqing Xie; Xinwei Wang; Wang, X., Highly Efficient Method for Preparing Homogeneous and Stable Colloids Containing Graphene Oxide. Nanoscale Res. Lett. 6 (2011): 1-7.
- [123] Du, H.; Ye, J.; Zhang, J.; Huang, X.; Yu, C., A voltammetric sensor based on graphene-modified electrode for simultaneous determination of catechol and hydroquinone. J. Electroanal. Chem. 650(2) (2011): 209-213.

- [124] Peng, J. Y.; Hou, C. T.; Liu, X. X.; Li, H. B.; Hu, X. Y., Electrochemical behavior of azithromycin at graphene and ionic liquid composite film modified electrode. Talanta 86(2011): 227-232.
- [125] Pruneanu, S.; Pogacean, F.; Biris, A. R.; Ardelean, S.; Canpean, V.; Blanita, G.; Dervishi, E.; Biris, A. S., Novel Graphene-Gold Nanoparticle Modified Electrodes for the High Sensitivity Electrochemical Spectroscopy Detection and Analysis of Carbamazepine. J. Phys.Chem. C 115(47) (2011): 23387-23394.
- [126] Zubero, M. B.; Aurrekoetxea, J. J.; Ibarluzea, J. M.; Arenaza, M. J.; Rodríguez, C.; Sáenz, J. R., Heavy metal levels (Pb, Cd, Cr and Hg) in the adult general population near an urban solid waste incinerator. Sci. Total Environ. 408(20) (2010): 4468-4474.
- [127] Marino, G.; Bergamini, M. F.; Teixeira, M. F. S.; Cavalheiro, s. d. T. G., Evaluation of a carbon paste electrode modified with organofunctionalized amorphous silica in the cadmium determination in a differential pulse anodic stripping voltammetric procedure. Talanta 59(5) (2003): 1021-1028.
- [128] Pittsburgh Conference on Analytical Chemistry. Anal. Chem. 24(3) (1952): 596-608.
- [129] Yáñez-Sedeño, P.; Pingarrón, J. M.; Riu, J.; Rius, F. X., Electrochemical sensing based on carbon nanotubes. TrAC Trends Anal.Chem. 29(9) (2010): 939-953.
- [130] Marek, T., Analytical applications of carbon nanotubes: a review. TrAC Trends Anal. Chem. 25(5) (2006): 480-489.
- [131] Injang, U.; Noyrod, P.; Siangproh, W.; Dungchai, W.; Motomizu, S.; Chailapakul, O., Determination of trace heavy metals in herbs by sequential injection analysis-anodic stripping voltammetry using screen-printed carbon nanotubes electrodes. Anal. Chim. Acta 668(1) (2010): 54-60.
- [132] Gao, Z.; Wang, G.; Li, P.; Zhao, Z., Differential pulse voltammetric determination of cobalt with a perfluorinated sulfonated polymer-2,2-

- bipyridyl modified carbon paste electrode. Anal. Chem. 63(10) (1991): 953-957.
- [133] Hwang, G.-H.; Han, W.-K.; Park, J.-S.; Kang, S.-G., An electrochemical sensor based on the reduction of screen-printed bismuth oxide for the determination of trace lead and cadmium. Sens. Actuators, B 135(1) (2008): 309-316.
- [134] Hwang, G. H.; Han, W. K.; Park, J. S.; Kang, S. G., Determination of trace metals by anodic stripping voltammetry using a bismuth-modified carbon nanotube electrode. Talanta 76(2) (2008): 301-308.
- [135] Mohammad Hadi, P., Graphene paste electrode for detection of chlorpromazine. Electrochem. Commun. 13(4) (2011): 366-369.
- [136] Li, F.; Li, J.; Feng, Y.; Yang, L.; Du, Z., Electrochemical behavior of graphene doped carbon paste electrode and its application for sensitive determination of ascorbic acid. Sens. Actuators, B 157(1) (2011): 110-114.
- [137] Pittcon: Pittcon 2000. Anal. Chem. 72(3) (1968): 117 A-163 A.
- [138] Meucci, V.; Laschi, S.; Minunni, M.; Pretti, C.; Intorre, L.; Soldani, G.; Mascini, M., An optimized digestion method coupled to electrochemical sensor for the determination of Cd, Cu, Pb and Hg in fish by square wave anodic stripping voltammetry. Talanta 77(3) (2009): 1143-1148.
- [139] John F, D., Dispersion and induction interactions of graphene with nanostructures. Surf. Sci. 605(17-18) (2011): 1621-1632.
- [140] Guo, J.; Ren, L.; Wang, R.; Zhang, C.; Yang, Y.; Liu, T., Water dispersible graphene noncovalently functionalized with tryptophan and its poly(vinyl alcohol) nanocomposite. Composites Part B 42(8) (2011): 2130-2135.
- [141] Shen, X.; Jiang, L.; Ji, Z.; Wu, J.; Zhou, H.; Zhu, G., Stable aqueous dispersions of graphene prepared with hexamethylenetetramine as a reductant. J. Colloid Interface Sci. 354(2) (2011): 493-497.
- [142] Chen, X.; Zhu, J.; Xi, Q.; Yang, W., A high performance electrochemical sensor for acetaminophen based on single-walled carbon nanotube-graphene nanosheet hybrid films. Sens. Actuators, B 161(1) (2011): 648-654.

- [143] Pu, N.-W.; Wang, C.-A.; Liu, Y.-M.; Sung, Y.; Wang, D.-S.; Ger, M.-D., Dispersion of graphene in aqueous solutions with different types of surfactants and the production of graphene films by spray or drop coating. J.Taiwan Inst. Chem. E., 43(1) (2011): 140-146.
- [144] Battumur, T.; Mujawar, S. H.; Truong, Q. T.; Ambade, S. B.; Lee, D. S.; Lee, W.; Han, S.-H.; Lee, S.-H., Graphene/carbon nanotubes composites as a counter electrode for dye-sensitized solar cells. Curr. Appl. Phys., In Press, Corrected Proof.
- [145] Chuanuwatanakul, S.; Dungchai, W.; Chailapakul, O.; Motomizu, S., Determination of trace heavy Metals by Sequential Injection-Anodic Stripping Voltammetry Using Bismuth Film Screen-printed Printed Carbon Electrode. Anal. Sci. 24(5) (2008): 589-594.
- [146] Mikysek, T. s.; Svancara, I.; Kalcher, K.; BartosĚ, M.; VytrĚas, K.; Ludvik, J. i., New Approaches to the Characterization of Carbon Paste Electrodes Using the Ohmic Resistance Effect and Qualitative Carbon Paste Indexes. Anal. Chem. 81(15) (2009): 6327-6333.
- [147] Baldrianova, L.; Svancara, I.; Vlcek, M.; Economou, A.; Sotiropoulos, S., Effect of Bi(III) concentration on the stripping voltammetric response of in situ bismuth-coated carbon paste and gold electrodes. Electrochim. Acta 52(2) (2006): 481-490.
- [148] Wu, Y.; Li, N. B.; Luo, H. Q., Simultaneous measurement of Pb, Cd and Zn using differential pulse anodic stripping voltammetry at a bismuth/poly(p-aminobenzene sulfonic acid) film electrode. Sens. Actuators, B 133(2) (2008): 677-681.
- [149] Kefala, G.; Economou, A.; Voulgaropoulos, A.; Sofoniou, M., A study of bismuth-film electrodes for the detection of trace metals by anodic stripping voltammetry and their application to the determination of Pb and Zn in tapwater and human hair. Talanta 61(5) (2003): 603-610.
- [150] Juan Sánchez, E. C., Piedad Corredor, Jesús Ágrede, Determination of Mercury by Anodic Stripping Voltammetry in Aqua Regia Extracts. Portugaliae Electrochim. Acta 29(3) (2011): 197-210.

APPENDICES

APPENDICES A

Table 1-A The SWASV peak currents of $50 \mu\text{g L}^{-1}$ Cd^{2+} and Pb^{2+} in 1.0 M HCl using the carbon electrode in the micro-flow sensor coupled with the SIA operating system at various deposition potential.

Ions	Deposition potential (V)	Peak current (μA)				
		$N=1$	$N=2$	$N=3$	Average \pm SD	%RSD
Cd^{2+}	-0.9	-	-	-	-	
	-1.0	3.78	4.26	3.89	3.98 ± 0.25	6.33
	-1.1	5.38	5.91	5.59	5.63 ± 0.27	4.74
	-1.2	9.02	8.97	8.94	8.98 ± 0.04	0.45
	-1.3	10.78	10.45	10.58	10.60 ± 0.17	1.57
	-1.4	14.97	14.62	14.78	14.79 ± 0.18	1.18
	-1.5	18.83	19.49	17.69	18.67 ± 0.91	4.88
Pb^{2+}	-0.9	7.09	6.97	7.02	7.03 ± 0.06	0.86
	-1.0	7.05	7.27	7.15	7.16 ± 0.11	1.54
	-1.1	8.19	8.65	8.32	8.39 ± 0.24	2.83
	-1.2	10.43	10.15	10.31	10.30 ± 0.14	1.36
	-1.3	11.30	11.07	11.20	11.19 ± 0.12	1.03
	-1.4	13.60	13.28	13.18	13.35 ± 0.22	1.64
	-1.5	14.29	13.88	14.69	14.29 ± 0.41	2.83

Table 2-A The SWASV peak currents of $50 \mu\text{g L}^{-1}$ Cd^{2+} and Pb^{2+} in 1.0 M HCl using the carbon electrode in the micro-flow sensor coupled with the SIA operating system at various frequencies.

Ions	Frequency (Hz)	Peak current (μA)				
		$N = 1$	$N = 2$	$N = 3$	Average \pm SD	%RSD
Cd^{2+}	10	1.96	1.86	1.91	1.91 ± 0.05	2.52
	25	3.62	3.99	3.83	3.81 ± 0.18	4.79
	50	6.95	6.80	6.89	6.88 ± 0.08	1.10
	75	2.34	2.24	2.30	2.29 ± 0.05	2.16
Pb^{2+}	10	2.37	2.27	2.31	2.32 ± 0.05	2.00
	25	4.92	5.33	5.41	5.22 ± 0.26	5.03
	50	9.81	9.96	9.89	9.89 ± 0.07	0.72
	75	3.28	3.41	3.33	3.34 ± 0.06	1.93

Table 3-A The SWASV peak currents of $50 \mu\text{g L}^{-1}$ of Cd^{2+} and Pb^{2+} in 1.0 M HCl using the carbon electrode in the micro-flow sensor coupled with the SIA operating system at various potential steps.

Ions	Potential step (V)	Peak current (μA)				
		$N = 1$	$N = 2$	$N = 3$	Average \pm SD	%RSD
Cd^{2+}	0.0100	4.97	5.11	5.03	5.04 ± 0.07	1.39
	0.0075	4.67	4.51	4.58	4.59 ± 0.08	1.75
	0.0050	4.40	4.69	4.57	4.55 ± 0.15	3.20
	0.0025	3.63	3.67	3.64	3.65 ± 0.02	0.57
Pb^{2+}	0.0100	7.00	7.32	7.14	7.15 ± 0.16	2.24
	0.0075	6.44	6.39	6.43	6.42 ± 0.03	0.41
	0.0050	5.47	5.43	5.46	5.45 ± 0.02	0.38
	0.0025	3.31	3.51	3.42	3.41 ± 0.10	2.94

Table 4-A The SWASV peak currents of $50 \mu\text{g L}^{-1}$ of Cd^{2+} and Pb^{2+} in 1.0 M HCl using the carbon electrode in the micro-flow sensor coupled with the SIA operating system at various potential amplitudes.

Ions	Potential amplitude (V)	Peak currents				
		$N = 1$	$N = 2$	$N = 3$	Average \pm SD	%RSD
Cd^{2+}	0.075	8.97	9.19	8.94	9.03 ± 0.14	1.51
	0.050	5.46	5.73	5.52	5.57 ± 0.14	2.55
	0.025	3.40	3.59	3.51	3.50 ± 0.10	2.73
	0.010	1.60	1.46	1.52	1.53 ± 0.07	4.60
Pb^{2+}	0.075	7.19	7.89	7.53	7.54 ± 0.35	4.64
	0.050	6.98	6.93	6.98	6.96 ± 0.30	0.41
	0.025	5.36	5.61	5.48	5.48 ± 0.13	2.28
	0.010	3.27	2.99	3.00	3.09 ± 0.16	5.15

VITAE

Name: Wanida Wonsawat
Birthdate: June, 16 1976
Place of Birth: Chonburi, Thailand
Education:
 Oct 2007- Present Chulalongkorn University Thailand, Ph.D. student
 Jun 2004- Mar 2006 Chulalongkorn University Thailand, M.Sc. student
 Jun 1995- Mar 1999 Burapha University, Bachelor of Education
 (Chemistry Teaching) B.Ed (Chemistry Teaching)

Publications

1. O.Chailapakul, W. Wonsawat, W. Siangproh, K.Grudpan, Y. Zhao, and Z. Zhu, "Analysis of Sudan I, Sudan II, Sudan III, and Sudan IV in Food by HPLC with Electrochemical Detection: Comparison of Glassy Carbon Electrode with Carbon Nanotube-Ionic Liquid Gel Modified Electrode" **Food Chem.**, **2008**, 109, 876-882.
2. W.Wonsawat, C.Kraiya, S.Chuanuwatanakul, O.Chailapakul, and S.Motomizu, "Electrochemical Characterization of Carbon Electrode in m-Flow Sensor by On-line Automated Flow System" **J.Flow Injection Anal.**, **2009**, 26, 43-47.
3. W.Wonsawat, W.Dungchai, S.Motomizu, S.Chuanuwatanakul, O.Chailapakul, "Highly Sensitive Determination of Cadmium and Lead Using a Low-cost Electrochemical Flow-through Cell Based on a Carbon Paste Electrode" **Anal. Sci.**, **2012**, 28, 141-146.

Scholarship

2005 CU. Graduate School Thesis Grant
 2006-2007 The 90th Years Anniversary of Chulalongkorn University (Ratchadphiseksomphot Endowment Fund)
 2007- 2008 Asian Development Bank (ADB)
 2007-2010 The Higher Educational Strategic Scholarships for Frontier Research Network Project, Thailand
 2007 Japan Student Services Organization under JASSO-Short-Term Student Exchange Promotion Program (Inbound) Scholarship
 2011-2012 The 90th Anniversary of Chulalongkorn University Fund (Ratchadaphiseksomphot Endowment Fund)

Award

Outstanding poster presentation "*Low-cost and portable electrochemical flow-through cell based on carbon paste electrode for highly sensitive determination of lead and cadmium*" –RGJ Seminar Series LXXXV "Contemporary Analytical Chemistry and Analytical Technology", September 9th, 2011